International School for Advanced Studies

Physics Area / Condensed Matter

Ph.D. thesis

Thermalization and relaxation after a quantum quench in disordered Hamiltonians

Candidate
Simone Ziraldo

Supervisor
Prof. Giuseppe E. Santoro

October 2013
Via Bonomea 265, 34136 Trieste - ITALY

Abstract

In the present thesis we study the unitary dynamics and the thermalization properties of free-fermion-like Hamiltonians after a sudden quantum quench in presence of disorder. With analytical and numerical arguments, we show that the existence of a stationary state and its description with a generalized Gibbs ensemble (GGE) depend crucially on the observable considered (local versus extensive, one-body versus many-body) and on the localization properties of the final Hamiltonian. We then show an extension of the Wang-Landau algorithm which allows the computation of weighted distributions associated to quantum quenches, like the diagonal and the GGE ensemble expectation-value distributions. We present results on three one-dimensional models, the Anderson model, a disordered one-dimensional fermionic chain with long-range hopping, and the disordered Ising/XY spin chain.

CONTENTS

1 INTRODUCTION

The concept of ergodicity is at the core of classical statistical mechanics: it establishes a connection between long-time averages of observables and statistical ensemble averages [1]. The extension of the ergodic theorem to quantum mechanics was pioneered in 1929 by von Neumann [2, 3] in a seminal paper on the unitary dynamics of closed quantum systems. The experimental possibility of studying the nonequilibrium dynamics of isolated quantum systems – most notably cold atomic species in optical lattices [4, 5] – has stimulated new interest in the subject. A highly debated issue in the recent literature is the characterization of the long-time dynamics of a quantum system taken out of equilibrium. The simplest setting for such a non-equilibrium situation is that of a quantum quench: starting from an initial state, eigenstate of an initial Hamiltonian, a system's parameter is suddenly changed and the dynamics is then governed by the new Hamiltonian. If an extensive amount of energy is suddenly injected in the system, will the resulting dynamics tend to a well defined stationary state? And what is the statistical ensemble describing it? Since the energy is conserved, it is reasonable to expect that an ergodic evolution in the Hilbert space will lead to time averages which are reproduced by the microcanonical ensemble: this is what von Neumann discussed for macroscopic observables [2, 3], and is generally expected to occur [6–8], independently of the initial state.

In classical physics, violations of ergodicity arise in many situations: on one extreme, for systems that are integrable [9] or close enough to being integrable [10–13]; on the other, for systems with a glassy dynamics, be it due to interactions providing dynamical constraints [14], or to genuine disorder [15]. Quantum mechanically, dangers to ergodicity come from very similar sources: integrability, interactions, and disorder.

Integrability implies the existence of many constants of motion, and this clearly restricts the ergodic exploration of the microcanonical energy shell, leading to what one might call a breakdown of thermalization [16, 17]. It often results in a kind of generalized thermalization described by a statistical ensemble which maximizes entropy in the presence of constraints, an ensemble introduced long ago by Jaynes [18] and known as generalized Gibbs ensemble (GGE) [19–23].

Another type of ergodicity crisis derives, apparently, from dynamical constraints imposed by interactions [24]. When quenching a Bose-Hubbard model starting with a non-homogeneous initial state at integer filling, the ensuing dynamics leads to a fast relaxation/thermalization for quenches at small interaction, while the relaxation is extremely slow (and the more so, the more the size of the system increases) and the dynamics appears effectively freezed for interaction greater than a critical value [24].

Concerning ergodicity breaking due to genuine disorder, both Anderson localization, at the single-particle level [25], and many-body localization, in the presence of interactions [26], are well-known examples of disorder-induced phenomena occurring in equilibrium physics. Recent studies hinted towards nontrivial effects due to the breaking of translational invariance. In integrable systems, breaking translational invariance in the initial state could introduce correlations among different constants of motion, persisting in the long-time evolution, and relevant for finite-size systems [27, 28]. However their effect has been argued to be negligible in predicting with GGE the stationary state attained by local observables [23]. While in the thermodynamic limit the breaking of translational invariance may not have a significant effect, localization could in turn play an important role, to the extent of resulting in the absence of thermalization even in non-integrable chains [29]. This observation appears to be consistent with earlier numerical analysis in disordered Ising or XY spin chains (characterized by localization of the eigenstates), where a discrepancy between the expected GGE and the effective

stationary state was observed [28]. Quantum quenches in the presence of disorder and interactions have also been studied, in the framework of many-body localization [30–33], but the physical picture is far from being fully understood.

Besides the problem of thermalization with respect to the relevant ensemble there is another key question: does an out-of-equilibrium system reach a stationary state for long times? The approach to equilibrium has been carefully investigated for one-dimensional Bose-Hubbard models describing quench experiments in optical lattices and super-lattices [34–37]. Starting from non-homogeneous half-filled initial states (density waves) and evolving the system with the Bose-Hubbard Hamiltonian, the long-time evolution of local observables relaxes to stationary values. This occurs both at the integrable points (zero and infinite interaction) where analytic solutions are possible [37], and at general (non-integrable) values of the interaction (analyzed through time-dependent density-matrix renormalization group [38, 39]). The physical picture emerging has led to the so-called "local relaxation conjecture" [34]: although the system is in a pure state, when measured upon locally in a finite region, the resulting (mixed) reduced density matrix relaxes towards a stationary Gibbs state of maximum entropy compatible with the constants of motion. This relaxation is strongly tight to the locality of the observable one measures, and results from information transfer carried by the excitations along the system [34, 35, 37], which eventually "thermalizes" any finite region, the rest of the system acting as an effective bath. Remarkably, such an approach to equilibrium does not require time averages [34]. Experimentally, a fast dynamical relaxation was recently observed [40] in a system of cold atoms which can be modeled with a one-dimensional Bose-Hubbard model.

In this thesis we will focus on the issue of thermalization and relaxation following a quantum quench with disordered Hamiltonians which can be mapped to free-fermion systems. On the basis of analytical calculations, corroborated by numerics, we argue that the existence of a stationary state depends crucially on the spectral properties of the final (i.e., after-quench) Hamiltonian, and not on the initial state. Indeed, we show that, in agreement with recent works [23], breaking of translational invariance and disorder in the initial state have apparently little or no effect on the ensuing relaxation of local observables towards a stationary state in the thermodynamic limit if the after-quench Hamiltonian has a continuous spectrum associated to delocalized states. On the contrary, in the presence of localization in the final Hamiltonian, the long-time after-quench dynamics does not relax towards a stationary state, and time fluctuations generally persist in the expectation values of local operators, even in the thermodynamic limit. This is essentially due to the presence of a pure-point spectrum of the final Hamiltonian associated to localized wave functions, as opposed to the smooth continuum of a system with extended states. One can view this persistence of time fluctuations in local measurements as a result of the inability of the system to carry information around [34], due to localization. When long-time fluctuations do not vanish in the thermodynamic limit, time averages are, therefore, mandatory in comparing dynamical quantities to statistical ensemble averages. We also show analytically that time averages of one-body local observables are perfectly well reproduced by the GGE, which is the relevant statistical ensemble being the considered models, essentially, free-fermion ones. This is not generally the case for many-body operators, unless time fluctuations of one-body Green's functions vanish for large times. We will show an explicit case in which, when this condition is not fulfilled, the time average of a many-body operator has clear deviations from the GGE prediction. We will exemplify these ideas on three models: the Anderson model, a disordered one-dimensional fermionic chain with long-range hopping, and disordered Ising/XY models. Finally, we will introduce a generalization of the Wang-Landau Monte Carlo algorithm [41–43] which is able to give us information on several distribution functions for relevant observables: such distribution functions cannot be generally calculated analytically, even for our free-fermion models, due to the exponential growth of the Hilbert space dimensions.

The structure of the present thesis is as follows. We start, in Chap. 2, by stating in a more precise way the problem we want to analyze. We briefly overview the problem of ergodicity in classical physics and of thermalization in quantum physics, and we introduce the concept of quantum quenches, the tool we have used to study the out-of-equilibrium quantum dynamics. Next, in Chap. 3, we describe the models we have investigated, focusing on their localization properties in presence of disorder. In Chap. 4 we present our original results on quantum quenches: we first show the essential reason why GGE works perfectly well in predicting infinite-time averages of one-body operators and why it may fail for many-body operators; next we present and analyze our numerical results for the three studied models. In Chap. 5 we introduce an extension the Wang-Landau algorithm, a Monte Carlo method which allows to compute numerically the density of states. With this modification we are able to compute weighted density of states, more precisely distribution functions of observables, which are useful quantities to look at when considering thermalization issues. We apply this technique to the quantum quenches studied in Chap. 4. Finally, Chap. 6 contains a final discussion with our conclusions and perspectives on the topic.

The results presented in Chap. 4 are contained in two publications:

1. S. Ziraldo, A. Silva and G.E. Santoro, Phys. Rev. Lett. **109**, 247205 (2012).

2. S. Ziraldo and G.E. Santoro, Phys. Rev. B **87**, 064201 (2013).

The results presented in Chap. 5 will appear in a manuscript which is still in preparation.

2 OUT OF EQUILIBRIUM STATISTICAL MECHANICS: PRELIMINARIES

Two important and fascinating aspects of statistical mechanics concern the concepts of ergodicity [44–47] and mixing [45, 46]. The first, ergodicity, is a hypothesis introduced by Boltzmann and Maxwell while laying the foundations of statistical mechanics; remarkably, it is still an open problem, widely studied in the mathematical and physics community. The concept of mixing is instead connected to how a classical out-of-equilibrium state reaches thermal equilibrium and is deeply connected to irreversibility, probably one of the most intriguing concepts of thermodynamics. In the first section of this chapter we briefly remind the reader about these aspects of classical statistical mechanics, particularly the notions of time and ensemble averages. In Sec. 2.2 we turn to quantum physics, and introduce the concepts of diagonal averages and quantum ensembles. Quantum quenches, which is the topic of Sec. 2.3, are the simplest way to study the out-of-equilibrium quantum dynamics and the foundations of quantum statistical mechanics. The importance of quantum quenches comes from their experimental feasibility: in Sec. 2.4 we recall how they can be realized with cold atoms experiments.

2.1 STATISTICAL MECHANICS OF CLASSICAL SYSTEMS: ERGODICITY AND MIXING

In this section we briefly overview the classical statistical ensembles, discussing their usefulness for the description of macroscopic systems. We will in particular touch on the concepts of ergodicity and mixing, which are the main ingredients in understanding relaxation and thermalization in classical physics.

We start by considering an isolated classical system described by a Hamiltonian $H(\mathbf{x})$ [9], where $\mathbf{x}$ is a f-dimensional vector which identifies uniquely the system's configuration. In a gas, for instance, $\mathbf{x}$ is the set of positions and momenta of all particles. The volume Γ spanned by all the possible configurations is known as phase space [1]. Given an initial state, the time evolution causes the configuration to move around, drawing a trajectory $\mathbf{x}(t)$ inside Γ. Since the system is isolated, the energy E is a constant of motion and the trajectory $\mathbf{x}(t)$ lies on a $(f-1)$-dimensional surface S_E, given by all the $\mathbf{x}$ such that $H(\mathbf{x}) = E$. Given a dynamical observable $A(\mathbf{x})$, we want to compute its value at time t, namely $A(\mathbf{x}(t))$. To get $\mathbf{x}(t)$ we have to solve the Hamilton's equations associated to the Hamiltonian $H(\mathbf{x})$ [9], i.e., we should integrate a set of f first-order differential equations. But, even before integrating the Hamilton's equations, we need the initial state, which would actually require knowing the positions and momenta of all the particles at time $t = 0$, $\mathbf{x}(0)$. This information is inaccessible in most of the real experimental setups, especially when the number of degrees of freedom f is large. (In a gas, for instance, f is of the order of the Avogadro's number.) Besides this obvious experimental limitation, there is also a more fundamental intrinsic issue: if the system is chaotic [9] we will not be able to follow its exact dynamics, because any small error in the initial state, even infinitesimal, is exponentially amplified, generating trajectories which are far apart in phase space. Experimentally, however, in measuring macroscopic quantities for large systems one does not generally find such a violent sensitivity on the choice of the initial condition. How does this comes about?

A fruitful alternative to this "dynamical approach" consists in using a "statistical approach". Rather than considering a single system and its time evolution in phase

Ensembles

space, one considers an infinite number of identical copies of the system, continuously distributed throughout the phase space. This set of systems is called an ensemble and we define $\rho(\mathbf{x})$ as the probability density describing the distribution of the states over the phase space. In this framework the dynamical observable $A(\mathbf{x})$ will be characterized by appropriate averages over the ensemble distribution, and its mean value

$$\langle A \rangle \equiv \int_\Gamma d\mathbf{x}\, \rho(\mathbf{x}) A(\mathbf{x}) \,, \tag{2.1}$$

is known as ensemble average. The selected probability density $\rho(\mathbf{x})$ usually depends on a small set of macroscopic quantities associated to the system. The advantage of the statistical approach is clear: we do not need to know exactly the initial state at $t = 0$ and to follow its time evolution, but rather have control of a small set of properties, which are usually experimentally accessible. For instance, when the system is isolated the energy doesn't change in time, and the usual choice is the so called microcanonical ensemble: $\rho_{mc}(\mathbf{x})$ is nonzero and constant only over the surface of constant energy S_E. In the microcanonical ensemble the phase average is therefore:

$$\langle A \rangle_{mc} \equiv \frac{1}{Z_{mc}} \int_{S_E} d\mathbf{x}\, A(\mathbf{x}) \,, \tag{2.2}$$

where $Z_{mc} = \int_{S_E} d\mathbf{x}$ is the microcanonical partition function. Other important ensembles are obtained by considering "open" portions of a larger isolated system. For instance, in the canonical ensemble the energy can change but the temperature is fixed; in the grancanonical ensemble, in addition to the energy, also the number of particles is free to fluctuate. We refer the reader to any standard textbook for details [1].

Once the ensemble has been chosen, we are in principle able to compute the phase averages of any physical observable. However we still lack a link with the experiment: what is the experimental counterpart of the ensemble average of the observable $A(\mathbf{x})$? At the end of the nineteenth century, Boltzmann argued that the measurement of a physical quantity necessarily requires a finite amount of time. Hence, the result of a measurement provides us with an average over a certain finite time interval. This time interval is usually much greater than any characteristic time-scale of the corresponding microscopic dynamics. Hence, it is legitimate to assume that a measurement of $A(\mathbf{x})$ will be essentially given by the infinite time average of $A(\mathbf{x})$:

Time average

$$\overline{A} \equiv \lim_{t\to\infty} \frac{1}{t} \int_0^t dt'\, A(\mathbf{x}(t')) \,. \tag{2.3}$$

Now, the final link between this quantity and the ensemble average of $A(\mathbf{x})$ is given by the ergodic hypothesis: an isolated system is ergodic if for any observable $A(\mathbf{x})$ and almost any initial state $\mathbf{x}_0$

Ergodicity

$$\overline{A} = \lim_{t\to\infty} \frac{1}{t} \int_0^t dt'\, A(\mathbf{x}(t')) = \frac{1}{Z_{mc}} \int_{S_E} d\mathbf{x}\, A(\mathbf{x}) = \langle A \rangle_{mc} \,. \tag{2.4}$$

The ergodic condition can be written in many ways: an equivalent interesting geometrical definition is that a system is ergodic when the trajectory $\mathbf{x}(t)$ passes close to nearly all the states compatible with the conservation of energy, see Figure 2.1.

Ergodicity has been mathematically proved for a small set of systems, mainly billiards with hard core spheres [48, 49]. A lack of ergodicity could come from many factors: integrability, on one extreme, and glassiness, on the other. A classical system is integrable when there is a complete set of constants of motion which restricts the dynamics to essentially one-dimensional degrees of freedom. In this case ergodicity can be in some sense "recovered" by restricting the microcanonical average in Eq. (2.2) to the appropriate surface in which all the constants of motion are fixed. More interesting is the case of systems which are "close to integrability": when the Hamiltonian is slightly perturbed from an integrable one, the trajectories remain "trapped" in surfaces,

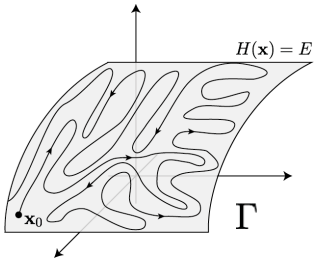

Figure 2.1: A sketch of an ergodic trajectory in phase space Γ. The gray surface is the set of configurations with energy E, where E is the energy of the initial state $\mathbf{x}_0$. An ergodic trajectory $\mathbf{x}(t)$ passes close to nearly all the sates with energy E as t approaches ∞.

called invariant tori, and they are unable to fill the available phase space. A numerical example of this effect was discovered by Fermi, Pasta, and Ulam [10]; the mathematics of it is contained in the famous Kolmogorov-Arnold-Moser (KAM) theorem [9, 11–13]. Glasses, at the other extreme, are a well known class of systems where ergodicity fails. In these systems the configuration is dynamically trapped in a subset of the phase space and the system is not able to fill the allowed S_E in any reasonable time-scale. Glassy dynamics has been shown even in simple systems, e.g., lattice Hamiltonians with density constraints, for instance when a particle on a lattice cannot have more than a given number of occupied neighboring sites [14]. Glassiness, and ergodicity breaking, is also present in disordered systems, like spin glasses [15], i.e., disordered magnets with frustrated interactions. Besides these well studied cases, it is commonly believed that in most of the non-trivial classical Hamiltonians with many degrees of freedom ergodicity is fulfilled [46].

Besides ergodicity, another important question is: if we start from an out-of-equilibrium state, will the observables approach their equilibrium value as time proceeds? The answer to this important question is deeply rooted in the concept of mixing. Mixing can be defined mathematically by introducing the concept of measure in phase space, but a physically quite transparent definition might be the following. Within the statistical approach, we start at time $t = 0$ from an out-of-equilibrium set of states with energy E, described by the initial ensemble $\rho_0(\mathbf{x})$. At any given time t, the new density will be $\rho_t(\mathbf{x})$, which for a Hamiltonian system will satisfy Liouville's theorem [1] (which say, essentially, $\rho_t(\mathbf{x}(t)) = \rho_0(\mathbf{x}(0))$). A system is said mixing if for any initial ensemble $\rho_0(\mathbf{x})$ and any observable $A(\mathbf{x})$ we have: *Mixing*

$$\lim_{t\to\infty} \int_{S_E} d\mathbf{x}\, A(\mathbf{x})\rho_t(\mathbf{x}) = \frac{1}{Z_{mc}} \int_{S_E} d\mathbf{x}\, A(\mathbf{x}) \,. \tag{2.5}$$

In words, this means that, in a mixing system, the mean value at time t of $A(\mathbf{x})$ approaches, for large times, the microcanonical average. To illustrate the concept of mixing, we sketch in Fig. 2.2 possible different types of flow in phase space starting from an initial ensemble which is concentrated in a finite volume of phase space (the deformed rectangles). During the time evolution the volume occupied by the initial ensemble moves and deforms, building a flow inside the phase space. From Liouville's theorem [1], the volume is conserved by the flow, but the shape can evolve and be deformed in many ways. The simplest case is illustrated in panel (a) of Fig. 2.2, in which the initial volume moves without distortion, returning to the initial position in phase space after a certain time: in this case, the flow sweeps a finite fraction of the available phase space. This flow is neither ergodic nor mixing. An example of ergodic flow is shown in panel (b) of Fig. 2.2, where the initial shape is only slightly altered, but it never returns to its initial location, and visits essentially every region of available phase space. Finally, panel (c) of Fig. 2.2 illustrates a mixing flow: here the shape of the initial distribution is highly distorted as time increases, and evolves into an octopus with contorted arms which grow into extremely fine filaments that spread out uniformly over the whole phase space. A familiar every-day example of a mixing flow is shown in Fig. 2.3. Essentially, in a mixing flow, starting from an initial out-of-equilibrium ensemble the distribution $\rho_t(\mathbf{x})$ evolves towards the equilibrium one, i.e., the microcanonical ensemble in the case of an isolated system. As one might guess by looking at the sketches of

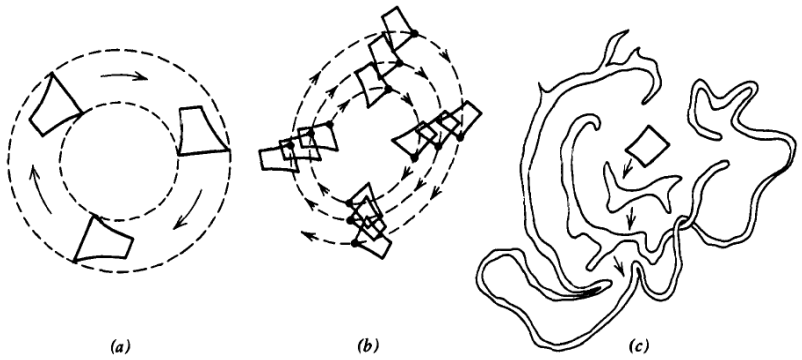

Figure 2.2.: Sketch of three types of flow in phase space. (a) non-ergodic: the initial sample moves without distortion, returning to the initial condition after a finite time; (b) ergodic: the shape of the initial sample is only slightly altered by time evolution but it never returns to the initial condition and it sweeps out the allowed portion of phase space; (c) mixing: the shape is distorted by time evolution and after an infinite time it spreads out over the whole allowed phase space. Figure taken from Ref. [46].

Fig. 2.2, mixing is a stronger condition than ergodicity: it implies ergodicity but is not implied by it. Like for ergodicity, mixing has been mathematically proven only for a few simple systems. The most known result is due to Sinai who proved, in 1962, that the hard-sphere gas is ergodic and mixing [48]. It has also been proved rigorously [50] that mixing is strongly connected to the instability of trajectories associated to a chaotic dynamics in phase space, and is deeply related to the issue of irreversibility [45].

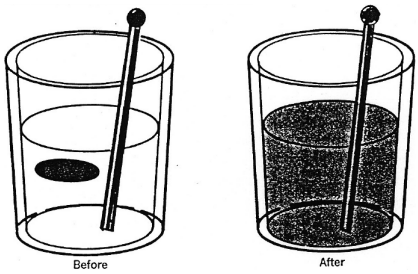

Figure 2.3: A familiar example of a mixing flow: rum (twenty percent) and cola (eighty percent) produce, after mixing, a "Cuba libre". Figure taken from Ref. [45].

2.2 STATISTICAL MECHANICS OF CLOSED QUANTUM SYSTEMS

In this section we briefly overview the statistical approach to closed quantum systems. A closed quantum system is described by a Hamiltonian $\hat{H}$, which is an Hermitian operator [51]. A state of the system is described by a wavefunction $|\Psi\rangle$ and the "phase space" is given by the associated Hilbert space [51]. The dynamics is governed by the Schrödinger equation, which is a linear first-order in time partial differential equation:

$$i\hbar\frac{\partial}{\partial t}|\Psi(t)\rangle = \hat{H}|\Psi(t)\rangle \,, \tag{2.6}$$

where $|\Psi(t)\rangle$ is the wavefunction at time t. We will denote by $|\Psi_0\rangle \equiv |\Psi(0)\rangle$ the initial state.

We start with some observations. Given an orthonormal basis set $\{|\alpha\rangle\}$ of the Hilbert space, the initial wavefunction $|\Psi_0\rangle$ can be expressed as

$$|\Psi_0\rangle = \sum_\alpha c_\alpha |\alpha\rangle \,, \tag{2.7}$$

where $c_\alpha \equiv \langle\alpha|\Psi_0\rangle$. An exact description of the initial state requires the knowledge of all the c_α's, whose number grows as the Hilbert space dimension, i.e., exponentially with the system size. Therefore, like in classical physics, a statistical approach is useful to deal with macroscopic systems. The second remark has to do with the linearity of the Schrödinger equation, as opposed to the generally non-linear Hamiltonian dynamics of classical physics. Due to linearity, if we work with a basis given by the eigenstates $|\alpha\rangle$ of the Hamiltonian $\hat{H}$, with eigenvalues E_α, the solution of Eq. (2.6) is:

$$|\Psi(t)\rangle = \sum_\alpha c_\alpha e^{-i\frac{E_\alpha t}{\hbar}}|\alpha\rangle \, . \tag{2.8}$$

If we regard this time evolution as a trajectory in phase space, quantum dynamics seems far from being ergodic. Indeed, the square modulus of $\langle\alpha|\Psi(t)\rangle = c_\alpha e^{-iE_\alpha t/\hbar}$ does not change in time during the evolution, $|\langle\alpha|\Psi(t)\rangle|^2 = |c_\alpha|^2$: as the time advances, only the phase of $\langle\alpha|\Psi(t)\rangle$ rotates in the complex plane. Let us denote by $E_0 \equiv \langle\Psi_0|\hat{H}|\Psi_0\rangle = \sum_\alpha E_\alpha |c_\alpha|^2$ the average energy of the initial state, which is a conserved quantity: $\langle\Psi(t)|\hat{H}|\Psi(t)\rangle = E_0$. In the Hilbert space, the "surface" of energy E_0 is given by all the normalized states $|\phi\rangle = \sum_\alpha \phi_\alpha|\alpha\rangle$ which satisfy the "ellipsoid" equation $E_0 = \langle\phi|\hat{H}|\phi\rangle = \sum_\alpha E_\alpha|\phi_\alpha|^2$. The states touched by $|\Psi(t)\rangle$ during the quantum dynamics are evidently just a small subset of such "ellipsoid", since the $|c_\alpha|^2$ are fixed: therefore, whatever is the Hamiltonian and the initial state, there is a huge set of normalized states $|\phi\rangle$ with energy E_0 which is neither touched nor close to the trajectory of $|\Psi(t)\rangle$. In summary, the conservation of the quantity $|\langle\alpha|\Psi(t)\rangle|^2 = |c_\alpha|^2$, directly implied by the linearity of the Schrödinger equation, seems to prevent any kind of ergodicity, at least in the classical sense. This fact was underlined by von Neumann [2, 3] in his seminal work on the quantum mechanical counterpart of the ergodic theorem. Indeed, ergodicity in quantum mechanics is far from a trivial concept, and we will not adventure in describing the large body of literature stimulated by von Neumann's work.

Ensembles

Abandoning the dynamical description (since we generally do not have access to the exact initial state) one can make profit of a statistical approach, defining quantum ensembles. As discussed for classical physics, the idea is that, instead of computing the expectation value of an operator over a single state, we average over all the states that are compatible with the experimentally accessible information. In other words, the single state is replaced by an ensemble of states $|\Psi^{(i)}\rangle$ with an associated probability w_i, such that $\sum_i w_i = 1$. Given an observable $\hat{A}$ (an Hermitian operator), the ensemble average is defined as:

$$\langle\hat{A}\rangle = \sum_i w_i \langle\Psi^{(i)}|\hat{A}|\Psi^{(i)}\rangle \, , \tag{2.9}$$

where $\langle\Psi^{(i)}|\hat{A}|\Psi^{(i)}\rangle$ is the expectation value of the observable $\hat{A}$ over the state $|\Psi^{(i)}\rangle$. If we expand these states over a basis, $|\Psi^{(i)}\rangle = \sum_\alpha c_\alpha^{(i)}|\alpha\rangle$, and define by $\hat{\rho}$ the operator $\langle\alpha|\hat{\rho}|\beta\rangle = \sum_i w_i c_\alpha^{(i)} c_\beta^{(i)*}$ then:

$$\langle\hat{A}\rangle \equiv \mathrm{Tr}\left[\hat{\rho}\hat{A}\right] \, . \tag{2.10}$$

The operator $\hat{\rho}$ is known as density matrix and is such that $\mathrm{Tr}\left[\hat{\rho}\right] = 1$.

For an isolated quantum system the natural choice for $\hat{\rho}$ is the microcanonical ensemble:

$$\hat{\rho}_{mc} \equiv \frac{1}{Z_{mc}} \sum_{\alpha|E_\alpha\in\Delta} |\alpha\rangle\langle\alpha| \, , \tag{2.11}$$

where the summation is over all the eigenstates $|\alpha\rangle$ of $\hat{H}$ such that E_α is inside a window $\Delta = [E_0 - \delta, E_0 + \delta]$ centered around the initial state energy $E_0 \equiv \langle\Psi_0|\hat{H}|\Psi_0\rangle$, and $Z_{mc} \equiv \sum_{\alpha|E_\alpha\in\Delta} 1$ is the microcanonical partition function, where δ can be arbitrary small, after the thermodynamic limit has been taken. This choice reminds the classical microcanonical ensemble, where $\rho_{mc}(\mathbf{x})$ is nonzero and constant only over the surface of constant energy S_E (see Eq. (2.2)), with a few important differences. Indeed, in quantum physics the initial wavefunction $|\Psi_0\rangle$ is in general a superposition of eigenstates

with different energies. This, obviously, has no counterpart in classical physics where each state is just a point in phase space possessing a definite energy. In this perspective, the definition of $\hat{\rho}_{mc}$ appears, at a first glance, a bit weak. An issue arises, for instance, if we consider a system with a finite gap in the energy spectrum, say around the energy $E = 0$; if we take a state $|\Psi_0\rangle$ which is a superposition of states of positive and negative energy such that $\langle\Psi_0|\hat{H}|\Psi_0\rangle = 0$, then the definition in Eq. (2.11) loses any meaning if 2δ is smaller than the gap. So, we need something more about the initial state $|\Psi_0\rangle$ we are trying to describe through the microcanonical ensemble. In a nutshell, we should require that most of the states that contribute to $|\Psi_0\rangle$ are arbitrarily close to E_0 in the thermodynamic limit [8, 52]. In more precise terms, if we define the (intensive) energy distribution of the initial state as:

$$\rho_D(\epsilon) \equiv \sum_\alpha |c_\alpha|^2 \delta(\epsilon - \epsilon_\alpha) \,, \tag{2.12}$$

where $\epsilon_\alpha \equiv E_\alpha/L$, then the width of this distribution goes to zero in the thermodynamic limit, a property which holds under very general conditions and physical meaningful situations [8]. We will come back to this property of $|\Psi_0\rangle$ in Chap. 5.

Another important and useful ensemble is the canonical one, which is built by considering an open portion of a large isolated system [1]. In this case the density matrix is:

$$\hat{\rho}_c \equiv \frac{1}{Z_c} e^{-\beta \hat{H}} \,, \tag{2.13}$$

where $\beta \equiv 1/K_B T$, K_B being the Boltzmann's constant and T the system's temperature, and $Z_c \equiv \mathrm{Tr}\left[e^{-\beta \hat{H}}\right]$. The canonical ensemble is often used also for isolated systems because usually simpler to use for both numerical and analytical computations. The crucial link between the two ensembles comes from the equivalence of the different ensembles, i.e., in the thermodynamic limit different ensembles should give equal phase averages [53]. In the thermodynamic limit, therefore, the microcanonical and canonical averages should coincide, and we might define the canonical temperature of our isolated system to be such that:

$$E_0 = \mathrm{Tr}\left[\hat{\rho}_c \hat{H}\right] \,. \tag{2.14}$$

In this thesis we are going to consider Hamiltonians with quadratic expansions over fermionic operators [54]. These are solvable non-interacting models that can be expressed as:

$$\hat{H} = \sum_\mu \epsilon_\mu \hat{\gamma}_\mu^\dagger \hat{\gamma}_\mu \,, \tag{2.15}$$

where $\hat{\gamma}_\mu^\dagger$ and $\hat{\gamma}_\mu$ are a set of fermionic operators which create and destroy a fermion in the single-particle state labeled by μ. These Hamiltonians commute with the occupation number operators $\hat{n}_\mu \equiv \hat{\gamma}_\mu^\dagger \hat{\gamma}_\mu$ and, therefore, we have more constraints (conserved quantities) than the usual isolated systems. The usual choice is a Gibbs-like statistical ensemble, called generalized Gibbs ensemble (GGE), for which the density matrix is [20]:

Generalized Gibbs ensemble

$$\hat{\rho}_{GGE} \equiv \frac{1}{Z_{GGE}} e^{-\sum_\mu \lambda_\mu \hat{\gamma}_\mu^\dagger \hat{\gamma}_\mu} \,, \tag{2.16}$$

where $Z_{GGE} \equiv \mathrm{Tr}\left[e^{-\sum_\mu \lambda_\mu \hat{\gamma}_\mu^\dagger \hat{\gamma}_\mu}\right]$, and the Lagrange multipliers λ_μ are fixed by requiring [1]

$$\langle\Psi_0|\hat{\gamma}_\mu^\dagger \hat{\gamma}_\mu|\Psi_0\rangle = \langle\hat{\gamma}_\mu^\dagger \hat{\gamma}_\mu\rangle_{GGE} \,. \tag{2.17}$$

1 Note that, in principle, the $\mathrm{Tr}[\cdot]$ appearing in the GGE ensemble could be assumed to be within the canonical Hilbert space with a fixed number of particles N, $\mathcal{H}_N$, or within the grand-canonical Hilbert space $\mathcal{H}$ where the number of particles can vary. Usually, the grand-canonical version is much easier to use (one can make use of Wick's theorem, for instance). Recall that the usual derivation of the Fermi-Dirac distribution in a free-fermion system proceeds in the grand-canonical Hilbert space.

This ensemble was first introduced by Jaynes [18], who called it the "maximum entropy ensemble", to describe the equilibrium state of a system possessing a set of constants of motion.

2.3 QUANTUM QUENCHES

The out-of-equilibrium quantum dynamics of a closed quantum system immediately poses two important questions. The first question is the quantum counterpart of the classical concept of mixing: given an initial state $|\Psi_0\rangle$, will the unitary quantum evolution be such that the interesting observables reach "stationary" values for very long times? The second question deals with a possible statistical description of such a stationary state: what is the most appropriate statistical ensemble, if any exist, to correctly describe and reproduce the time averages of the interesting observables? Quantum quenches represent the simplest framework to tackle analytically and numerically these questions.

In a quantum quench the initial state is a pure state $|\Psi_0\rangle$, which is assumed to be an eigenstate of some initial Hamiltonian $\hat{H}_0$, but the system is abruptly modified at time $t = 0$ in such a way that it evolves under a different time-independent Hamiltonian $\hat{H}$. This prescription can also describe real experimental situations where a parameter of the system is suddenly changed (an example is illustrated in Sec. 2.4).

2.3.1 Time and diagonal averages

Given a quantum quench, the expectation value of an observable $\hat{A}$ at time t can be always split into two terms:

$$A(t) \equiv \langle\Psi(t)|\hat{A}|\Psi(t)\rangle = \overline{A} + \delta A(t)\,, \tag{2.18}$$

in which the first term is the time average of $A(t)$: *Time average*

$$\overline{A} \equiv \lim_{t\to\infty} \frac{1}{t}\int_0^t dt'\, A(t') \tag{2.19}$$

and $\delta A(t)$ is the time fluctuating part, with (by definition) a vanishing time average.

An alternative standard decomposition of $A(t)$ proceeds by introducing the (many-body) eigenstates $|\alpha\rangle$ and eigenvalues E_α of $\hat{H}$ and uses Eq. (2.8) for representing $|\Psi(t)\rangle$:

$$\begin{aligned} A(t) &= \sum_{\alpha\beta} e^{-i(E_\alpha - E_\beta)\frac{t}{\hbar}} c_\alpha c_\beta^* A_{\beta\alpha} \\ &= \underbrace{\sum_{\alpha} |c_\alpha|^2 A_{\alpha\alpha}}_{\langle\hat{A}\rangle_D} + \sum_{\alpha\neq\beta} e^{-i(E_\alpha - E_\beta)\frac{t}{\hbar}} c_\alpha c_\beta^* A_{\beta\alpha}\,, \end{aligned} \tag{2.20}$$

where we have introduced the short-hand notation $A_{\beta\alpha} \equiv \langle\beta|\hat{A}|\alpha\rangle$, and, in the second line, we have split the summation into two terms: the first with only diagonal elements and the second with only off-diagonal ones. The first term is usually called diagonal average of $\hat{A}$ [2, 3, 8], and we denote it with $\langle\hat{A}\rangle_D \equiv \sum_\alpha |c_\alpha|^2 A_{\alpha\alpha}$. This average can be regarded as an ensemble average in which the density matrix is *Diagonal average*

$$\hat{\rho}_D = \sum_\alpha |c_\alpha|^2 |\alpha\rangle\langle\alpha|\,, \tag{2.21}$$

from which the name "diagonal" becomes clear.

To understand the relation between the two terms of Eq. (2.18) with the quantities in Eq. (2.20) let us consider a finite system in which there are no energy degeneracies

(i.e., $E_\alpha = E_\beta$ only if $\alpha = \beta$). In this case, for any $\alpha \neq \beta$ the spectral gap $|E_\alpha - E_\beta|$ is strictly positive and the time average of the second (off-diagonal) term of Eq. (2.20) is zero. Therefore, in absence of degeneracies the long-time average of $A(t)$ is:

$$\overline{A} = \sum_\alpha |c_\alpha|^2 A_{\alpha\alpha} = \langle \hat{A} \rangle_D \,, \tag{2.22}$$

and consequently the fluctuating part results solely from the off-diagonal terms:

$$\delta A(t) = \sum_{\alpha \neq \beta} e^{-i(E_\alpha - E_\beta)\frac{t}{\hbar}} c_\alpha c_\beta^* A_{\beta\alpha} \,. \tag{2.23}$$

Summarizing, for any finite system without degeneracies, the diagonal average coincides with the time average [2, 3, 8]. In principle, the non-degeneracy condition can, in some sense, be "enforced", at at the price, however, of knowing the initial state. [2]

Although not very often emphasized, Eq. (2.22) is correct for finite size systems where, in principle, the long-time dynamics suffers from inevitable "revivals" due to the finite gaps in the spectrum, as long as the integral is extended up to infinite times. An obvious issue, in considering the thermodynamical limit, is that in principle we should take it before computing, for instance, a $t \to \infty$ limit or a time-average. Since the summation over α and β in Eq. (2.20) is infinite and spectral gaps tend to close in the thermodynamics limit, it is not trivial to conclude that

$$\frac{1}{t}\int_0^t dt' \sum_{\alpha \neq \beta} e^{-i(E_\alpha - E_\beta)t'/\hbar} c_\alpha c_\beta^* A_{\beta\alpha} \overset{t\to\infty}{\longrightarrow} 0 \,, \tag{2.24}$$

i.e., that the time average of fluctuations actually vanishes for large t. This is not a purely mathematical difficulty: it might lead to physical consequences. When we increase the size of our system, the spectrum becomes more and more dense and the spectral gaps become smaller and smaller (while the energies E_α are extensive, i.e., they grow linearly with the size, the Hilbert space dimension grows exponentially with the size of the system). If Δ is the typical energy gap, the time t^* up to which we have to average $e^{i\Delta t}$ to see a vanishing contribution to the time average is proportional to $1/\Delta$. Such a time t^* becomes infinite in the thermodynamic limit, and this could lead to off-diagonal contributions to the time averages. In this case Eq. (2.22) might not be true. And even at finite, but large, sizes t^* could be impractically large to actually test the validity of Eq. (2.22). Obviously, the previous arguments are oversimplified, because in addition to the phases $e^{-i(E_\alpha - E_\beta)t/\hbar}$ there are weights, $c_\alpha c_\beta^* A_{\beta\alpha}$, that may cancel this effect.

Although often assumed and probably correct in many physical situations, the equality expressed by Eq. (2.22) between the diagonal average $\langle \hat{A} \rangle_D$ and the time average $\overline{A}$ is by no means guaranteed. An important physical example in which Eq. (2.22) appears to "fail" has been recently discussed in the literature [24]. The model considered was a one dimensional Bose-Hubbard Hamiltonian:

$$\hat{H}_{BH} = -J \sum_{j=1}^{L} \left(\hat{b}_j^\dagger \hat{b}_{j+1} + \text{h.c.} \right) + \frac{U}{2} \sum_{j=1}^{L} \hat{n}_j \left(\hat{n}_j - 1 \right) \,, \tag{2.25}$$

where $\hat{b}_j^\dagger$ and $\hat{b}_j$ creates and destroys, respectively, a boson on site j with periodic boundary conditions, i.e., $\hat{b}_{L+1} = \hat{b}_1$, and $\hat{n}_j \equiv \hat{b}_j^\dagger \hat{b}_j$ is the local density operator. The parameter J tunes the hopping between nearest-neighbor sites, and U is the local (Hubbard) repulsion between bosons. At equilibrium and for a filling of one-boson per site, the Hamiltonian $\hat{H}_{BH}$ is known to possess a transition for $(U/J)_c \approx 3.5$ [55] between a low-U superfluid phase and a large-U Mott-Hubbard localized phase. This

2 We can always perform a basis rotation such that just one eigenstate in the degenerate subset has $c_\alpha \neq 0$. This gives $c_\alpha c_\beta^* = 0$ if $\alpha \neq \beta$ whenever $E_\alpha = E_\beta$; with this new basis Eq. (2.22) is still valid.

Mott transition is accompanied by a change in the spectral gap statistics, from a Wigner-Dyson to a Poisson distribution [56, 57]. Let's now define $\hat{T}_r$ as the translation operator by r sites (r being an integer). The Hamiltonian is translationally invariant. Hence $\hat{H}_{BH}$ commutes with $\hat{T}_r$, and they possess a complete orthonormal set of common eigenstates, which we denote by $\{|\alpha\rangle\}$. The expectation value of the local density of bosons at site $j+r$ in the eigenstate $|\alpha\rangle$ is:

$$\langle\alpha|\hat{n}_{j+r}|\alpha\rangle = \langle\alpha|\hat{T}_r\hat{n}_j\hat{T}_r^\dagger|\alpha\rangle = \langle\alpha|\hat{n}_j|\alpha\rangle \,, \tag{2.26}$$

where we exploited the fact that $\hat{n}_{j+r} = \hat{T}_r\hat{n}_j\hat{T}_r^\dagger$ and that $\hat{T}_r$ is unitary and its eigenvalues have norm one. Therefore, the diagonal elements $\langle\alpha|\hat{n}_j|\alpha\rangle$ do not depend on the site j and consequently the diagonal average of $\hat{n}_j$ is translational invariant: $\langle\hat{n}_j\rangle_D = N_B/L$, where N_B is the total number of bosons in the initial state $|\Psi_0\rangle$. In Ref. [24] Carleo *et al.* studied the time evolution of the local density $n_j(t) = \langle\Psi(t)|\hat{n}_j|\Psi(t)\rangle$, starting from a wavefunction $|\Psi_0\rangle$ in which all the sites are alternatively either empty or doubly occupied $|\Psi_0\rangle = |2,0,2,0,\ldots,2,0\rangle$ (see the upper-right corner of Fig. 2.4). For any finite size Eq. (2.22) is valid and the infinite time average of $n_j(t)$ is translational invariant. But, depending on the value of (U/J) and upon increasing the size, the characteristic time τ_R needed for the system to relax towards the equilibrium uniform value of the density shows a remarkable crossover: when U/J exceeds a specific value $(U/J)_c$ (related to the equilibrium transition between the superfluid phase and the Mott-localized one) the value of τ_R has a sudden increase which becomes sharper and sharper as the system size increases, see Fig. 2.4. Hence, it appears that above $(U/J)_c$, the system has a tendency to remaining dynamically trapped into long-lived inhomogeneous configurations (see the inset of Fig. 2.4). This suggest that, in the thermodynamic limit, there might be some transition beyond which the off-diagonal terms, i.e. $t^{-1}\int_0^t dt' \sum_{\alpha\neq\beta} e^{-i(E_\alpha-E_\beta)t'/\hbar} c_\alpha c_\beta^* A_{\beta\alpha}$, give a finite contribution to the time average, leading to non-translational invariant time averages.

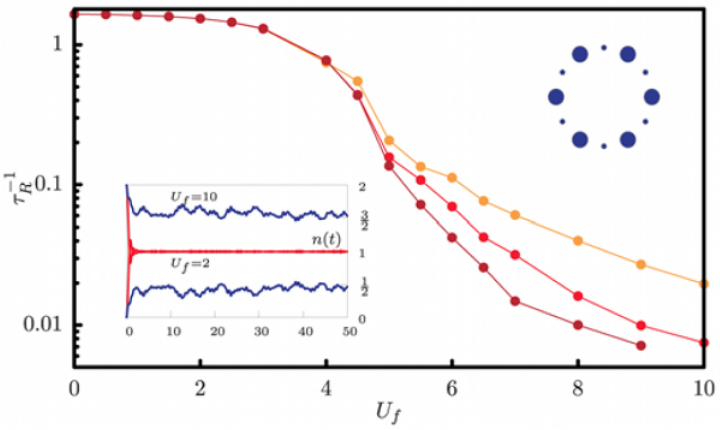

Figure 2.4.: Inverse of the relaxation time τ_R for the local density as a function of the after-quench interaction U/J. τ_R is the time for which $n_j(t)$ approaches its homogeneous value after a quantum quench with the Hamiltonian $\hat{H}_{BH}$, defined in Eq. (2.25). Darker points mark larger systems, respectively $L = 8, 10$ and 12 and the data are obtained with exact diagonalizations. In the upper-right corner there is a sketch of the initial state: alternatively empty and doubly occupied sites. In the inset the time evolution of $n_j(t)$ as a function of time for odd and even sites for to different values of U/J, one smaller than $(U/J)_c$ and one larger. Figure taken from Ref. [24].

2.3.2 Thermalization

The problem of thermalization focuses on the equivalence between time and ensemble averages. We say that $A(t)$ thermalizes with respect to a given ensemble if $\overline{A} = \langle\hat{A}\rangle$,

where $\langle \hat{A} \rangle$ denotes the ensemble average. For non-integrable Hamiltonians, one expects, generically, that the quantum microcanonical ensemble should apply, and the statement of thermalization for the observable $\hat{A}$ reads:

$$\overline{A} = \langle \hat{A} \rangle_{mc} \qquad \Longrightarrow \qquad \sum_{\alpha} |c_\alpha|^2 A_{\alpha\alpha} = \frac{1}{Z_{mc}} \sum_{\alpha | E_\alpha \in \Delta} A_{\alpha\alpha} \,, \tag{2.27}$$

where the left-hand side comes from Eq. (2.22) and the right-hand side from Eq. (2.11). Thermodynamical universality is evident in this equality: although the left-hand side depends on the details of the initial conditions through the set of coefficients c_α, the right-hand side depends only on the total energy, which is the same for many different initial conditions. A proposed explanation for the validity of Eq. (2.27) is the so-called "eigenstate thermalization hypothesis" (ETH) [6–8, 16]. The ETH, roughly speaking, says that the $A_{\alpha\alpha}$'s almost do not fluctuate at all between eigenstates that are close in energy. In this case, Eq. (2.27) holds without exception for all initial states that are "narrow in energy". For integrable models, like the ones we will consider in the following, Eq. (2.27) is not true and indeed the ETH is not fulfilled [16]. This is not surprising since the meaningful ensemble to use for these Hamiltonians is not the microcanonical one, but rather the GGE ensemble [19, 20]. It has been shown that GGE averages correctly predict the asymptotic momentum distribution functions for many systems [58], from Luttinger liquids [59, 60], free bosonic theories [61], integrable hard-core boson models [20], and Hubbard-like models [62, 63]. But the GGE does not always give a complete description of the asymptotic state of the system. For instance, GGE has been shown to fail when translational invariance is not present [28], or in the localized phase of some disordered Hamiltonians [64]. An important open question is therefore to understand under which general circumstances the GGE can be applied. In this thesis we will show that the applicability of the GGE depends crucially on the observable considered (one-body versus many-body) and on the localization properties of the final Hamiltonian. We will show that time averages of one-body operators are perfectly reproduced by GGE, while time averages of many-body operators might show clear deviations from the GGE when localization of the eigenstates is at play.

2.3.3 Relaxation

The problem of relaxation focuses on the long-time behavior of the fluctuating part of $A(t)$, i.e. $\delta A(t)$. We say that $A(t)$ relaxes if $\delta A(t) \to 0$ for $t \to \infty$.

When Eq. (2.22) applies, $\delta A(t)$ can be recast as a Fourier transform:

$$\delta A(t) = \int_{-\infty}^{+\infty} d\Omega \, e^{-i\Omega t/\hbar} F_A(\Omega) \,, \tag{2.28}$$

where

$$F_A(\Omega) \equiv \sum_{\alpha \neq \beta} c_\alpha c_\beta^* A_{\beta\alpha} \delta\left(\Omega - E_\alpha + E_\beta\right) \tag{2.29}$$

is a weighted joint (many-body) density of states. The behavior of the fluctuating part $\delta A(t)$, decaying to 0 for large t or remaining finite (with persistent oscillations) for $t \to \infty$ is strongly tied to the smoothness of $F_A(\Omega)$. For finite systems, $F_A(\Omega)$ is always a series of discrete Dirac's deltas, hence $\delta A(t)$ will never go to zero for $t \to \infty$, and "time revivals" will appear. If the many-body spectrum $\{E_\alpha\}$, in the thermodynamic limit, is a smooth continuum and the weights $c_\beta^* A_{\beta\alpha} c_\alpha$ make $F_A(\Omega)$ still integrable, then $\delta A(t)$ will decay to zero for large t, due to the destructive interference induced by the strongly oscillating phase $e^{-i\Omega t/\hbar}$ (see the Riemann-Lebesgue lemma in App. A). If, on the contrary, $\{E_\alpha\}$ has an important pure-point spectrum part, i.e., Dirac's delta functions associated to localized eigenstates, then one should expect persistent time fluctuations for certain operators. Indeed, in next chapters we will see that when the eigenstate of the final Hamiltonian are localized in space than the time fluctuations of

the local density, and many other operators, remain finite. When instead the eigenstates are extended (even if in presence of disorder in the final Hamiltonian) the same set of observables will relax.

Relaxation may seem, at a first sight, in conflict with the fact that we are dealing with closed quantum system, in which the time evolution is strictly unitary. The state $|\Psi(t)\rangle$ is "rotating" in the Hilbert space and a pure state will remain such as long as the time evolution is unitary. Indeed, we can always build operators which do not relax in time, and a trivial example of this is the operator $\hat{P}_{\alpha\beta} \equiv |\alpha\rangle\langle\beta| + |\beta\rangle\langle\alpha|$ for which $P_{\alpha\beta}(t) = 2\,\mathrm{Re}\left[c_\alpha c_\beta^* e^{-i(E_\alpha - E_\beta)t/\hbar}\right]$. These observations, however, do not exclude the possibility that, when measuring local observables, the system may appear to be perfectly relaxed, without the need for time averages. This is, in essence, the statement of the local relaxation conjecture [34, 35, 37]. For instance, for the Bose-Hubbard Hamiltonian in Eq. (2.25), it has been shown [35] that the local relaxation conjecture strictly holds when considering quenches in which $|\Psi_0\rangle$ has the odd sites occupied by exactly a single boson and all even sites empty $|\Psi_0\rangle = |1,0,1,0,\ldots,1,0\rangle$ (i.e., a half-filled state, at variance with the Carleo *et al.* [24] integer filling case considered before). Clear signatures of local relaxation are observed for the local densities and for correlations between nearest-neighbors sites, i.e., $\hat{b}_j^\dagger \hat{b}_{j+1}$ [35]. In Fig. 2.5 we report the results for the local density of bosons as a function of time for different values of the local interaction U (here $J = 1$). The limiting cases $U = 0$ and $U = \infty$ can be mapped onto free fermion models, and with exact calculations [35] one can show that the relaxation is proportional to the zeroth order Bessel function, which goes like $t^{-1/2}$. For intermediate values of U, the results of time-dependent density-matrix renormalization-group calculations (t-DMRG) show a similar relaxation with even faster power laws [35].

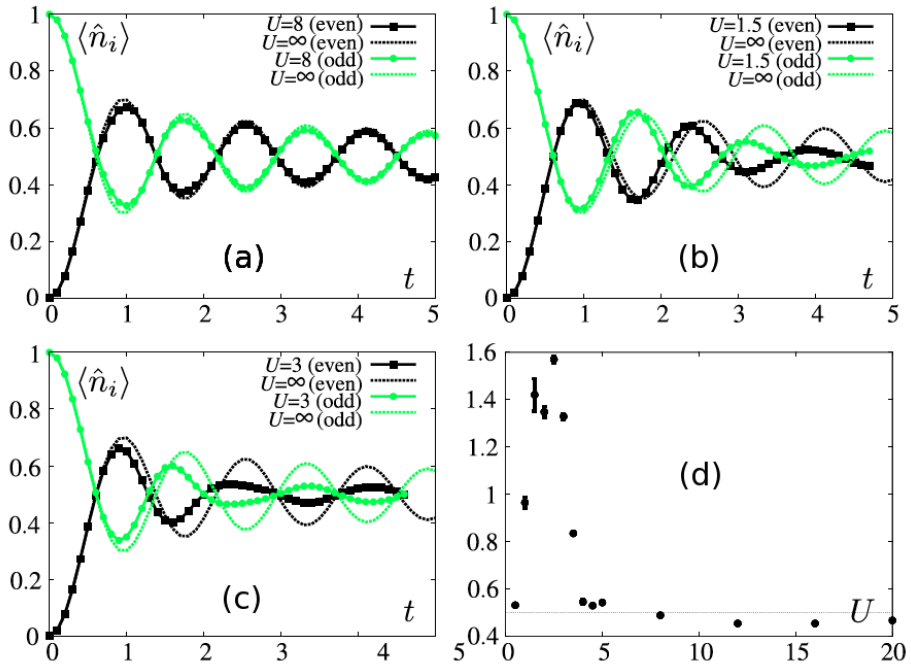

Figure 2.5.: (a), (b) and (c): Expectation value of the local density as a function of time for a quench in the Bose-Hubbard Hamiltonian $\hat{H}_{BH}$, Eq. (2.25), in which the initial state has odd sites occupied by one boson and even sites empty. Different panels correspond to different values of U (here $J = 1$). (d): Estimated exponent ν of the asymptotic power-law decay, $\delta n_j(t) \sim 1/t^\nu$, as a function of U. Figure taken from Ref. [35].

Intuitively, this process of local relaxation can be thought in the following way: during the time evolution, a wave-front emerges from each site, moving at finite speed and carrying information around; as time progresses more and more excitations pass

through a given site; the cumulative effect of these successive excitations results in an effective averaging process, and the information stored in one site becomes infinitely diluted across the lattice.

In this thesis we will see that, when considering solvable quadratic models, this traveling of "information" around the system is possible when the final Hamiltonian has extended eigenstates. On the contrary, when the final Hamiltonian possesses localized eigenstates, the local relaxation conjecture is in principle no longer valid, because the "information" remains trapped in the localized eigenstates.

2.4 QUENCHES WITH COLD ATOMS EXPERIMENTS

Ultracold atomic gases in optical lattices are one of the most important experimental quantum simulator for probing fundamental condensed matter physics [5] and out-of-equilibrium quantum quench dynamics [58]. In these experiments an artificial potential for atoms is built by the interference of laser beams, which creates a spatially periodic pattern. Indeed, the interference of two counter propagating laser beams forms an optical standing wave with halved period. With this device, by using many beams one can obtain one, two or three dimensional periodic potentials, see Fig. 2.6. When neutral atoms are cooled to very low temperatures, the optical potential may trap atoms via the Stark shift [65]. The structure of the potential and the resulting arrangement of trapped atoms resembles a crystal lattice. The power of these systems is that they are highly tunable: the geometry can be changed by making laser beams to interfere under different angles and frequencies and the depth of the potential can be changed by increasing or decreasing the intensity of the beams. Time-dependent Hamiltonians can also be investigated by just modulating in time the laser beams.

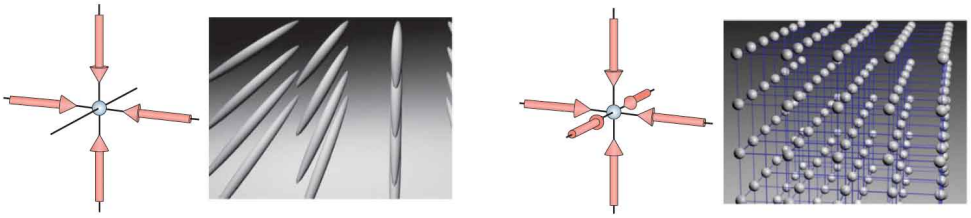

(a) square lattice **(b)** simple cubic lattice

Figure 2.6.: Optical lattices are obtained using the interference pattern of laser beams. One-dimensional lattices are obtained using two counter propagating laser beams, which build effectively an array of two-dimensional disks. Panel (a): two orthogonal optical standing waves create an array of one-dimensional tubes which resembles a two-dimensional square lattice. Panel (b): three orthogonal beans produce a three-dimensional simple cubic lattice in which each trapping site is like a confining harmonic oscillator potential. Figure taken from Ref. [66].

An example, strictly connected to the discussion at the end of the previous section, is the experiment done by Trotzky *et al.* [40]. They use a Bose-Einstein system of about 45×10^3 atoms of ^{87}Rb in an optical lattice, which can be modeled with the following Hamiltonian:

$$\hat{H}_{BH+H} = -J \sum_j \left(\hat{b}_j^\dagger \hat{b}_{j+1} + \text{h.c.} \right) + \frac{U}{2} \sum_j \hat{n}_j \left(\hat{n}_j - 1 \right) + \frac{K}{2} \sum_j j^2 \hat{n}_j \,, \tag{2.30}$$

where, as before, $\hat{b}_j^\dagger$ and $\hat{b}_j$ create and destroy, respectively, a boson at site j, and $\hat{n}_j \equiv \hat{b}_j^\dagger \hat{b}_j$ is the local density operator. This is exactly the Bose-Hubbard Hamiltonian introduced in Eq. (2.25) plus an external harmonic trap whose intensity is controlled by the parameter K. The system is initially prepared in a half-filled state such that only

even sites are occupied with one boson and no hopping coupling is present, namely $|\Psi_0\rangle = |0,1,0,1,\ldots,0,1\rangle$. A quench is then performed to a given set of positive parameters J, U and K and the system follow the dynamics with the Hamiltonian $\hat{H}_{BH+H}$. Finally, the tunneling between nearest sites is suppressed again, and a measurement is performed on the final state. Experimentally, one can measure local densities, local currents and momentum distributions. In Fig. 2.7 we report the results for the local densities in the odd sites. Damped oscillations which converge towards a steady value of $\approx 1/2$ are observed for a wide range of interactions. The authors have also performed t-DMRG calculations with parameters obtained from the respective set of experimental control parameters: For the time accessible in the t-DMRG simulations, they found a good agreement with the experimental results. Only for small U/J systematic deviations have been found that can be attributed to the breakdown of the nearest-neighbors tight-binding approximation for shallow lattice. Indeed, by introducing next-nearest neighbor hopping terms (dashed line in Fig. 2.7) the agreements between simulations and experiments seems to improve.

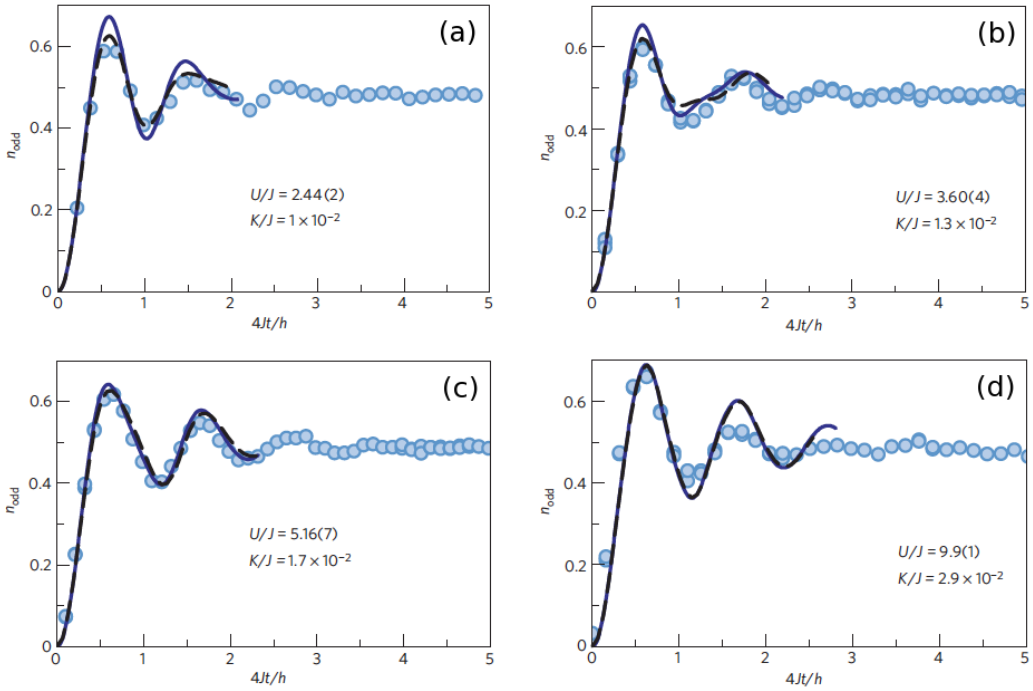

Figure 2.7.: Local density as a function of time, in quenches in which the initial state has a boson only on even sites. The points are experimental data obtained performing a quench in a cold atom system with ^{87}Rb atoms (see text for details). The system can be modeled with the Hamiltonian $\hat{H}_{BH+H}$ in Eq. (2.30) and the straight lines are data obtained performing t-DMRG calculations without free parameters (i.e., the values of U/J and K/J are fixed by the experiment). The dashed lines represent simulations including next-nearest neighbor hoppings. The experimental data, in agreement with numerical computations, show vanishing long-time fluctuations. Figure taken from Ref. [40].

This example shows the power of cold atom experiments for investigating quantum quenches and out-of-equilibrium physics. Many other examples can be found in the literature, see Ref. [4] for a review.

3 THE QUADRATIC FERMIONIC MODELS WE STUDY

In this chapter we introduce the systems for which we will characterize, in the next chapter, the out-of-equilibrium quantum dynamics following a sudden quench of the parameters. The systems we will consider are, or can be reduced to, quadratic fermionic models, which can be tackled essentially in an exact (albeit often only numerical) way. In particular, we will focus on the nature and main properties of their eigenvalues and eigenstates.

We start by briefly overviewing, in Sec. 3.1, the idea behind the well known tight-binding approximation, leading to the Anderson model. In Sec. 3.2 we introduce and describe a disordered tight-binding chain in which the hopping amplitude decreases with a power law of the distance between the sites. In Sec. 3.3 we illustrate the clean and disordered one-dimensional quantum Ising/XY models, and we show how to map these Hamiltonians onto quadratic fermion models, illustrating the differences with the previously introduced tight-binding models. Finally, in Sec. 3.4 we will show an experiment demonstrating Anderson localization in cold atomic systems.

3.1 TIGHT-BINDING APPROXIMATION AND THE ANDERSON MODEL

The general many-body problem for electrons in solids and crystals is a hard problem, even at equilibrium [67]. So hard that, even neglecting electron-phonon interaction, the problem of interacting electrons in a crystal lattice is still too complicated and essentially unsolved. In second quantization [54], the Hamiltonian of such a system can be written as:

$$\begin{aligned}\hat{H}_{el} \equiv &\sum_{\sigma} \int d\mathbf{x}\, \Psi^{\dagger}_{\sigma}(\mathbf{x}) \left[-\frac{\hbar^2}{2m}\nabla^2 + v(\mathbf{x}) \right] \Psi_{\sigma}(\mathbf{x}) \\ &+ \sum_{\sigma\sigma'} \frac{1}{2} \int d\mathbf{x}\, d\mathbf{x}'\, \Psi^{\dagger}_{\sigma'}(\mathbf{x}') \Psi^{\dagger}_{\sigma}(\mathbf{x}) \frac{e^2}{|\mathbf{x}-\mathbf{x}'|} \Psi_{\sigma}(\mathbf{x}) \Psi_{\sigma'}(\mathbf{x}') \,, \end{aligned} \tag{3.1}$$

where $\Psi^{\dagger}_{\sigma}(\mathbf{x})$ ($\Psi_{\sigma}(\mathbf{x})$) is the fermionic field operator which creates (destroys) an electron in position $\mathbf{x}$ with spin σ, $v(\mathbf{x})$ is the external potential felt by the electrons, and e and m are the electronic charge and mass. The field operators can be expanded in any one-particle basis set. A quite convenient choice, for our purposes, is the set of Wannier states [67]. These states, which will be denoted with $w_{n\mathbf{r}}(\mathbf{x})$, are as many as the bands (labeled by n) and the lattice sites (labeled by $\mathbf{r}$), and roughly localized around each lattice site $\mathbf{r}$. With this basis set, we can define the annihilation operator $\hat{c}_{n\mathbf{r}\sigma}$ and the creation $\hat{c}^{\dagger}_{n\mathbf{r}\sigma}$ such that:

$$\Psi_{\sigma}(\mathbf{x}) = \sum_{n,\mathbf{r}} w_{n\mathbf{r}}(\mathbf{x}) \hat{c}_{n\mathbf{r}\sigma} \qquad\qquad \Psi^{\dagger}_{\sigma}(\mathbf{x}) = \sum_{n,\mathbf{r}} w^{*}_{n\mathbf{r}}(\mathbf{x}) \hat{c}^{\dagger}_{n\mathbf{r}\sigma} \,, \tag{3.2}$$

where the summation is over all the bands n and lattice sites $\mathbf{r}$. For the orthonormality property of the Wannier states, it follows that $\hat{c}_{n\mathbf{r}\sigma}$ and $\hat{c}^{\dagger}_{n\mathbf{r}\sigma}$, which, respectively, de-

stroy and create an electron in the Wannier state $w_{n\mathbf{r}}(\mathbf{x})$, are good fermionic operators, namely they verify the anticommutation rules:

$$\begin{aligned}\left\{\hat{c}_{n\mathbf{r}\sigma}, \hat{c}^{\dagger}_{n'\mathbf{r}'\sigma'}\right\} &= \delta_{n\mathbf{r}\sigma,n'\mathbf{r}'\sigma'}\\ \left\{\hat{c}^{\dagger}_{n\mathbf{r}\sigma}, \hat{c}^{\dagger}_{n'\mathbf{r}'\sigma'}\right\} &= \left\{\hat{c}_{n\mathbf{r}\sigma}, \hat{c}_{n'\mathbf{r}'\sigma'}\right\} = 0\,.\end{aligned} \tag{3.3}$$

We could rewrite $\hat{H}_{el}$ using these new operators but to make progress we need further approximations. In many cases, one can single-out one important conduction band and disregard all the other bands. Denoting with $w_{\mathbf{r}}(\mathbf{x})$ the Wannier orbitals of that "important" band, and with $\hat{c}^{\dagger}_{\mathbf{r}\sigma}$, and $\hat{c}_{\mathbf{r}\sigma}$ the corresponding operators, the Hamiltonian $\hat{H}_{el}$ is approximated to:

$$\begin{aligned}\hat{H}^{1b.}_{el} &= \sum_{\sigma}\sum_{\mathbf{r}\mathbf{r}'} J_{\mathbf{r}'\mathbf{r}}\hat{c}^{\dagger}_{\mathbf{r}'\sigma}\hat{c}_{\mathbf{r}\sigma} + \frac{1}{2}\sum_{\sigma\sigma'}\sum_{\mathbf{r}_1\mathbf{r}_2\mathbf{r}'_1\mathbf{r}'_2} U_{\mathbf{r}_1\mathbf{r}_2\mathbf{r}'_1\mathbf{r}'_2}\hat{c}^{\dagger}_{\mathbf{r}'_2\sigma'}\hat{c}^{\dagger}_{\mathbf{r}'_1\sigma}\hat{c}_{\mathbf{r}_1\sigma}\hat{c}_{\mathbf{r}_2\sigma'}\\ J_{\mathbf{r}'\mathbf{r}} &\equiv \int d\mathbf{x}\, w^{*}_{\mathbf{r}'}(\mathbf{x})\left[-\frac{\hbar^2}{2m}\nabla^2 + v(\mathbf{x})\right] w_{\mathbf{r}}(\mathbf{x})\\ U_{\mathbf{r}_1\mathbf{r}_2\mathbf{r}'_1\mathbf{r}'_2} &\equiv \int d\mathbf{x}\, d\mathbf{x}'\, w^{*}_{\mathbf{r}'_2}(\mathbf{x}')w^{*}_{\mathbf{r}'_1}(\mathbf{x})\frac{e^2}{|\mathbf{x}-\mathbf{x}'|}w_{\mathbf{r}_1}(\mathbf{x})w_{\mathbf{r}_2}(\mathbf{x}')\,.\end{aligned} \tag{3.4}$$

The first term in $\hat{H}^{1b.}_{el}$ is "one-body" and describes the electrons hopping on the lattice. It originates from the kinetic energy and the external potential (first line of Eq. (3.1)). The second term is instead a "two-body" contribution and describes the Coulomb interaction between the electrons (second line of Eq. (3.1)). Using the operators $\hat{c}_{\mathbf{r}\sigma}$ and $\hat{c}^{\dagger}_{\mathbf{r}\sigma}$ we have now a discrete representation of the Hamiltonian: the continuous integration over $\mathbf{x}$ is now hidden in the parameters $J_{\mathbf{r}'\mathbf{r}}$ and $U_{\mathbf{r}_1\mathbf{r}_2\mathbf{r}'_1\mathbf{r}'_2}$. In addressing model systems, these parameters will be fixed without knowing much about the details of the underlying Hamiltonian (for instance, $v(\mathbf{x})$) or the form of the Wannier states $w_{\mathbf{r}}(\mathbf{x})$.

In this thesis we will focus on free tight-binding models in which the interaction term is set to zero, i.e., $U_{\mathbf{r}_1\mathbf{r}_2\mathbf{r}'_1\mathbf{r}'_2} = 0$. As we shall see, the one-body nature of the resulting Hamiltonian allows us to reduce the diagonalization of $\hat{H}$ in the many-body Hilbert space, whose dimension is of order 2^L where L is the number of lattice sites, to the simpler diagonalization of a single-particle Hamiltonian in the one-body Hilbert space of dimension L. Moreover, since the hopping term does mix spins, we can safely drop the spin index and consider spinless fermions. Even thought these approximations seems to be crude, this is a good starting point for understanding many quantum effects for both equilibrium and out-of-equilibrium systems.

Disorder-free tight-binding

Let us therefore start with the simplest case: a translationally invariant (homogeneous) one-dimensional chain with nearest-neighbor hopping. The lattice site $\mathbf{r}$ is now an integer which labels the sites, and $J_{\mathbf{r}'\mathbf{r}}$ is non-zero only for $\mathbf{r}' = \mathbf{r}$ and nearest-neighbor sites. The Hamiltonian reads:

$$\hat{H}_{hom} \equiv -J\sum_{j=1}^{L}\left[\hat{c}^{\dagger}_{j}\hat{c}_{j+1} + h.c.\right] + h\sum_{j=1}^{L}\hat{c}^{\dagger}_{j}\hat{c}_{j}\,, \tag{3.5}$$

where L is the chain size, J the hopping amplitude and h the on-site energy. We use periodic boundary conditions, namely $\hat{c}^{\dagger}_{L+1} = \hat{c}^{\dagger}_{1}$: the chain can be actually thought as a ring. The Hamiltonian is quadratic in $\hat{c}^{\dagger}_{j}$ and $\hat{c}_{j}$ and can be diagonalized by performing a canonical transformation of these operators. Since $\hat{H}_{hom}$ is translational invariant, the simplest (and indeed correct) choice is to use the operators which create and destroy a fermion in a plane wave with wave-number k:

$$\hat{c}_{k} \equiv \frac{1}{\sqrt{L}}\sum_{j=1}^{L} e^{-ikj}\hat{c}_{j} \qquad\qquad \hat{c}^{\dagger}_{k} \equiv \frac{1}{\sqrt{L}}\sum_{j=1}^{L} e^{ikj}\hat{c}^{\dagger}_{j}\,, \tag{3.6}$$

where $k = 2\pi n/L$ and $n = 0, \ldots, L-1$ (this restriction is obtained by inverting the previous canonical transformation, and imposing periodic boundary conditions). With these new fermionic operators the Hamiltonian is:

$$\hat{H}_{\text{hom}} = \sum_k \epsilon_k \hat{c}_k^\dagger \hat{c}_k \,, \tag{3.7}$$

where $\epsilon_k \equiv -2J\cos k + h$ are the single-particle energies. The many-body eigenstates are Slater determinants of the single-particle eigenstates. If $|0\rangle$ is the empty state, i.e., the state without fermions, all eigenstates are constructed by applying repeatedly to $|0\rangle$ creation operators $\hat{c}_k^\dagger$ with different values of k (we cannot have more than one fermion in the same single-particle state, by Pauli principle). The many-body wavefunction $|\alpha\rangle = \prod_k \hat{c}_k^{\dagger\, n_k^\alpha}|0\rangle$, where $n_k^\alpha = 0$ if the single particle state k is empty and $n_k^\alpha = 1$ if it is occupied, is an eigenstate of $\hat{H}_{\text{hom}}$ with energy $E_\alpha = \sum_k n_k^\alpha \epsilon_k$. The ground state (known as filled Fermi sea) is obtaining by creating fermions, $n_k^\alpha = 1$, on all k-modes with $\epsilon_k < 0$. Notice that by changing h and J the eigenstates of $\hat{H}_{\text{hom}}$ are always the same, only their energies change.

The homogeneous chain described by $\hat{H}_{\text{hom}}$ is an idealized system, and we expect that in any experimental situation there will be a certain amount of disorder, due to impurities and defects. There are many ways to take into account these effects, and a pioneering example is the model introduced by Anderson in 1958 [25]. In a one-dimensional exemplification, on top of $\hat{H}_{\text{hom}}$ we add disorder in the form of an external potential:

Anderson model

$$\hat{H}_A \equiv -J\sum_{j=1}^{L}\left(\hat{c}_j^\dagger \hat{c}_{j+1} + \text{h.c.}\right) + \sum_{j=1}^{L} h_j \hat{c}_j^\dagger \hat{c}_j \,, \tag{3.8}$$

where h_j is an on-site random potential, usually assumed to be uncorrelated and uniformly distributed in the range $[-W/2, W/2]$. In principle, disorder could also be added to the hopping term or we could use different uncorrelated random distributions, but the phase diagram and the key futures of $\hat{H}_A$ remain almost unchanged. This Hamiltonian is still quadratic, like $\hat{H}_{\text{hom}}$, but cannot be analytically diagonalized by switching to (Bloch) plane waves, due to the random on-site energies h_j. Obviously, we can always obtain the correct single-particle modes $u_{j\mu}$, with associated energy ϵ_μ, numerically. In terms of the new fermionic operators:

$$\hat{c}_\mu \equiv \sum_{j=1}^{L} u_{j\mu}^* \hat{c}_j \qquad\qquad \hat{c}_\mu^\dagger \equiv \sum_{j=1}^{L} u_{j\mu} \hat{c}_j^\dagger \,, \tag{3.9}$$

the Hamiltonian is diagonalized:

$$\hat{H}_A = \sum_{\mu=1}^{L} \epsilon_\mu \hat{c}_\mu^\dagger \hat{c}_\mu \,. \tag{3.10}$$

The explicit first-quantization equations for the wavefunctions $u_{j\mu}$ are easy to obtain:

$$-Ju_{j-1\mu} - Ju_{j+1\mu} + h_j u_{j\mu} = \epsilon_\mu u_{j\mu} \qquad \forall j = 1, \ldots, L \,. \tag{3.11}$$

This is evidently an eigenvalue problem:

$$H_A \mathbf{u}_\mu = \epsilon_\mu \mathbf{u}_\mu \,, \tag{3.12}$$

where $\mathbf{u}_\mu$ is the vector of components $u_{j\mu}$ and H_A is the following $L \times L$ matrix:

$$H_A = \begin{pmatrix} h_1 & -J & 0 & \ldots & -J \\ -J & h_2 & -J & \ldots & 0 \\ 0 & -J & h_3 & \ldots & 0 \\ \vdots & \vdots & \vdots & \ddots & \vdots \\ -J & 0 & \ldots & -J & h_L \end{pmatrix} . \tag{3.13}$$

Therefore, given a realization of the on-site energies h_j's we can compute eigenvalues ϵ_μ and the associated eigenvectors $u_{j\mu}$ by numerically diagonalizing the $L \times L$ matrix H_A. Since all matrix elements are real, we can always take all the $u_{j\mu}$ to be real. [1] Once the L eigenvalues and eigenstates have been obtained, we can build the many-body eigenstates using the same procedure described for the Hamiltonian $\hat{H}_{hom}$.

It has been mathematically proven [68] that, in one dimension and in presence of even the smallest disorder, all the single-particle eigenstates of $\hat{H}_A$ are exponentially localized around a lattice site, i.e., $|u_{j\mu}|^2 \sim e^{-2|j-\bar{j}_\mu|/\xi}$, where $\bar{j}_\mu$ is the site over which μ is localized and ξ takes the name of localization length. An example of a localized state, obtained by diagonalizing numerically $\hat{H}_A$, is shown in Fig. 3.1. The existence of localized states is simple to understand in the limit of very strong disorder, by perturbation theory arguments [51]. The zeroth-order description, for strong disorder, amounts to neglecting the kinetic energy: the eigenstates are orbitals localized at each site. Perturbation theory in the hopping ($\hat{H}_{hom}$ is actually the perturbation) generates a mixture between different orbitals. However such mixture does not produce an extended state built of a linear combinations of infinitely many localized orbitals. Indeed orbitals that are nearby in space, so that their wavefunctions overlap significantly, have in general very different energies, so that their admixture is small because of the large energy denominator. On the other hand, states that are nearly degenerate, are in general very far apart in space, so that their overlap is exponentially small. Thus, one would argue that, in the strongly disordered limit, wavefunctions must be exponentially localized. In the low disorder limit, an argument like this is difficult to make, as the one-dimensional nature of the lattice and the nearest-neighbor geometry turn out to be crucial.

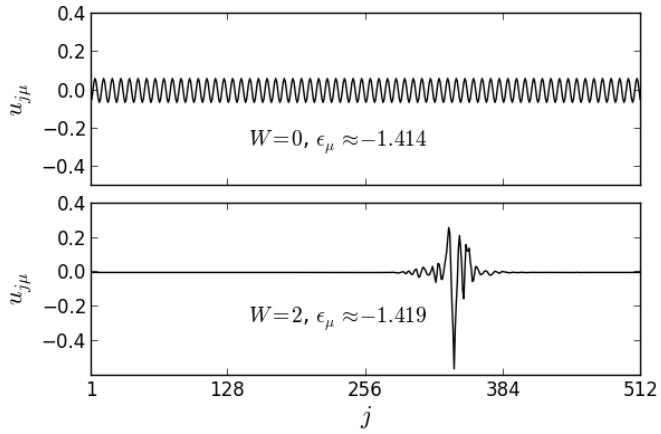

Figure 3.1.: Single-particle eigenfunctions obtained diagonalizing $\hat{H}_A$. In the upper panel we use $W = 0$ (in this case $\hat{H}_A$ is equal to $\hat{H}_{hom}$ with $h = 0$) while in the lower one $W = 2$. The system size is $L = 512$ and we have chosen two eigenstates with similar energies.

Indeed, the properties of disordered systems depend crucially on the dimensionality. In three dimensions, the disorder can drive a true metal-to-insulator transition. In fact, in the presence of disorder, localization occurs first for states with energies in the regions where the density of states is low [69]; indeed, the density of states acquires tails of exponentially localized states [70]. If the disorder amplitude is not so large as to localize all states, then two mobility edges separate localized states, in the band tails, from extended states in the band center (see Fig. 3.2), and a metal-insulator transition can be triggered by sweeping the chemical potential across the mobility edge. The chemical potential can be moved across the mobility edge by doping the system;

1 For $W = 0$ we actually get $\hat{H}_A = \hat{H}_{hom}$ and the real eigenfunctions are given by a linear combination of the two degenerate plane-waves with opposite k defined in Eq. (3.6).

alternatively the metal-insulator transition can be achieved by increasing the density of impurities/defects. [2]

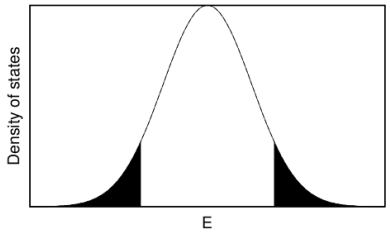

Figure 3.2.: Density of states of a three-dimensional system with a disorder smaller than the critical value. The black filled area is the portion of the spectrum whose states are localized. The energies which separate extended and localized states are called mobility edges.

A good way to detect numerically the localization of single-particle wavefunctions on a lattice consists in computing the inverse participation ratio (IPR):

Inverse participation ratio

$$\mathrm{IPR}_\mu \equiv \sum_j |u_{j\mu}|^4 \ . \tag{3.14}$$

The IPR_μ lies in the range $]0,1]$, since $\sum_j |u_{j\mu}|^2 = 1$. For a wavefunction completely localized at one site, the wavefunction $u_{j\mu}$ is a Kronecker's delta and consequently the IPR is one. On the contrary, for a plain wave $|u_{jk}| = |e^{ikj}/\sqrt{L}| = 1/\sqrt{L}$ and thus

$$\mathrm{IPR}_k = \sum_j \frac{1}{L^2} = \frac{1}{L} \ , \tag{3.15}$$

which goes to zero for $L \to \infty$. Similarly, if $\mathrm{IPR} \to 0$ for $L \to \infty$ the associated wavefunction is said to be extended, while if the IPR remains finite for $L \to \infty$ the wavefunction is said to be localized. For any eigenstate of $\hat{H}_A$, at any finite value W the IPR_μ saturates to a finite value for $L \to \infty$, since all the eigenstates are localized. An example is shown in Fig. 3.3, where we plot the IPR_μ averaged over the disorder as a function of L.

The IPR strongly depends on the basis set on which we expand the eigenstates. If we expand the eigenstates over the basis of plane-waves, see definitions in Eq. (3.6), the wavefunctions are the discrete Fourier transform of $u_{j\mu}$:

$$u_{k\mu} \equiv \frac{1}{\sqrt{L}} \sum_{j=1}^{L} e^{-ikj} u_{j\mu} \ , \tag{3.16}$$

where $k = 2\pi n/L$, with $n = 0, \ldots, L-1$. The associated IPR therefore reads:

$$\mathrm{IPR}^k_\mu \equiv \sum_k |u_{k\mu}|^4 \ , \tag{3.17}$$

which is evidently different from the spatial IPR defined in Eq (3.14). For instance, if we consider a pure plane-wave we have $\mathrm{IPR} = 1/L$ and $\mathrm{IPR}^k = 1$ (the Fourier transform of a plane-wave is a Kronecker's delta). Therefore, quite trivially, the eigenstates of $\hat{H}_{\mathrm{hom}}$ are extended in real space and localized in reciprocal space. In Fig. 3.3 we see that for the eigenstates of $\hat{H}_A$ the behavior is opposite: localized in real space and extended in reciprocal space. One would expect that an extended real-space wavefunction should always look localized in momentum space, i.e., composed of a small number of k waves.

2 It turns out that two dimensions is the lower critical dimension for a metal-insulator transition, as conjectured by Abrahams *et al.* on the basis of a scaling ansatz [71]. Hence, also in two dimensions, all the single-particle wavefunctions are localized by an arbitrarily weak disorder.

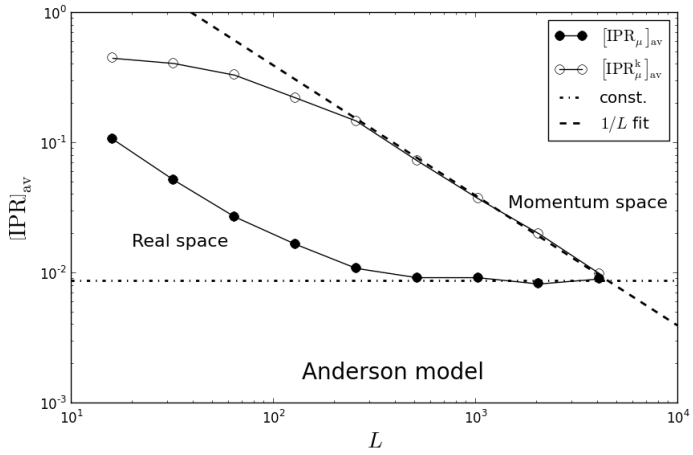

Figure 3.3.: Plot of the mean real-space IPR (IPR_μ) and reciprocal space IPR (IPR^k_μ) as a function of size for the eigenstates of $\hat{H}_A$. The dashed line is a $1/L$ fit which describe well the behavior at large L for the IPR^k_μ. This plot shows that in real space the eigenstates of $\hat{H}_A$ are localized while in reciprocal space they are delocalized. The mean is computed diagonalizing numerically 50 realizations and selecting the eigenstate in the middle of the spectrum. The errorbars are smaller than the markers.

This expectation, quite reasonable for ordinary extended states of non-disordered systems, is not correct, in general, in the presence of disorder. We will see an example of this curious fact in the next section.

Let us now look at the spectral properties of $\hat{H}_A$, and let us consider the single-particle density of states:

$$\rho(\epsilon) \equiv \frac{1}{L}\sum_\mu \delta(\epsilon - \epsilon_\mu)\,, \tag{3.18}$$

where $\delta(x)$ is the Dirac delta function. For $W = 0$ we can compute it analytically, $\rho(\epsilon) = 1/(\pi\sqrt{4-\epsilon^2})$ (shown in Fig. 3.4a), and it shows two van Hove singularities [67] of the kind $\rho(\epsilon) \sim 1/\sqrt{\pm 2 - \epsilon}$, typical of one-dimensional systems. As we see in Fig. 3.4a, when we add disorder these singularities are washed out and the density of states is much smoother. Note that we did not average over the disorder and the $\rho(\epsilon)$ is computed using a single realization. The quantity which changes completely look, when localization is at play, is the local density of states:

$$\rho_j(\epsilon) \equiv \sum_\mu |u_{j\mu}|^2 \delta(\epsilon - \epsilon_\mu)\,, \tag{3.19}$$

where $u_{j\mu}$ are the single-particle eigenfunctions. For $W = 0$ the eigenstates are plane-waves and $\rho_j(\epsilon) = \rho(\epsilon)$, which means that the spectrum is equally distributed on any lattice site. This is not true when localization is at play. In this case, see 3.4b, the local density is much more structured with spikes arranged along the spectrum. Indeed since the eigenstates are localized, in the summation of Eq. (3.19), only the energies whose eigenstates are localized in j contribute to $\rho_j(\epsilon)$ making it a highly discontinuous function. This is, essentially, what one refers to as having a pure-point spectrum. Using the normalization property of the eigenstates we have that the site average of the local density of states is equal to the density of states: $\rho(\epsilon) = \sum_j \rho_j(\epsilon)/L$. This clearly shows how the site average is able to wash out the irregularities of $\rho_j(\epsilon)$, making $\rho(\epsilon)$ a smooth function of ϵ.

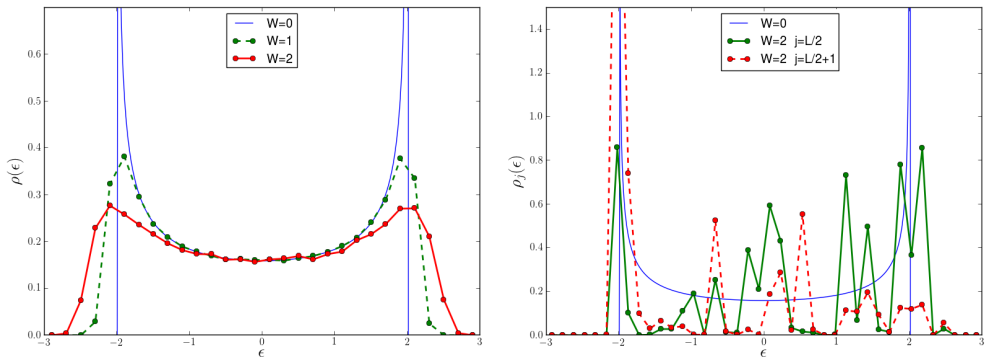

(a) Density of states **(b)** Local density of states

Figure 3.4.: Single-particle density of states for a single realization of $\hat{H}_A$, in panel (a), and single-particle local density of states $\rho_j(\epsilon)$, in panel (b). In presence of disorder the pure-point property of the spectrum emerges. The line is the density of states in the thermodynamic limit for $W = 0$ obtained using its analytical expression. For the $W \neq 0$ data we have diagonalized a single realization of $\hat{H}_A$ with $L = 16384$.

3.2 LONG-RANGE HOPPING HAMILTONIAN

In the previous section we have discussed the Anderson model and we have seen that for $\hat{H}_A$, in one dimension and with short-range hoppings, any amount of disorder is able to localize all the eigenstates. In this section we shall see that this picture changes drastically when one considers long-range hoppings: even in one-dimensional system, allowing for long-range hoppings can lead to an Anderson transition at a finite disorder.

Let us consider a disordered chain with spinless fermions in which the hopping integrals connects sites at any distance, as follows:

$$\hat{H}_{lrh} \equiv \sum_{j_1,j_2=1}^{L} J_{j_1 j_2} \left(\hat{c}^\dagger_{j_1} \hat{c}_{j_2} + \text{h.c.} \right) , \tag{3.20}$$

where $J_{j_1 j_2}$ is the (real) hopping integral between sites j_1 and j_2. We will take the $J_{j_1 j_2}$'s to be random and long-ranged, with a Gaussian distribution of zero mean, $\langle J_{j_1 j_2} \rangle = 0$, and variance given by [72]:

$$\langle J^2_{j_1 j_2} \rangle = \frac{1}{1 + \left(\frac{|j_1 - j_2|}{\beta} \right)^{2\alpha}} . \tag{3.21}$$

Here α is a real positive parameter setting how fast the hoppings' variance decays with distance. For this Hamiltonian we use open boundary condition [3], i.e., null wavefunctions outside the chain. Like $\hat{H}_A$, this Hamiltonian is still quadratic in the fermionic operators $\hat{c}^\dagger_j$ and $\hat{c}_j$. We can therefore define a new set of fermionic operators $\hat{c}_\mu$ and $\hat{c}^\dagger_\mu$ (see the definitions in Eqs. (3.9)) such that the Hamiltonian reads:

$$\hat{H}_{lrh} = \sum_{\mu} \epsilon_\mu \hat{c}^\dagger_\mu \hat{c}_\mu , \tag{3.22}$$

where the ϵ_μ are the single-particle energies. To get this canonical transformation we follow the same steps performed with $\hat{H}_A$, arriving at the following set of equations:

$$\sum_{l=1}^{L} \left(J_{lj} + J_{jl} \right) u_{l\mu} = \epsilon_\mu u_{j\mu} \qquad \forall j = 1, \ldots, L , \tag{3.23}$$

3 Here the periodic boundary conditions would have the following issue: given a site j, the sites $j-1$ and $j+1$ are the nearest neighbors, but they are also the "virtual" sites at distance $nL+1$ from j, where n is any integer.

where $u_{j\mu}$ are the wavefunctions of the single-particle eigenstates. This is again an eigenvalue problem:

$$H_{lrh}\mathbf{u}_\mu = \epsilon_\mu \mathbf{u}_\mu \,, \tag{3.24}$$

where $\mathbf{u}_\mu$ is the vector of components $u_{j\mu}$, and H_{lrh} is the following $L \times L$ matrix:

$$H_{lrh} = \begin{pmatrix} 2J_{11} & J_{12}+J_{21} & \dots & J_{1L}+J_{L1} \\ J_{21}+J_{12} & 2J_{22} & \dots & J_{2L}+J_{L2} \\ \vdots & \vdots & \ddots & \vdots \\ J_{L1}+J_{1L} & J_{L2}+J_{2L} & \dots & 2J_{LL} \end{pmatrix} . \tag{3.25}$$

Given the realization of the hoppings $J_{j_1 j_2}$ we can therefore compute numerically eigenvalues and eigenvectors by diagonalizing H_{lrh}. These matrices belong to the set of power-law banded random matrices, the name coming from the fact that each "band" at a given distance from the main diagonal follows the same statistics with a variance that decreases as a power law.

The peculiarity of this long-range-hopping model is that, regardless of the value of β (which hereafter is fixed to 1), it has an Anderson transition from (metallic) extended eigenstates, for $\alpha < 1$, to (insulating) localized eigenstates for $\alpha > 1$ [72–74]. At variance with $\hat{H}_A$, for $\alpha > 1$, the wavefunctions are localized with integrable power-law tails of the form $|u_{j\mu}|^2 \sim |j - \bar{j}_\mu|^{-2\alpha}$, where $\bar{j}_\mu$ is the localization site [72, 75]. At the critical value $\alpha = 1$ the system exhibits multifractality and spectral statistics intermediate between the Wigner-Dyson and Poisson statistics [72–74]. Physically, this transition is due to the fact that, for small α, long-range hoppings are capable of overcoming the localization due to disorder.

To catch the Anderson transition we can compute numerically the IPR (see Eq. (3.14)). In Fig. 3.5 there is a plot of the mean IPR_μ as a function of L. For $\alpha = 1/2$, we have $IPR_\mu \sim 1/L$ for large sizes (i.e., extended eigenstates), while for $\alpha = 2$, we have a finite IPR for $L \to \infty$ (i.e., localized eigenstates). We can in principle compute the mean IPR_μ as a function of L for many α's, and for each of them fit the data with a power law $IPR_\mu = A/L^\nu$. If ν is 1 the eigenstates are extended, while if ν is 0 the eigenstates are localized. In Fig. 3.6 we report ν as a function of α as computed in Ref. [72] for a similar Hamiltonian: the data show a crossover from the behavior typical of extended states ($\nu = 1$) to that typical of localized states ($\nu = 0$), centered approximately at the critical point $\alpha = 1$. The deviations from a sharp transition are due to finite-size effects, which are quite pronounced in this model due to the long-range nature of the off-diagonal coupling.

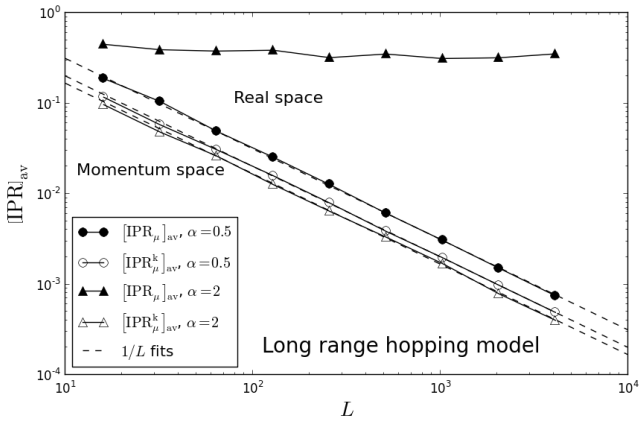

Figure 3.5.: Mean IPR_μ and IPR^k_μ as a function of size for the eigenstates of $\hat{H}_{lrh}$. The mean is computed taking the eigenstate in the middle of the spectrum and averaging over 50 realizations of $\hat{H}_{lrh}$. The errorbars are smaller than the markers.

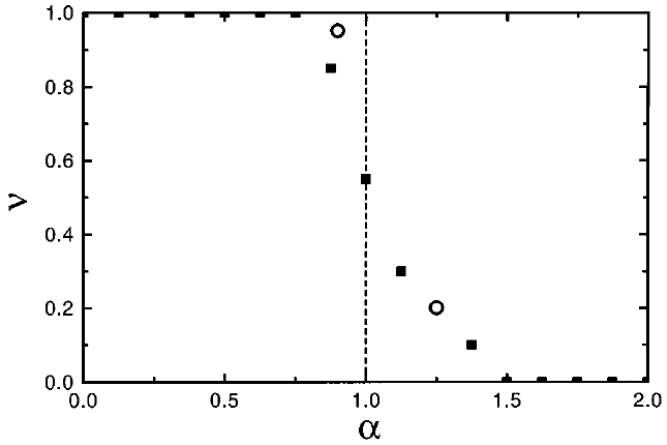

Figure 3.6.: Index ν characterizing the dependence of the inverse participation ratio IPR on the system size L via IPR $\sim 1/L^{\nu}$, as a function of α. Points refer to the best-fit values obtained from sizes between $L = 100$ and $L = 1000$ (squares) or $L = 2400$ (circles). The dashed line is the theoretical prediction for the transition from $\nu = 1$ (extended eigenstates), at small α, to $\nu = 0$, at large α (localized eigenstates). Figure taken from Ref. [72], where they use a slightly modified matrix H for the numerical diagonalization: $H_{ij} = G_{ij}\, a(|i-j|)$, where G comes from the Gaussian orthogonal ensemble and $a(r) = r^{-\alpha}$ for $r > 1$ and $a(r) = 1$ for $r \leqslant 1$.

As shown in Fig. 3.5 another interesting future of this Hamiltonian is that for $\alpha < 1$ the eigenstates are extended both in real space and reciprocal space, i.e. both IPR_{μ} and IPR^{k}_{μ} go to zero for large L. Therefore for the extended eigenstates of $\hat{H}_{\mathrm{lrh}}$ the usual link "extended in real space" - "localized in reciprocal space" is not valid. A simple example demonstrates the crucial role played by disorder on the destruction of this correspondence. Consider a toy real-space extended wavefunction with $u_j = w_j/\sqrt{L}$ where $w_j = \pm 1$ is a random sign on every site. Without w_j, the momentum space function $u_k \equiv \sum_j u_j e^{-ikj}/\sqrt{L}$ would be localized, with a peak at $k = 0$. When w_j is accounted for, $|u_k|^2$ becomes extremely irregular but extended over all k points, see Fig. 3.7. In the presence of disorder, therefore, the fact of being extended in real-space does not imply a sharply defined momentum.

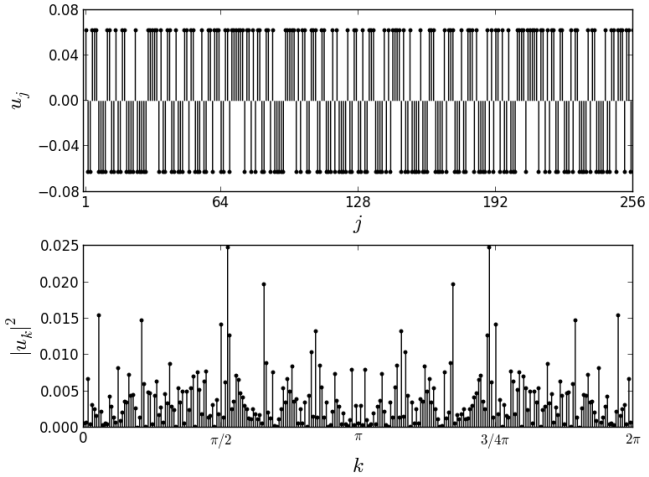

Figure 3.7.: Wavefunction expressed with two different basis sets: in real space (u_j) and reciprocal space (u_k). The wavefunction is $u_j = w_j/\sqrt{L}$ where $w_j = \pm 1$ is a random sign on every site, and in reciprocal space $u_k = \sum w_j e^{-ikj}/\sqrt{L}$. These states are extended in both the basis sets.

3.3 ISING/XY CHAIN

In this section we discuss one-dimensional chains in which at each lattice site there is a spin-1/2 which interacts with the neighboring spins in the usual Ising way. We will see that, with an appropriate transformation, this Hamiltonian can be mapped onto a quadratic fermionic chain. We will overview both disordered and clean chains and show that, also for this set of Hamiltonians, localization appears in presence of disorder.

The Hamiltonian of a disordered Ising/XY chain in a transverse field [76] reads:

$$\hat{H}_{XY} \equiv -\sum_{j=1}^{L} \left(J_j^x \hat{\sigma}_j^x \hat{\sigma}_{j+1}^x + J_j^y \hat{\sigma}_j^y \hat{\sigma}_{j+1}^y \right) - \sum_{j=1}^{L} h_j \hat{\sigma}_i^z \,, \tag{3.26}$$

where L is the chain size, $\hat{\sigma}_j^\mu$ ($\mu = x, y, z$) are spin-1/2 Pauli matrices for the j site, and periodic boundary conditions are assumed, i.e., $\hat{\sigma}_{L+1}^\mu = \hat{\sigma}_1^\mu$. J_j^x, J_j^y and h_j are real and describe, respectively, the nearest-neighbor spin couplings and the transverse magnetic field. By means of the Jordan-Wigner transformation [77], the one-dimensional Ising model can be reduced to a free-fermion model. One first writes the spin operators in terms of hard-core bosons $\hat{a}_j$ and $\hat{a}_j^\dagger$ in a representation that maps the state $|\sigma_z^j = +1\rangle \to \hat{a}_j^\dagger |0\rangle_j$ and $|\sigma_z^j = -1\rangle \to |0\rangle_j$ (where $|0\rangle_j$ is the state without bosons at site j), with the hard-core constraint $\left(\hat{a}_j^\dagger\right)^2 |0\rangle_j = 0$. In term of these operator the spin components for each site are:

$$\hat{\sigma}_j^z = 2\hat{a}_j^\dagger \hat{a}_j - 1 \qquad \hat{\sigma}_j^x = \hat{a}_j + \hat{a}_j^\dagger \qquad \hat{\sigma}_j^y = -i\left(\hat{a}_j^\dagger - \hat{a}_j\right) \,. \tag{3.27}$$

Then the hard-core boson operators $\hat{a}_j$ are re-expressed in terms of spinless fermions operators $\hat{c}_j$: $\hat{a}_j = e^{i\pi \sum_{l<j} \hat{c}_l^\dagger \hat{c}_l} \hat{c}_j$. In terms of these fermionic operators $\hat{H}_{XY}$ reads:

$$\hat{H}_{XY} = -\sum_{j=1}^{L} J_j \left(\hat{c}_j^\dagger \hat{c}_{j+1} + \gamma \hat{c}_j^\dagger \hat{c}_{j+1}^\dagger + \text{h.c.} \right) - \sum_{j=1}^{L} h_j (2\hat{c}_j^\dagger \hat{c}_j - 1) \,, \tag{3.28}$$

where $J_j = J_j^x + J_j^y$, and we have introduced the (uniform) anisotropy parameter γ in terms of which $J_j^x = J_j(1+\gamma)/2$ and $J_j^y = J_j(1-\gamma)/2$. The periodic boundary conditions for spins give rise to two different boundary conditions for fermions: periodic boundary conditions $\hat{c}_{L+1} = \hat{c}_1$ when the number of fermions is odd, anti-periodic boundary conditions $\hat{c}_{L+1} = -\hat{c}_1$ when the number of fermions is even [77]. Notice that total number of fermions $\hat{N}_F = \sum_i \hat{c}_i^\dagger \hat{c}_i$ is not conserved by $\hat{H}_{XY}$, but its parity is conserved because fermions are created (and destroyed) in pairs, like in a BCS model: $(-1)^{N_F}$ is therefore a constant of motion with value $+1$ or -1.

The model in Eq. (3.28) can can be diagonalized through a Bogoliubov rotation [77–79], by introducing the new fermionic operators $\hat{\gamma}_\mu$ and $\hat{\gamma}_\mu^\dagger$:

$$\hat{\gamma}_\mu \equiv \sum_{j=1}^{L} \left(u_{j\mu}^* \hat{c}_j + v_{j\mu}^* \hat{c}_j^\dagger \right) \qquad \hat{\gamma}_\mu^\dagger \equiv \sum_{j=1}^{L} \left(v_{j\mu} \hat{c}_j + u_{j\mu} \hat{c}_j^\dagger \right) \,. \tag{3.29}$$

These new operators are still fermionic and therefore u and v are $L \times L$ matrices which fulfill the relations $u^\dagger u + v^\dagger v = \mathbb{1}$, $u^\dagger v^* + v^\dagger u^* = 0$ (where $\mathbb{1}$ is the identity and 0 the matrix with all zero elements). Notice that, differently from $\hat{H}_A$ and $\hat{H}_{lrh}$, the modes are now linear combinations of particles and holes. The inverse transformation is:

$$\hat{c}_j = \sum_{\mu=1}^{L} \left(u_{j\mu} \hat{\gamma}_\mu + v_{j\mu}^* \hat{\gamma}_\mu^\dagger \right) \qquad \hat{c}_j^\dagger = \sum_{\mu=1}^{L} \left(v_{j\mu} \hat{\gamma}_\mu + u_{j\mu}^* \hat{\gamma}_\mu^\dagger \right) \,. \tag{3.30}$$

Plugging these relations into Eq. (3.28) and imposing the diagonalization we find a set of 2L Bogoliubov-de Gennes equations. These equations can be written compactly by defining the L-dimensional vectors $\mathbf{u}_\mu$ and $\mathbf{v}_\mu$ whose components are $u_{j\mu}$ and $v_{j\mu}$:

$$\begin{aligned} A\mathbf{u}_\mu + B\mathbf{v}_\mu &= \epsilon_\mu \mathbf{u}_\mu \\ -B\mathbf{u}_\mu - A\mathbf{v}_\mu &= \epsilon_\mu \mathbf{v}_\mu \,, \end{aligned} \tag{3.31}$$

where ϵ_μ is the energy of the mode μ and A and B are real $L \times L$ matrices whose non-zero elements are given by $A_{jj} = -h_j$, $A_{jj+1} = A_{j+1j} = -J_j/2$, $B_{jj+1} = -B_{j+1j} = -\gamma J_j/2$, and, due to the boundary conditions, the additional matrix elements $A_{L1} = A_{1L} = (-1)^{N_F}(J_L/2)$, and $B_{L1} = -B_{1L} = (-1)^{N_F}\gamma(J_L/2)$. These equations can be written as an eigenvalue problem:

$$\begin{pmatrix} A & B \\ -B & -A \end{pmatrix} \begin{pmatrix} \mathbf{u}_\mu \\ \mathbf{v}_\mu \end{pmatrix} = \epsilon_\mu \begin{pmatrix} \mathbf{u}_\mu \\ \mathbf{v}_\mu \end{pmatrix} , \tag{3.32}$$

where the matrix, that can be diagonalized numerically, is $2L \times 2L$ [78–80]. The 2L modes are not independent because of the particle-hole symmetry, which is present even in the general disordered case [78, 79]. Indeed this symmetry implies that for every positive eigenvalue $\epsilon_\mu > 0$, with associated eigenvector $(\mathbf{u}_\mu, \mathbf{v}_\mu)$, there is a negative eigenvalue $-\epsilon_\mu$ associated to $(\mathbf{v}_\mu^*, \mathbf{u}_\mu^*)$. Redefining with ϵ_μ the positive eigenvalues (μ now goes from 1 to L), the Hamiltonian $\hat{H}_{XY}$ can be written as:

$$\hat{H}_{XY} = \sum_{\mu=1}^{L} \left(\epsilon_\mu \hat{\gamma}_\mu^\dagger \hat{\gamma}_\mu - \epsilon_\mu \hat{\gamma}_\mu \hat{\gamma}_\mu^\dagger \right) = \sum_{\mu=1}^{L} 2\epsilon_\mu \left(\hat{\gamma}_\mu^\dagger \hat{\gamma}_\mu - \frac{1}{2} \right) . \tag{3.33}$$

With these notations the ground state of $\hat{H}_{XY}$ is the Bogoliubov vacuum state $|\emptyset\rangle$ annihilated by all the $\hat{\gamma}_\mu$'s, i.e. $\hat{\gamma}_\mu|\emptyset\rangle = 0$ for $\mu = 1, \ldots, L$, and its energy is $E_0 = -\sum_{\mu=1}^{L} \epsilon_\mu$. The many-body exited eigenstates are obtained by applying $\hat{\gamma}_\mu^\dagger$ to the ground state and their energy will be $E_0 + 2\sum_\mu n_\mu \epsilon_\mu$, where $n_\mu = 1$ ($n_\mu = 0$) if the mode μ is occupied (empty).

In our calculations we will assume a uniform anisotropy $\gamma = 1$ (Ising anisotropy), and we will take $J_j = 1 + \epsilon\eta_j$, and $h_j = h + \epsilon\xi_j$, where ϵ sets the disorder strength and η_j, ξ_j are uncorrelated uniform random numbers in $[-1, 1[$. As in the standard one-dimensional Anderson model case $\hat{H}_A$, for any finite disorder amplitude ϵ, the Hamiltonian $\hat{H}_{XY}$ has localized states. To analyze this localization we extend the definition of the IPR in Eq. (3.14):

Inverse participation ratio

$$\mathrm{IPR}_\mu^{XY} \equiv \sum_{j=1}^{L} \left(|u_{j\mu}|^4 + |v_{j\mu}|^4 \right) , \tag{3.34}$$

which still lies in the range $]0, 1]$. Once again, $\mathrm{IPR}_\mu^{XY} \to 0$ for $L \to \infty$ for extended states, while it remains finite for localized states. For illustration, we plot in Fig. 3.8 the mean IPR_μ^{XY} in the middle of the spectrum as a function of L for different values of ϵ: there is a clear signal of a finite IPR_μ^{XY} and of spatially localized states. This is not surprising since the eigenvalue problem defined in Eq. (3.32), can be thought as a conventional tight-binding system with two-coupled chains of L sites and short-range hopping. Indeed, if we look at the matrix elements we realize that the sites can be organized in two rings of length L, see Fig. 3.9, the outer ring corresponding to the first half components ($u_{j\mu}$, the "particles") and the inner ring to the second half components ($v_{j\mu}$, the "holes"). The hopping is local and the model is still effectively one-dimensional: this is the reason why we localization is present for any finite amount of disorder.

To simplify the notation we introduce the Nambu formalism [78, 79] and we define the Nambu vectors $\hat{\Psi} \equiv \left(\hat{c}_1, \ldots, \hat{c}_L, \hat{c}_1^\dagger, \ldots, \hat{c}_L^\dagger\right)$ and $\hat{\Gamma} \equiv \left(\hat{\gamma}_1, \ldots, \hat{\gamma}_L, \hat{\gamma}_1^\dagger, \ldots, \hat{\gamma}_L^\dagger\right)$.

Nambu formalism

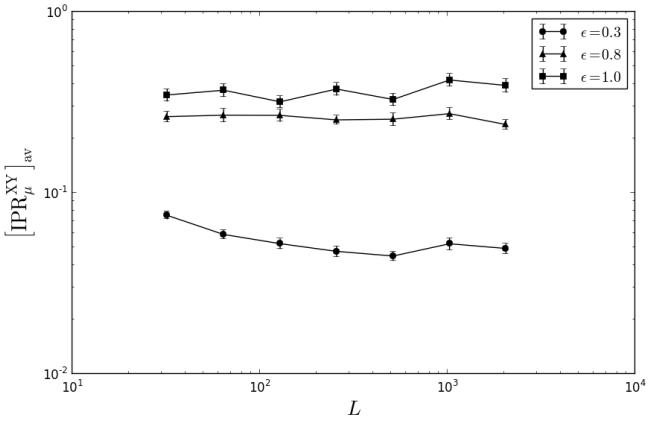

Figure 3.8.: Mean $\mathrm{IPR}_\mu^{\mathrm{XY}}$ as a function of size for different values of the disorder amplitude ϵ. The mean is computed by taking the eigenstate in the middle of the spectrum and averaging over 50 realizations of $\hat{H}_{\mathrm{XY}}$.

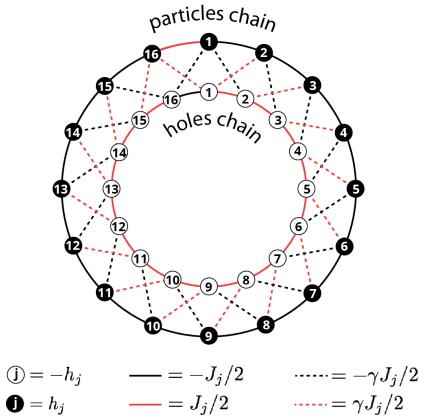

Figure 3.9.: A representation of the Ising/XY Hamiltonian using a tight-binding fermionic chain for $L = 16$. We focused on the case of an even number of fermions, hence anti-periodic boundary conditions on fermions. See text for details.

Using Eq. (3.29), the transformation between the two vectors is:

$$\hat{\Psi} = U\hat{\Gamma} \qquad\qquad \hat{\Gamma} = U^\dagger\hat{\Psi}\,, \tag{3.35}$$

where U is a $2L \times 2L$ unitary matrix given by:

$$U \equiv \begin{pmatrix} u & v^* \\ v & u^* \end{pmatrix}\,. \tag{3.36}$$

With this notation the Hamiltonian can be compactly written as:

$$\hat{H}_{\mathrm{XY}} = \sum_{\mu}^{2L} \tilde{\epsilon}_\mu \hat{\Gamma}_\mu^\dagger \hat{\Gamma}_\mu\,, \tag{3.37}$$

where $\tilde{\epsilon}_\mu$ are $2L$ single particle energies such that $\tilde{\epsilon}_\mu = \epsilon_\mu \geqslant 0$ and $\tilde{\epsilon}_{\mu+L} = -\epsilon_\mu \leqslant 0$ with $\mu = 1, \ldots, L$. Notice that now $\hat{H}_{\mathrm{XY}}$ has exactly the same diagonal form of $\hat{H}_A$ and $\hat{H}_{\mathrm{lrh}}$ in Eq. (3.10) and Eq. (3.22). The only difference is that $\hat{\Psi}_j$ with $j = 1, \ldots, L$ (which is $\hat{c}_j$) does not anticommute with $\hat{\Psi}_{j+L} = \hat{c}_j^\dagger$. This will introduces a factor 2 in the energies of the single-particle eigenstates (see Eq. (3.33)).

Disorder-free Ising/XY chain

In our calculations we will also use the disorder-free (or clean) version of $\hat{H}_{\mathrm{XY}}$, where $J_i = J$ and $h_i = h$ for $i = 1, \ldots, L$. In this case we can exploit the translational invariance

as we have done in Sec. 3.1. We first switch to momentum space with the transformations of Eqs. (3.6). The different boundary conditions on the fermion operators lead to two conditions on k depending on the parity of the number of fermions N_F: if N_F is odd, the allowed momenta can be taken to be $k = 2\pi n/L$, with $n = 0, \dots, L-1$, while if N_F is even then $k = \pi(2n+1)/L$, where $n = 0, \dots, L-1$. Expressing $\hat{c}_j$, $\hat{c}_j^\dagger$ in terms of $\hat{c}_k$, $\hat{c}_k^\dagger$ and inserting this expansion into (3.28) we get:

$$\hat{H}_{\text{cleanXY}} = \sum_{0 \leqslant k \leqslant \pi} \hat{H}_k \,, \tag{3.38}$$

where the summation is only over the admitted k values, and therefore changes according to the parity of N_F (boundary condition):

$$\hat{H}_{k=0} = -2(J+h)\hat{c}_0^\dagger \hat{c}_0 + h \tag{3.39}$$

$$\hat{H}_{k=\pi} = +2(J-h)\hat{c}_\pi^\dagger \hat{c}_\pi + h \tag{3.40}$$

$$\begin{aligned}\hat{H}_k = &-2J\left[\cos k\left(\hat{c}_k^\dagger \hat{c}_k - \hat{c}_{-k}\hat{c}_{-k}^\dagger\right) + i\gamma \sin k\left(\hat{c}_k^\dagger \hat{c}_{-k}^\dagger - \hat{c}_{-k}\hat{c}_k\right)\right] \\ &-2h\left(\hat{c}_k^\dagger \hat{c}_k - \hat{c}_{-k}\hat{c}_{-k}^\dagger\right) \,.\end{aligned} \tag{3.41}$$

The full Hamiltonian is now split into a set of k-Hamiltonians which acts on different two-dimensional subspaces. For $k = 0$ and $k = \pi$, present only when the fermion number is odd (periodic boundary conditions), $\hat{H}_k$ is trivially diagonal. For the other values of k, $\hat{H}_k$ mixes the momentum k and $-k$ and therefore the diagonalization of $\hat{H}_{\text{cleanXY}}$ can be reduced to the diagonalization of 2×2 matrices. Introducing again the Nambu formalism, we define the fermionic two-component spinor:

$$\hat{\Psi}_k \equiv \begin{pmatrix} \hat{c}_k \\ \hat{c}_{-k}^\dagger \end{pmatrix} \qquad\qquad \hat{\Psi}_k^\dagger \equiv \begin{pmatrix} \hat{c}_k^\dagger, \hat{c}_{-k} \end{pmatrix} \,. \tag{3.42}$$

which verify standard fermionic commutation relations. $\hat{H}_k$, with $0 < k < \pi$, reads:

$$\hat{H}_k = \hat{\Psi}_k^\dagger \begin{pmatrix} a_k & -ib_k \\ ib_k & -a_k \end{pmatrix} \hat{\Psi}_k \,, \tag{3.43}$$

where $a_k \equiv -2J\cos k - 2h$ and $b_k \equiv 2\gamma J \sin k$. The two modes are therefore given by the following Bogoliubov transformation:

$$\begin{pmatrix} \hat{\gamma}_k \\ \hat{\gamma}_{-k}^\dagger \end{pmatrix} \equiv \begin{pmatrix} u_k^* & v_k^* \\ -v_k & u_k \end{pmatrix} \hat{\Psi}_k \,, \tag{3.44}$$

where:

$$u_k = \frac{\epsilon_k + a_k}{\sqrt{2\epsilon_k(\epsilon_k + a_k)}} \,, \tag{3.45}$$

$$v_k = \frac{ib_k}{\sqrt{2\epsilon_k(\epsilon_k + a_k)}} \tag{3.46}$$

and ϵ_k is the dispersion of the quasiparticles with momentum k:

$$\epsilon_k = \sqrt{a_k^2 + b_k^2} = 2J\sqrt{\cos^2 k + \gamma^2 \sin^2 k + \left(\frac{h}{J}\right)^2 + 2\frac{h}{J}\cos k} \,. \tag{3.47}$$

Finally, in terms of the γ_k-fermions the Hamiltonian reads: [4]

$$\hat{H}_{\text{cleanXY}} = \sum_{0<k<\pi} \epsilon_k \left(\hat{\gamma}_k^\dagger \hat{\gamma}_k + \hat{\gamma}_{-k}^\dagger \hat{\gamma}_{-k} - 1\right) \qquad \left[+\hat{H}_{k=0} + \hat{H}_{k=\pi}\right] \,, \tag{3.48}$$

4 Notice that with the definitions done here, the single-particle energies ϵ_k are twice the energies ϵ_μ introduced in the disordered case (see Eq. (3.33)).

where the last two terms are present only when N_F is odd. Again the ground state of this Hamiltonian has even fermion number parity, and is the vacuum state of the fermionic Bogoliubov quasiparticles $\hat{\gamma}_k$, with energy $E_0 = -\sum_{0<k<\pi} \epsilon_k$. The IPR for the modes of $\hat{H}_{\text{cleanXY}}$ can be computed analytically by writing the modes $\hat{\gamma}_k^\dagger$ in terms of $\hat{c}_j$ and $\hat{c}_j^\dagger$:

$$\hat{\gamma}_k = \sum_{j=1}^{L} \left(\frac{u_k^*}{\sqrt{L}} e^{-ikj} \right) \hat{c}_j + \left(\frac{v_k^*}{\sqrt{L}} e^{-ikj} \right) \hat{c}_j^\dagger \,, \tag{3.49}$$

from which we deduce that $u_{jk} = u_k e^{ikj}/\sqrt{L}$ and $v_{jk} = v_k e^{ikj}/\sqrt{L}$. Using Eq. (3.29) we then calculate:

$$\text{IPR}_k = \sum_{j=1}^{L} \left(\frac{|u_k|^4}{L^2} + \frac{|v_k|^4}{L^2} \right) = \frac{|u_k|^4 + |v_k|^4}{L} \,, \tag{3.50}$$

which goes to zero for $L \to \infty$. Therefore, as expected, the eigenstates are extended and the IPR vanishes in the disorder-free case.

3.4 ANDERSON LOCALIZATION IN COLD ATOMS EXPERIMENTS

In this section we will briefly comment on recent experimental tests of Anderson's localization, in the framework of cold atoms systems (see Sec. 2.4 for some details).

Anderson localization, originally predicted in the context of electrons in disordered crystals [25], was first observed with light waves in disordered media [81, 82]. Recently, thanks to the great advances in the field of cold atoms in optical lattices, Anderson localization has been shown in lattice systems [83, 84].

In Ref. [84], Roati *et al.* study the localization phenomena in a one-dimensional lattice of bosonic atoms perturbed by a periodic but incommensurate external potential (created by a secondary laser beam). The system can be modeled with a tight-binding Hamiltonian for hard-core bosons with an external periodic potential which is incommensurate with respect to the underlying lattice, as in the well known Aubry-André model [85]:

$$\hat{H}_{AA} = -J \sum_j \left(\hat{b}_j^\dagger \hat{b}_{j+1} + \hat{b}_{j+1}^\dagger \hat{b}_j \right) + \lambda \sum_j \cos\left(2\pi\xi j\right) \hat{b}_j^\dagger \hat{b}_j \,, \tag{3.51}$$

where $\hat{b}_j^\dagger$ ($\hat{b}_j$) creates (destroys) a hard-core boson at site j, J is the hopping amplitude, λ is the strength, and $2\pi\xi$ the wavevector, of the incommensurate potential. In the experiment, the two relevant energies J and λ can be controlled independently by changing the intensity of the lattice potential and of the secondary beam. To get an incommensurate potential the parameter ξ must be irrational, and the usual choice for a theoretician would be the golden mean $\xi = (\sqrt{5}-1)/2$. The hard-core boson Hamiltonian $\hat{H}_{AA}$ can be reduced, by a Jordan-Wigner transformation [86], to an equivalent free-fermion tight-binding system, as in the original Aubry-André model [85], which can then be tackled using the tools described in Sec. 3.1. For this Hamiltonian the single-particle eigenstates shows a localization-delocalization transition at the critical incommensurate potential strength $\lambda_c = 2J$ [85, 87, 88]. For $\lambda < \lambda_c$ the single-particle states are extended, while for $\lambda > \lambda_c$ they are exponentially localized.

In the experimental setup of Roati *et al.* [84] the quasiperiodic optical potential, acting on ^{39}K atoms, is obtained by superimposing two standing waves created with laser beams of wavelengths $\lambda_1 \approx 1032$ nm (primary lattice) and $\lambda_2 \approx 862$ nm. These values correspond to a $\xi \approx 1.1972$. The ^{39}K atoms are initially confined within an harmonic

potential, which is then abruptly switched off, letting the atoms expand along the one-dimensional lattice. The spatial distribution of the atoms at increasing evolution times is then monitored using absorption images, see Fig. 3.10, panel (a), to test for diffusion. The absence of diffusion when Anderson localization is at play is indeed one of the cornerstones of the subject, the title of Anderson's original paper [25] being "Absence of Diffusion in Certain Random Lattices". Consistently with the properties of $\hat{H}_{AA}$, the experiment shows that the system expand ballistically for $\lambda/J = 0$, while no diffusion is instead observed in the limit of large incommensurability, $\lambda/J > 7$. Between the two regimes there is a clear crossover, revealed by Fig. 3.10, panel (b), where the width of the atomic distribution after 750 ms is plotted as a function of the incommensurability strength λ/J. The different curves, obtained using different values of J, show that that parameter controlling the crossover to the localized regime is indeed λ/J, in agreement with the predictions on the Aubry-André Hamiltonian $\hat{H}_{AA}$.

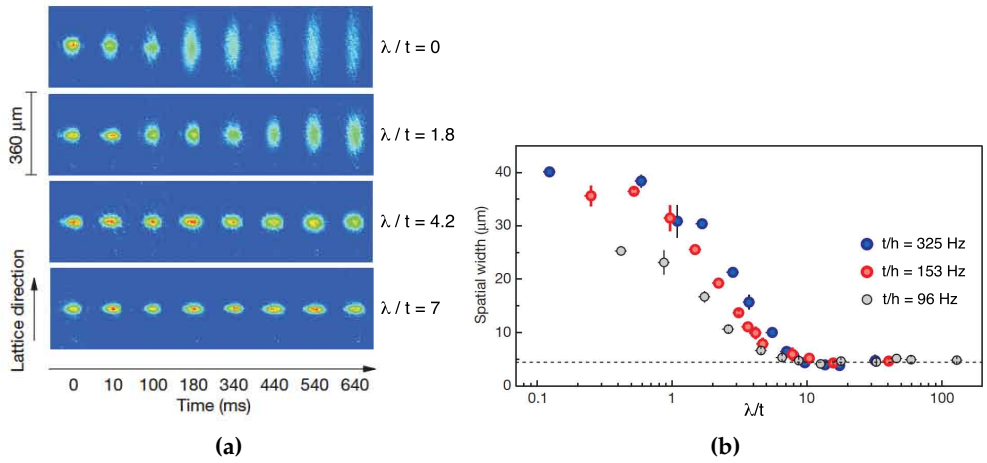

Figure 3.10.: (a) Spatial distribution of a cloud of ^{39}K atoms diffusing along the quasiperiodic lattice with $J/h = 153$Hz (where h is Planck's constant). (b) Spatial width of the condensate for different values of J after 750 ms as a function of the strength of the periodic potential. The dashed line indicates the initial size of the condensate. Plots taken from Ref. [84]. In both panels t denotes the hopping amplitude, which we denote by J.

4 QUENCHES WITH QUADRATIC FERMIONIC MODELS

In this chapter we are going to study the relaxation and the thermalization properties after a sudden quantum quench with quadratic fermionic models in presence of disorder. We show that existence of a stationary state and its description with the GGE depend on the observable considered (local versus extended, one-body versus many-body) and on the localization properties of the final Hamiltonian. We analytically prove that, while time averages of one-body operators are perfectly reproduced by GGE, time averages of many-body operators might show clear deviations from the GGE prediction when disorder-induced localization of the eigenstates is at play.

In Sec. 4.1 we show that, for the set of Hamiltonians we have studied, the time evolution of a given observable can be computed using expansions over one-body Green's functions and we obtain their expression. In Sec. 4.2 we prove that GGE works perfectly well in predicting infinite-time averages of one-body operators, and we show why this is not generally the case for many-body operators. Next, in Secs. 4.3, 4.4, 4.5 and 4.6 we present our results for quenches with the models we have introduced in Chap. 3. Finally, in Sec. 4.7, we compare our results with the ones obtained in some recent papers.

4.1 TIME EVOLUTION AND TIME FLUCTUATIONS

In this section we show how we can compute the time-evolved expectation value of an observable $\hat{A}$ after a quantum quench using one-body Green's functions.

We consider quenches in which the initial state $|\Psi_0\rangle$ is the ground state of an initial Hamiltonian $\hat{H}_0$ and it evolves under a different Hamiltonian $\hat{H}$, where $\hat{H}_0$ and $\hat{H}$ are both quadratic fermionic models. Given an observable $\hat{A}$, its expectation value at time t is equal to:

$$A(t) \equiv \langle\Psi(t)|\hat{A}|\Psi(t)\rangle = \langle\Psi_0|e^{i\hat{H}t}\hat{A}e^{-i\hat{H}t}|\Psi_0\rangle = \langle\Psi_0|\hat{A}_H(t)|\Psi_0\rangle\,, \tag{4.1}$$

where we take $\hbar = 1$ and $\hat{A}_H(t) \equiv e^{i\hat{H}t}\hat{A}e^{-i\hat{H}t}$ is the Heisenberg representation of $\hat{A}$. In our systems, any observable $\hat{A}$ can be expressed as a linear combination of powers of the fermionic operators $\hat{c}_j$ and $\hat{c}_j^\dagger$, which destroy and create a fermion at site j. Examples are the local density $\hat{n}_j \equiv \hat{c}_j^\dagger\hat{c}_j$ and the density-density correlation $\hat{\rho}_{j_1j_2} \equiv \hat{n}_{j_1}\hat{n}_{j_2}$, for the tight-binding Hamiltonians, and the local spin σ_j^z and the spin-spin correlations $\sigma_{j_1}^x\sigma_{j_2}^x$, $\sigma_{j_1}^z\sigma_{j_2}^z$, for the Ising/XY ones. Being $\hat{H}_0$ and $\hat{H}$ quadratic free-fermion Hamiltonians, the initial state $|\Psi_0\rangle$ is a BCS-Slater determinant, and we can apply Wick's theorem [89]. We can therefore expand $A(t)$ as a sum of products of one-body Green's functions: *Green's functions*

$$\begin{aligned} G_{j_1j_2}(t) &\equiv \langle\Psi(t)|\hat{c}_{j_1}^\dagger\hat{c}_{j_2}|\Psi(t)\rangle = \langle\Psi_0|\hat{c}_{j_1H}^\dagger(t)\hat{c}_{j_2H}(t)|\Psi_0\rangle\,, \\ F_{j_1j_2}(t) &\equiv \langle\Psi(t)|\hat{c}_{j_1}^\dagger\hat{c}_{j_2}^\dagger|\Psi(t)\rangle = \langle\Psi_0|\hat{c}_{j_1H}^\dagger(t)\hat{c}_{j_2H}^\dagger(t)|\Psi_0\rangle\,. \end{aligned} \tag{4.2}$$

To make things more clear, let us consider, for instance, the density-density correlation $\hat{\rho}_{j_1j_2} \equiv \hat{n}_{j_1}\hat{n}_{j_2}$ with $j_1 \neq j_2$, a two-body operator whose Wick's expansion reads:

$$\begin{aligned} \rho_{j_1j_2}(t) &= \langle\Psi(t)|\hat{c}_{j_1}^\dagger\hat{c}_{j_1}\hat{c}_{j_2}^\dagger\hat{c}_{j_2}|\Psi(t)\rangle \\ &= G_{j_1j_1}(t)G_{j_2j_2}(t) - |G_{j_1j_2}(t)|^2 + |F_{j_1j_2}(t)|^2\,. \end{aligned} \tag{4.3}$$

Clearly, the presence of long-time fluctuations in $\rho_{j_1 j_2}(t)$ is strongly linked to the long-time fluctuations of $G_{j_1 j_2}(t)$ and $F_{j_1 j_2}(t)$. Indeed, establishing that $G_{j_1 j_2}(t)$ and $F_{j_1 j_2}(t)$ approach a well-defined limit for large t (i.e., their fluctuations decay) allows us to make similar statements for any $A(t)$ which has a finite expansion over $G_{j_1 j_2}(t)$ and $F_{j_1 j_2}(t)$. This is a consequence of two elementary properties of limits: the limit of a sum is equal to the sum of the limits, and the limit of a product is equal to the product of the limits.

Let us now consider the expressions of $G_{j_1 j_2}(t)$ and $F_{j_1 j_2}(t)$. We address separately the cases of tight-binding Hamiltonians and Ising/XY ones. In the tight-binding case, as shown in Chap. 3, the Hamiltonian can be expressed in a diagonal form as:

$$\hat{H} = \sum_{\mu} \epsilon_{\mu} \hat{c}^{\dagger}_{\mu} \hat{c}_{\mu} \, , \tag{4.4}$$

where $\hat{c}_{\mu}$ and $\hat{c}^{\dagger}_{\mu}$ are the fermionic operators associated to the quasiparticle mode μ, of energy ϵ_{μ}. Using the expansions in Eqs. (3.9) for $\hat{c}_{\mu}$ and $\hat{c}^{\dagger}_{\mu}$, the operators $\hat{c}_{jH}(t)$ and $\hat{c}^{\dagger}_{jH}(t)$ read:

$$\begin{aligned}
\hat{c}_{jH}(t) &= e^{i\hat{H}t} \hat{c}_j e^{-i\hat{H}t} = \sum_{\mu} u_{j\mu} e^{i\hat{H}t} \hat{c}_{\mu} e^{-i\hat{H}t} = \sum_{\mu} u_{j\mu} e^{-i\epsilon_{\mu} t} \hat{c}_{\mu} \, , \\
\hat{c}^{\dagger}_{jH}(t) &= e^{i\hat{H}t} \hat{c}^{\dagger}_j e^{-i\hat{H}t} = \sum_{\mu} u^{*}_{j\mu} e^{i\hat{H}t} \hat{c}^{\dagger}_{\mu} e^{-i\hat{H}t} = \sum_{\mu} u^{*}_{j\mu} e^{i\epsilon_{\mu} t} \hat{c}^{\dagger}_{\mu} \, .
\end{aligned} \tag{4.5}$$

The tight-binding Hamiltonian conserves the number of fermions and therefore $F_{j_1 j_2}(t)$ is always zero, while $G_{j_1 j_2}(t)$ reads:

$$\begin{aligned}
G_{j_1 j_2}(t) &= \langle \Psi_0 | \hat{c}^{\dagger}_{j_1 H}(t) \hat{c}_{j_2 H}(t) | \Psi_0 \rangle \\
&= \sum_{\mu_1 \mu_2} u^{*}_{j_1 \mu_1} u_{j_2 \mu_2} e^{i(\epsilon_{\mu_1} - \epsilon_{\mu_2})t} G^{0}_{\mu_1 \mu_2} \, ,
\end{aligned} \tag{4.6}$$

in which $G^{0}_{\mu_1 \mu_2} \equiv \langle \Psi_0 | \hat{c}^{\dagger}_{\mu_1} \hat{c}_{\mu_2} | \Psi_0 \rangle$ is the $t = 0$ one-body Green's function of the quasiparticle modes. If $u^{0}_{j\nu}$ denote the single-particle eigenstates of $\hat{H}_0$, $G^{0}_{\mu_1 \mu_2}$ is:

$$G^{0}_{\mu_1 \mu_2} = \sum_{\nu} \sum_{j_1 j_2} n^{0}_{\nu} u_{j_1 \mu_1} u^{*}_{j_2 \mu_2} u^{0*}_{j_1 \nu} u^{0}_{j_2 \nu} \, , \tag{4.7}$$

where $n^{0}_{\nu} = 0, 1$ are the occupations number of the quasiparticle modes of $\hat{H}_0$ in the initial state $|\Psi_0\rangle$, and we used the relations $\hat{c}^{\dagger}_{\mu} = \sum_j u_{j\mu} \hat{c}^{\dagger}_j$ and $\hat{c}^{\dagger}_j = \sum_{\nu} u^{0*}_{j\nu} \hat{c}^{0\dagger}_{\nu}$.

For the quenches with Ising/XY chains the equations are similar. The changes are due to the fact that the Bogoliubov quasiparticle modes now mix particles and holes. Using the Nambu formalism, see Eqs. (3.35), the Hamiltonian, after diagonalization, is:

$$\hat{H}_{XY} = \sum_{\mu=1}^{2L} \tilde{\epsilon}_{\mu} \hat{\Gamma}^{\dagger}_{\mu} \hat{\Gamma}_{\mu} \, , \tag{4.8}$$

where $\tilde{\epsilon}_{\mu}$ are the $2L$ energies associated to the Bogoliubov quasiparticles, ordered in such a way that $\tilde{\epsilon}_{\mu+L} = -\tilde{\epsilon}_{\mu} \leqslant 0$, with $\mu = 1, \ldots, L$. With this formalism the Heisenberg representation of $\hat{\Gamma}_{\mu}$ and $\hat{\Gamma}^{\dagger}_{\mu}$ is:

$$\hat{\Gamma}_{\mu H}(t) = e^{-2i\tilde{\epsilon}_{\mu}} \hat{\Gamma}_{\mu} \qquad\qquad \hat{\Gamma}^{\dagger}_{\mu H}(t) = e^{2i\tilde{\epsilon}_{\mu}} \hat{\Gamma}^{\dagger}_{\mu} \, , \tag{4.9}$$

where the factor 2 appearing in the exponent can be traced back to the fact that $\hat{\Gamma}_{\mu} = \hat{\Gamma}^{\dagger}_{\mu+L}$ for $\mu = 1, \ldots L$, and hence, in the sum appearing in Eq. (4.8) there are two terms in-

volving the same mode: $\tilde{\epsilon}_\mu \hat{\Gamma}^\dagger_\mu \hat{\Gamma}_\mu$ and $\tilde{\epsilon}_{\mu+L} \hat{\Gamma}^\dagger_{\mu+L} \hat{\Gamma}_{\mu+L}$. Using Eqs. (3.35), the Heisenberg representation of the $\hat{\Psi}_j$ fermions is:

$$\hat{\Psi}_{jH}(t) = \sum_{\mu=1}^{2L} U_{j\mu} e^{i\hat{H}_{XY}t} \hat{\Gamma}_\mu e^{-i\hat{H}_{XY}t} = \sum_{\mu=1}^{2L} e^{-2i\tilde{\epsilon}_\mu} U_{j\mu} \hat{\Gamma}_\mu \,,$$
$$\hat{\Psi}^\dagger_{jH}(t) = \sum_{\mu=1}^{2L} U^*_{j\mu} e^{i\hat{H}_{XY}t} \hat{\Gamma}^\dagger_\mu e^{-i\hat{H}_{XY}t} = \sum_{\mu=1}^{2L} e^{2i\tilde{\epsilon}_\mu} U^*_{j\mu} \hat{\Gamma}^\dagger_\mu \,. \tag{4.10}$$

The pairs $\hat{c}^\dagger_{j_1} \hat{c}_{j_2}$ and $\hat{c}^\dagger_{j_1} \hat{c}^\dagger_{j_2}$ entering in the one-body standard $G_{j_1 j_2}(t)$ and anomalous $F_{j_1 j_2}(t)$ Green's functions can both be obtained from the Nambu pairs $\hat{\Psi}^\dagger_{j_1} \hat{\Psi}_{j_2}$ (where now j_1 and j_2 run from 1 to 2L), i.e., in terms of Nambu Green's functions $\mathcal{G}_{j_1 j_2}(t) \equiv \langle \Psi(t) | \hat{\Psi}^\dagger_{j_1} \hat{\Psi}_{j_2} | \Psi(t) \rangle$, whose expression closely resembles Eq. (4.6):

$$\begin{aligned} \mathcal{G}_{j_1 j_2}(t) &\equiv \langle \Psi(t) | \hat{\Psi}^\dagger_{j_1} \hat{\Psi}_{j_2} | \Psi(t) \rangle \\ &= \sum_{\mu_1 \mu_2} U^*_{j_1 \mu_1} U_{j_2 \mu_2} e^{2i(\tilde{\epsilon}_{\mu_1} - \tilde{\epsilon}_{\mu_2})t} \mathcal{G}^0_{\mu_1 \mu_2} \,, \end{aligned} \tag{4.11}$$

where $\mathcal{G}^0_{\mu_1 \mu_2} \equiv \langle \Psi_0 | \hat{\Gamma}^\dagger_{\mu_1} \hat{\Gamma}_{\mu_2} | \Psi_0 \rangle$ is the $t = 0$ Nambu one-body Green's function of the after-quench Bogoliubov modes. Denoting by $U^0_{j\nu}$ the single-particle eigenstates of $\hat{H}_0$, $\mathcal{G}^0_{\mu_1 \mu_2}$ will read:

$$\mathcal{G}^0_{\mu_1 \mu_2} = \sum_{\nu=L+1}^{2L} \sum_{j_1 j_2} U_{j_1 \mu_1} U^*_{j_2 \mu_2} U^{0*}_{j_1 \nu} U^0_{j_2 \nu} \,, \tag{4.12}$$

where we used the relations $\hat{\Gamma}^\dagger_\mu = \sum_j U_{j\mu} \hat{\Psi}^\dagger_j$ and $\hat{\Psi}^\dagger_j = \sum_\nu U^{0*}_{j\nu} \hat{\Gamma}^{0\dagger}_\nu$, and we exploited the fact that $|\Psi_0\rangle$ is the vacuum of the Bogoliubov quasiparticles of $\hat{H}_0$.

4.2 GGE AVERAGES

In this section we first show how we can compute GGE averages. Then we prove that, for one-body operators, the GGE average coincides with the time-average, i.e., the latter can be said to "GGE-thermalize" while, for many-body operator, additional requirements are needed in order for GGE-thermalization to occur [90].

All the Hamiltonians described in Chap. 3, after diagonalization, can be expressed as:

$$\hat{H} = \sum_\mu \epsilon_\mu \hat{\gamma}^\dagger_\mu \hat{\gamma}_\mu + E_0 \,, \tag{4.13}$$

where $\epsilon_\mu \geqslant 0$ is the positive excitation energy of the state $\hat{\gamma}^\dagger_\mu |\emptyset\rangle$ and E_0 is the energy of the state $|\emptyset\rangle$ annihilated by all the $\hat{\gamma}_\mu$'s. For $\hat{H}_{XY}$ these operators are exactly the one defined in Eq. (3.29), while for the tight-binding Hamiltonians we have to perform an intermediate step. In diagonalizing $\hat{H}_A$ and $\hat{H}_{lrh}$ we generally obtain some negative eigenvalues ϵ_μ: in such a case, it is enough to perform a particle-hole transformation $\gamma_\mu = \hat{c}^\dagger_\mu$ to change the sign of ϵ_μ, where $\hat{c}^\dagger_\mu$ is the fermionic operator associated to the quasiparticle μ, defined in Eq. (3.9). Physically, that implies that all negative energies are occupied in the ground state $|\emptyset\rangle$, and the resulting excitations describe particles or holes. We define U as the $2L \times 2L$ unitary transformation which goes from the $\hat{c}_j$, $\hat{c}^\dagger_j$ to the $\hat{\gamma}_j$, $\hat{\gamma}^\dagger_j$ operators. In the remaining part of this section we assume the Hamiltonian has been expressed in the form of Eq. (4.13): all the observations made are valid for al the models described in Chap. 3.

As discussed in Chap. 2, GGE is the most natural ensemble here. The GGE density matrix is:

$$\hat{\rho}_{GGE} \equiv \frac{1}{Z_{GGE}} e^{-\sum_\mu \lambda_\mu \hat{\gamma}^\dagger_\mu \hat{\gamma}_\mu} \,, \tag{4.14}$$

where $Z_{GGE} \equiv \mathrm{Tr}\left[e^{-\sum_\mu \lambda_\mu \hat{\gamma}_\mu^\dagger \hat{\gamma}_\mu}\right]$ and the Lagrange multipliers λ_μ are fixed by imposing the occupations of the initial state $|\Psi_0\rangle$:

$$\langle \hat{\gamma}_\mu^\dagger \hat{\gamma}_\mu \rangle_{GGE} = \langle \Psi_0 | \hat{\gamma}_\mu^\dagger \hat{\gamma}_\mu | \Psi_0 \rangle \ . \tag{4.15}$$

Notice that, in the GGE ensemble we fix the mean number of particles, but in general the number of particles can fluctuate in a grand-canonical way. [1] Using Eq. (4.14), the left-hand side is:

$$\langle \hat{\gamma}_\mu^\dagger \hat{\gamma}_\mu \rangle_{GGE} = \frac{1}{e^{\lambda_\mu} + 1} \ , \tag{4.16}$$

which clearly resembles the Fermi-Dirac distribution $1/(e^{\beta(\epsilon_\mu - \bar{\mu})} + 1)$, where $\bar{\mu}$ is the chemical potential. The right-hand side of Eq. (4.15) coincides with $\mathcal{G}^0_{\mu\mu}$, whose expression is given in Eq (4.12).

4.2.1 Why GGE works for one-body observables

In this subsection we are going to show that, for a free-fermion Hamiltonian of the form given in Eq. (4.13), the long-time average (and the diagonal average) of any one-body operator coincides with the corresponding GGE average, for any system size L, and any possible quench [90]:

$$\overline{A_{1-body}} = \langle \hat{A}_{1-body} \rangle_D = \langle \hat{A}_{1-body} \rangle_{GGE} \ , \tag{4.17}$$

with some important remarks to be made when there are degeneracies in the one-body spectrum (see below). As we shall see, this can be traced back to the constraints that the GGE sets through the constants of motion $\hat{n}_\mu \equiv \hat{\gamma}_\mu^\dagger \hat{\gamma}_\mu$. We stress that, remarkably, this equality holds even for a finite-size chain L, while, usually, statistical ensembles need a thermodynamic limit.Examples of one-body operators are, in real space, $\hat{c}_{j_1}^\dagger \hat{c}_{j_2}$ or $\hat{c}_{j_1}^\dagger \hat{c}_{j_2}^\dagger$, the local density $\hat{n}_j \equiv \hat{c}_j^\dagger \hat{c}_j$, the density $\hat{n} \equiv \sum_j \hat{n}_j / L$, and, in momentum space, $\hat{c}_k^\dagger \hat{c}_k$ (where $\hat{c}_k^\dagger = \sum_j e^{ikj} \hat{c}_j^\dagger / \sqrt{L}$), etc.

A one-body fermionic operator can always be written, neglecting irrelevant constants and rewriting the $\hat{c}_j$'s in terms of the $\hat{\gamma}_\mu$ (using Eqs. (3.9) or (3.30)), as:

$$\hat{A}_{1-body} = \sum_{\mu_1 \mu_2} \left[a_{\mu_1 \mu_2} \hat{\gamma}_{\mu_1}^\dagger \hat{\gamma}_{\mu_2} + b_{\mu_1 \mu_2} \hat{\gamma}_{\mu_1}^\dagger \hat{\gamma}_{\mu_2}^\dagger + d_{\mu_1 \mu_2} \hat{\gamma}_{\mu_1} \hat{\gamma}_{\mu_2} \right] \ , \tag{4.18}$$

where a, b, and d are $L \times L$ matrices. We start showing that $\langle \hat{A}_{1-body} \rangle_D = \langle \hat{A}_{1-body} \rangle_{GGE}$. If $|\alpha\rangle = \hat{\gamma}_{\mu_1}^\dagger \hat{\gamma}_{\mu_2}^\dagger \cdots |\emptyset\rangle$ denotes a general many-body eigenstate of $\hat{H}$, then clearly only the diagonal elements of a enter in the diagonal matrix elements:

$$\langle \alpha | \hat{A}_{1-body} | \alpha \rangle = \sum_\mu a_{\mu\mu} \langle \alpha | \hat{\gamma}_\mu^\dagger \hat{\gamma}_\mu | \alpha \rangle \ , \tag{4.19}$$

where $\langle \alpha | \hat{\gamma}_\mu^\dagger \hat{\gamma}_\mu | \alpha \rangle = 0, 1$ is the occupation number of eigenmode μ in the eigenstate $|\alpha\rangle$. In terms of $\langle \alpha | \hat{A}_{1-body} | \alpha \rangle$, the diagonal average of $\hat{A}_{1-body}$ is readily expressed as:

$$\begin{aligned}
\langle \hat{A}_{1-body} \rangle_D &= \sum_\alpha \sum_\mu |c_\alpha|^2 a_{\mu\mu} \langle \alpha | \hat{\gamma}_\mu^\dagger \hat{\gamma}_\mu | \alpha \rangle \\
&= \sum_\mu a_{\mu\mu} \sum_\alpha \langle \Psi_0 | \alpha \rangle \langle \alpha | \hat{\gamma}_\mu^\dagger \hat{\gamma}_\mu | \alpha \rangle \langle \alpha | \Psi_0 \rangle \\
&= \sum_\mu a_{\mu\mu} \sum_{\alpha\alpha'} \langle \Psi_0 | \alpha \rangle \langle \alpha | \hat{\gamma}_\mu^\dagger \hat{\gamma}_\mu | \alpha' \rangle \langle \alpha' | \Psi_0 \rangle \\
&= \sum_\mu a_{\mu\mu} \langle \Psi_0 | \hat{\gamma}_\mu^\dagger \hat{\gamma}_\mu | \Psi_0 \rangle \ ,
\end{aligned} \tag{4.20}$$

1 Indeed, in the definition of $\hat{\rho}_{GGE}$ there is no projection operator which fixes the total number of particles; in some sense, the GGE can be regarded as an integrable version of the grand-canonical ensemble. This is crucial in calculating the occupations in terms of the Lagrange multipliers, see Eq. (4.16).

where we have added an extra sum over α', using $\langle\alpha|\hat{\gamma}^\dagger_\mu\hat{\gamma}_\mu|\alpha'\rangle = \delta_{\alpha\alpha'}\langle\alpha|\hat{\gamma}^\dagger_\mu\hat{\gamma}_\mu|\alpha\rangle$, and then recognized two resolutions of the identity $\sum_\alpha |\alpha\rangle\langle\alpha|$. Notice, therefore, that the initial state enters only through $\langle\Psi_0|\hat{\gamma}^\dagger_\mu\hat{\gamma}_\mu|\Psi_0\rangle$, i.e., exactly the constants of motion which are constrained and reproduced by the GGE averages: $\langle\hat{\gamma}^\dagger_\mu\hat{\gamma}_\mu\rangle_{\mathrm{GGE}} = \langle\Psi_0|\hat{\gamma}^\dagger_\mu\hat{\gamma}_\mu|\Psi_0\rangle$. The conclusion is therefore simple, as the GGE average of $\hat{A}_{1-\mathrm{body}}$ is:

$$\begin{aligned}\langle\hat{A}_{1-\mathrm{body}}\rangle_{\mathrm{GGE}} &= \sum_\mu a_{\mu\mu}\langle\hat{\gamma}^\dagger_\mu\hat{\gamma}_\mu\rangle_{\mathrm{GGE}} \\ &= \sum_\mu a_{\mu\mu}\langle\Psi_0|\hat{\gamma}^\dagger_\mu\hat{\gamma}_\mu|\Psi_0\rangle\ , \end{aligned} \tag{4.21}$$

where we used that, by construction of the GGE, $\langle\hat{\gamma}^\dagger_{\mu_1}\hat{\gamma}_{\mu_2\neq\mu_1}\rangle_{\mathrm{GGE}} = \langle\hat{\gamma}^\dagger_{\mu_1}\hat{\gamma}^\dagger_{\mu_2}\rangle_{\mathrm{GGE}} = \langle\hat{\gamma}_{\mu_1}\hat{\gamma}_{\mu_2}\rangle_{\mathrm{GGE}} = 0$.

Concerning the equality $\overline{A_{1-\mathrm{body}}} = \langle\hat{A}_{1-\mathrm{body}}\rangle_D$, we should pay attention to the cases in which $\hat{H}$ has degenerate single-particle eigenvalues, $\epsilon_{\mu_1} = \epsilon_{\mu_2\neq\mu_1}$ (for instance, when $\hat{H}$ is a non-disordered chain). In these cases, the time average of $A_{1-\mathrm{body}}(t)$ suppresses all the oscillatory factors $e^{\pm i(\epsilon_{\mu_2}+\epsilon_{\mu_1})t}$ occurring in the b and d terms of Eq. (4.18), but all the factors $e^{i(\epsilon_{\mu_2}-\epsilon_{\mu_1})t}$ corresponding to degenerate eigenvalues appearing in the a terms survive. Therefore:

$$\begin{aligned}\overline{A_{1-\mathrm{body}}} &= \sum_{(\mu_1,\mu_2)}^{(\epsilon_{\mu_1}=\epsilon_{\mu_2})} a_{\mu_1\mu_2}\langle\Psi_0|\hat{\gamma}^\dagger_{\mu_1}\hat{\gamma}_{\mu_2}|\Psi_0\rangle \\ &= \langle\hat{A}_{1-\mathrm{body}}\rangle_D + \sum_{(\mu_1,\mu_2\neq\mu_1)}^{(\epsilon_{\mu_1}=\epsilon_{\mu_2})} a_{\mu_1\mu_2}\langle\Psi_0|\hat{\gamma}^\dagger_{\mu_1}\hat{\gamma}_{\mu_2}|\Psi_0\rangle\ , \end{aligned} \tag{4.22}$$

where we have singled out the diagonal elements, and the second sum runs over all the degenerate pairs (μ_1,μ_2), with $\mu_2\neq\mu_1$, such that $\epsilon_{\mu_1} = \epsilon_{\mu_2}$. Because of degeneracies, however, there is more freedom in the choice of the fermionic operators $\hat{\gamma}^\dagger_\mu$: we can always perform a unitary rotation in each degenerate subspace in such a way that $\langle\Psi_0|\hat{\gamma}^\dagger_{\mu_1}\hat{\gamma}_{\mu_2}|\Psi_0\rangle = 0$ for $\mu_1\neq\mu_2$. With such a choice of the $\hat{\gamma}^\dagger_\mu$'s, the extra terms in Eq. (4.22) vanish, and we recover the initial statement in Eq. (4.17), i.e., for any size and any quench, the long-time average of any one-body operator is equal to the GGE one. We stress the fact that, for any finite system, $A_{1-\mathrm{body}}(t)$ will have recurrent fluctuations $\delta A_{1-\mathrm{body}}(t)$, the so-called returns or revivals, due to the discreteness of the finite-size spectrum: nevertheless, integrating over all times (across revivals) is guaranteed to reproduce the GGE average:

$$\lim_{t\to\infty}\frac{1}{t}\int_0^t dt'\, A_{1-\mathrm{body}}(t') = \langle\hat{A}_{1-\mathrm{body}}\rangle_{\mathrm{GGE}}\ . \tag{4.23}$$

This statement, however, does not imply relaxation, i.e., that the fluctuating part $\delta A_{1-\mathrm{body}}(t)$ decreases to 0 for $t\to\infty$, as indeed evident from the presence of finite-size revivals. As we will see, $\delta A_{1-\mathrm{body}}(t)$ might indeed persist for all times even in the thermodynamic limit, when $\hat{H}$ has localized eigenstates: this in turn implies that $\lim_{t\to\infty} A_{1-\mathrm{body}}(t)$ might not exist in some cases, preventing a straightforward application of Wick's theorem to extend the equalities of averages in Eq. (4.17) to many-body operators.

4.2.2 GGE for many-body observables

In the previous subsection we have shown that the GGE average of a one-body operator coincides exactly with its long-time average. Here we will see that, for a general many-body observable $\hat{A}$, the situation is more complicated, and GGE can be proven

to correctly predict long-time averages under two additional requirements [90]: (1) $\hat{A}$ is a finite sum of powers of some fermionic operators, and (2) the time fluctuations of the one-body Green's functions associated to such fermionic operators are vanishing (i.e., they relaxes). Whenever either of the two conditions is not realized, $\langle\hat{A}\rangle_{GGE}$ is not guaranteed to coincide with $\overline{A}$: in the following sections (see Sec. 4.5.2) we will indeed discuss cases of a definite disagreement between the two averages because of a violation of condition (2) above, i.e., the persistence of time fluctuations of one-body Green's functions [90].

The key to the story is Wick's theorem [89], which clearly applies to the free-fermion Hamiltonians we are discussing [23]. As discussed in Sec. 4.1, for any any many-body observable $\hat{A}$, we can expand $\langle\Psi(t)|\hat{A}|\Psi(t)\rangle$, using Wick's theorem, as a sum of products of the one-body Green's functions $G_{j_1j_2}(t) \equiv \langle\Psi(t)|\hat{c}^\dagger_{j_1}\hat{c}_{j_2}|\Psi(t)\rangle$ and $F_{j_1j_2}(t) \equiv \langle\Psi(t)|\hat{c}^\dagger_{j_1}\hat{c}^\dagger_{j_2}|\Psi(t)\rangle$. For instance, the density-density correlations $\hat{\rho}_{j_1j_2} \equiv \hat{n}_{j_1}\hat{n}_{j_2}$ with $j_1 \neq j_2$, a two-body operator whose Wick's expansion reads:

$$\begin{aligned}\rho_{j_1j_2}(t) &= \langle\Psi(t)|\hat{c}^\dagger_{j_1}\hat{c}_{j_1}\hat{c}^\dagger_{j_2}\hat{c}_{j_2}|\Psi(t)\rangle \\ &= G_{j_1j_1}(t)G_{j_2j_2}(t) - |G_{j_1j_2}(t)|^2 + |F_{j_1j_2}(t)|^2 \,. \end{aligned} \tag{4.24}$$

This expansion clearly involves a finite number of terms (condition (1)). Now suppose (condition (2)) that the time fluctuations of the Green's functions vanish for large t, hence the limits $\lim_{t\to\infty} G_{j_1j_2}(t) = G_{j_1j_2}(\infty)$ and $\lim_{t\to\infty} F_{j_1j_2}(t) = F_{j_1j_2}(\infty)$ exist. From the analysis of the previous subsection, it is obvious that such limits must coincide with the corresponding GGE averages: $G^{GGE}_{j_1j_2} \equiv \langle\hat{c}^\dagger_{j_1}\hat{c}_{j_2}\rangle_{GGE} = G_{j_1j_2}(\infty)$, and $F^{GGE}_{j_1j_2} \equiv \langle\hat{c}^\dagger_{j_1}\hat{c}^\dagger_{j_2}\rangle_{GGE} = F_{j_1j_2}(\infty)$. It follows therefore that $\lim_{t\to\infty}\rho_{j_1j_2}(t)$ exists (i.e., its fluctuating part $\delta\rho_{j_1j_2}(t)$ vanishes for large t) and is given by:

$$\begin{aligned}\lim_{t\to\infty}\rho_{j_1j_2}(t) &= G^{GGE}_{j_1j_1}G^{GGE}_{j_2j_2} - |G^{GGE}_{j_1j_2}|^2 + |F^{GGE}_{j_1j_2}|^2 \\ &= \langle\hat{\rho}_{j_1j_2}\rangle_{GGE} \,, \end{aligned} \tag{4.25}$$

where the final step uses the fact that Wick's theorem also applies to GGE averages of free-fermion Hamiltonians [89]. Notice that, since long-time fluctuations of $\rho_{j_1j_2}(t)$ vanish, the infinite-time limit coincides with the time average, and this implies:

$$\overline{\rho_{j_1j_2}} = \lim_{t\to\infty}\rho_{j_1j_2}(t) = \langle\hat{\rho}_{j_1j_2}\rangle_{GGE} \,. \tag{4.26}$$

A similar proof works quite generally for all observables $\hat{A}$ provided the two stipulated conditions are satisfied. A few important remarks are in order: (*i*) The existence of time limits of Green's functions, as opposed to time averages, are crucial in applying Wick's theorem, because it is generally false that the "time average of a sum of products" coincides with the "sum of products of time averages"; (*ii*) For definiteness, we have chosen, above, the real-space fermions $\hat{c}^\dagger_j$ to expand $\hat{A}$, but similar arguments can be made in any one-body fermionic basis $\hat{f}^\dagger_l$, for instance, a momentum space basis. Notice, in this respect, that $\hat{A}$ might involve an infinite expansion in terms of the $\hat{c}^\dagger_j$'s and a finite one in terms of the $\hat{f}^\dagger_l$'s (condition (1)). In this case, if the time fluctuations of $G_{lm}(t) \equiv \langle\Psi(t)|\hat{f}^\dagger_l\hat{f}_m|\Psi(t)\rangle$ and $F_{lm}(t) \equiv \langle\Psi(t)|\hat{f}^\dagger_l\hat{f}^\dagger_m|\Psi(t)\rangle$ vanish (condition (2)) one can still conclude that $\overline{A} = \langle\hat{A}\rangle_{GGE}$; (*iii*) Whenever the time fluctuations of the one-body Green's functions do not vanish for large t, and/or the expansion of the operator $\hat{A}$ involves an infinite number of Wick's contractions, there is no guarantee that GGE will not reproduce long-time averages: we simply cannot prove it by using Wick's theorem. Nevertheless, we will later discuss (see Sec. 4.5.2) explicit cases where the persistence of one-body time fluctuations, due to disorder and to the presence of localized eigenstates, indeed leads to a definite discrepancy between $\overline{A}$ and $\langle\hat{A}\rangle_{GGE}$.

4.3 QUENCHES WITH NON-DISORDERED CHAINS

In this section we consider quenches with non-disordered chains. In this simple case we can compute analytic expressions for $G_{j_1 j_2}(t)$ and $F_{j_1 j_2}(t)$, and we will see that the long-time fluctuations of $G_{j_1 j_2}(t)$ and $F_{j_1 j_2}(t)$ go to zero with a power law in the thermodynamic limit. Therefore, for this set of quenches, the GGE averages correctly predict the time averages for any observable with a finite expansion over $\hat{c}_j^\dagger$ and $\hat{c}_j$. We will also see an explicit observable, the momentum occupation $\hat{c}_k^\dagger \hat{c}_k$, with an infinite expansion over $G_{j_1 j_2}(t)$ and $F_{j_1 j_2}(t)$ for which time fluctuations do not vanish.

For the clean tight-binding Hamiltonian (no BCS terms), any quench on the parameters J or h is rather trivial. The single-particle eigenstates of $\hat{H}_0$ and $\hat{H}$ are the same (see Sec. 3.1), and hence $|\Psi_0\rangle$ is an eigenstates of both the Hamiltonians. Clearly $G^0_{k_1 k_2}$ is diagonal and, from Eq. (4.6), $G_{j_1 j_2}(t)$ is constant in time.

Quenches with non-disordered Ising/XY chains are more interesting and have been largely studied in the literature [22, 91–97]. A detailed analysis of this problem is not the scope of our thesis (the reader can consult the large literature on this topic). Here we just consider the time evolution of the spatial one-body Green's functions. (For all the quantities associated to the initial Hamiltonian $\hat{H}_0$ we add a label 0.) Using Eq. (4.2) and Eq. (3.6) the standard and anomalous Green's functions are:

$$\begin{aligned} G_{j_1 j_2}(t) &= \frac{1}{L} \sum_{k_1 k_2} e^{-i(k_1 j_1 - k_2 j_2)} \langle \Psi_0 | \hat{c}^\dagger_{k_1 H}(t) \hat{c}_{k_2 H}(t) | \Psi_0 \rangle \,, \\ F_{j_1 j_2}(t) &= \frac{1}{L} \sum_{k_1 k_2} e^{-i(k_1 j_1 + k_2 j_2)} \langle \Psi_0 | \hat{c}^\dagger_{k_1 H}(t) \hat{c}^\dagger_{k_2 H}(t) | \Psi_0 \rangle \,. \end{aligned} \tag{4.27}$$

Now we expand $\hat{c}^\dagger_{kH}(t)$ and $\hat{c}_{kH}(t)$ using the fermionic operators associated to the single-particle modes of the initial Hamiltonian $\hat{\gamma}^{0\dagger}_k$ and $\hat{\gamma}^0_k$:

$$\hat{c}_{kH}(t) = u_k(t) \hat{\gamma}^0_k - v^*_k(t) \hat{\gamma}^{0\dagger}_{-k} \qquad \hat{c}^\dagger_{-kH}(t) = v_k(t) \hat{\gamma}^0_k + u^*_k(t) \hat{\gamma}^{0\dagger}_{-k} \,, \tag{4.28}$$

where the coefficient $u_k(t)$ and $v_k(t)$ are given by:

$$\begin{pmatrix} u_k(t) \\ v_k(t) \end{pmatrix} = \begin{pmatrix} u_k & -v^*_k \\ v_k & u^*_k \end{pmatrix} \begin{pmatrix} e^{-i\epsilon_k t} & 0 \\ 0 & e^{i\epsilon_k t} \end{pmatrix} \begin{pmatrix} u^*_k & v^*_k \\ -v_k & u_k \end{pmatrix} \begin{pmatrix} u^0_k \\ v^0_k \end{pmatrix} \,, \tag{4.29}$$

where we used Eq. (3.44), u_k and v_k (and u^0_k and v^0_k for $\hat{H}_0$) are defined in Eqs. (3.45) and (3.46), and ϵ_k is the single-particle energy of the final Hamiltonian. Using the fact that $|\Psi_0\rangle$ is the empty state with respect to $\hat{\gamma}^{0\dagger}_k$ and $\hat{\gamma}^0_k$, the Green's functions in Eqs. (4.27) read:

$$\begin{aligned} G_{j_1 j_2}(t) &= \frac{1}{L} \sum_k e^{-ik(j_1 - j_2)} \, |v_k(t)|^2 \,, \\ F_{j_1 j_2}(t) &= \frac{1}{L} \sum_k e^{-ik(j_1 - j_2)} v_{-k}(t) u^*_k(t) \,. \end{aligned} \tag{4.30}$$

Let us focus on $G_{j_1 j_2}(t)$, taking for simplicity $J_0 = J = 1$, $\gamma_0 = \gamma = 1$, and $h_0 \neq h$. Using Eq. (4.29) and the explicit expressions for u^0_k, v^0_k, u_k and v_k, after some algebra we arrive at:

$$|v_k(t)|^2 = \frac{1}{2} + \frac{\cos k + h_0}{\epsilon^0_k} + 4 \frac{\sin^2 k (h_0 - h)}{\epsilon^0_k \epsilon^2_k} \left[\cos(2\epsilon_k t) - 1 \right] \,. \tag{4.31}$$

Defining $\delta G_{j_1 j_2}(t) \equiv G_{j_1 j_2}(t) - \overline{G_{j_1 j_2}}$ as the time fluctuating part of the Green's function we get:

$$\begin{aligned}\delta G_{j_1 j_2}(t) &= 4(h_0 - h)\frac{2}{L}\sum_{k>0}\frac{\cos\left[k(j_1 - j_2)\right]\sin^2 k}{\epsilon_k^0 \epsilon_k^2}\cos\left(2\epsilon_k t\right) \\ &= 4(h_0 - h)\int_0^\pi \frac{dk}{\pi}\frac{\cos\left[k(j_1 - j_2)\right]\sin^2 k}{\epsilon_k^0 \epsilon_k^2}\cos\left(2\epsilon_k t\right) \ , \end{aligned} \tag{4.32}$$

where in the last step we have taken the thermodynamic limit. In Fig. 4.1 we plot $\delta G_{j_1 j_2}(t)$ as a function of time for $j_1 = j_2$, namely the time fluctuations of the local density. The time fluctuations of $\delta G_{j_1 j_2}(t)$ go to zero for $t \to \infty$ with a power law, and it was shown analytically in Ref. [98] that these fluctuations decay to 0 as $t^{-3/2}$ with oscillations. This is a consequence of the the Riemann-Lebesgue lemma (see App. A). Indeed, changing the integration domain in Eq. (4.32) from the momentum space to the energy domain, the continuous single-particle spectrum of the final Hamiltonian allows us to rewrite $\delta G_{j_1 j_2}(t)$ as the Fourier transform of a smooth function. A similar statement holds for $j_1 \neq j_2$ and for $F_{j_1 j_2}(t)$.

This analysis allows us to conclude that, for this set of quenches, for any observable with a finite expansion over $\hat{c}_j^\dagger$ and $\hat{c}_j$, the long-time fluctuations of the observable vanish, and GGE correctly predicts its time average. For observables with an infinite expansion in the thermodynamic limit we cannot predict the long-time behavior by just looking at the fluctuations of $G_{j_1 j_2}(t)$ and $F_{j_1 j_2}(t)$. An example are the occupations in momentum space $\hat{c}_k^\dagger \hat{c}_k$:

$$\langle \Psi(t)|\hat{c}_k^\dagger \hat{c}_k|\Psi(t)\rangle = |v_k(t)|^2 \ , \tag{4.33}$$

whose full expression is given in Eq. (4.31). Clearly, their long time fluctuations do not vanish. This is not surprising: $\hat{c}_k$ is a linear combination of just two modes of the final Hamiltonian and this "localization" with respect to the normal modes leads to non-vanishing time fluctuations. Indeed, the fluctuating part of $|v_k(t)|^2$ is the Fourier transform of two Dirac's deltas centered at $+2\epsilon_k$ and $-2\epsilon_k$, for which the Riemann-Lebesgue lemma does not apply (see App. A).

4.4 QUENCHES WITH THE ANDERSON MODEL

In this section we are going to study quenches with the Anderson model $\hat{H}_A$, introduced in Sec. 3.1, in which disorder is present either in the initial or final Hamiltonian. The results are all equivalent to what we have shown in Ref. [99], for XX chains with disorder both in the hopping and in the external field.

In App. B we analyze a simple set of quenches: the initial state $|\Psi_0\rangle$ is made by a set of perfectly localized fermions arranged in a disordered (or regular) fashion, and the final Hamiltonian is the clean chain $\hat{H}_{hom}$. With analytical calculations, we show that, in these cases, the long-time fluctuations of $G_{j_1 j_2}(t)$ vanish in the thermodynamic limit with a power law. However, for generic initial and final Hamiltonians, when disorder is present, simple analytical expressions for the eigenstates are lacking. To make progress we need an easy-to-compute quantitative discrimination of the persistence of fluctuations and we introduce the mean long-time squared fluctuations of $G_{j_1 j_2}(t)$ [99]:

Mean squared fluctuations

$$\delta^2_{j_1 j_2} \equiv \lim_{t\to\infty}\frac{1}{t}\int_0^t dt' \ \left|\delta G_{j_1 j_2}(t')\right|^2 \ , \tag{4.34}$$

where $\delta G_{j_1 j_2}(t) \equiv G_{j_1 j_2}(t) - \overline{G_{j_1 j_2}}$ is the time fluctuation with respect to the long-time average. This quantity is 0 when time fluctuations of $G_{j_1 j_2}(t)$ vanish, and finite if they persist. Physically, δ^2_{jj} is the averaged long-time fluctuation of the local density $\hat{c}_j^\dagger \hat{c}_j$.

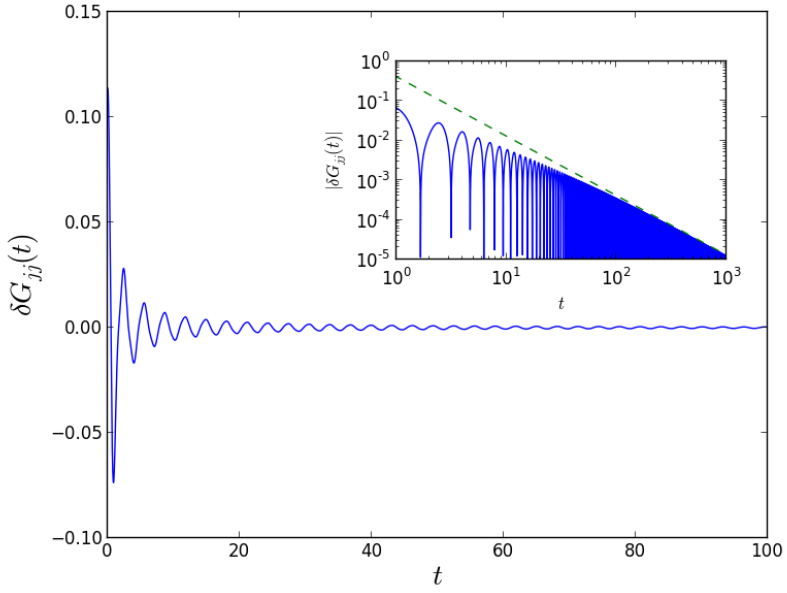

Figure 4.1.: Fluctuations around the time average of the Green's function $G_{jj}(t)$ in a quench with non-disordered Ising/XY chains. The fluctuations, after a transient, goes to zero for $t \to \infty$. In the inset we plot $|\delta G_{jj}(t)|$ as a function of time in log scale. The straight line is the envelope $f(t) = A/t^{\nu}$, with $\nu = 3/2$, obtained from Ref. [98]. Notice how one would get a wrong power-law exponent by looking at too small time-scales. The parameters are $J_0 = J = 1$, $\gamma_0 = \gamma = 1$, $h_0 = 0.9$ and $h = 0.5$.

Starting from Eq. (4.6) for $G_{j_1 j_2}(t)$ and assuming no energy degeneracy in the final Hamiltonian (i.e., $\epsilon_{\mu_1} = \epsilon_{\mu_2}$ only if $\mu_1 = \mu_2$) the time average of $G_{j_1 j_2}(t)$ is:

$$\overline{G_{j_1 j_2}} = \sum_{\mu} u^*_{j_1 \mu} u_{j_2 \mu} G^0_{\mu\mu} \, . \tag{4.35}$$

Therefore $\delta G_{j_1 j_2}(t)$ has the same expression as $G_{j_1 j_2}(t)$, except for the absence of the terms with $\mu_1 = \mu_2$. The integrand in Eq. (4.34) is therefore

$$\left|\delta G_{j_1 j_2}(t)\right|^2 = \sum_{\mu_1 \neq \mu_2} \sum_{\mu_3 \neq \mu_4} e^{i(\epsilon_{\mu_1} - \epsilon_{\mu_2} - \epsilon_{\mu_3} + \epsilon_{\mu_4})t} \\ u^*_{j_1 \mu_1} u_{j_2 \mu_2} u_{j_1 \mu_3} u^*_{j_2 \mu_4} G^0_{\mu_1 \mu_2} G^{0*}_{\mu_3 \mu_4} \, .$$

With the further assumption of no gap degeneracy (i.e., $\epsilon_{\mu_1} - \epsilon_{\mu_2} = \epsilon_{\mu_3} - \epsilon_{\mu_4}$ only if $\mu_1 = \mu_3$ and $\mu_2 = \mu_4$, or $\mu_1 = \mu_2$ and $\mu_3 = \mu_4$) [2] we arrive at the key result [99]

$$\delta^2_{j_1 j_2} = \sum_{\mu_1 \neq \mu_2} |u_{j_1 \mu_1}|^2 |u_{j_2 \mu_2}|^2 |G^0_{\mu_1 \mu_2}|^2 \, , \tag{4.36}$$

expressing $\delta^2_{j_1 j_2}$ for a single realization as an eigenfunction-weighted sum of $|G^0_{\mu_1 \mu_2}|^2$. Disorder averages are performed after computing $\delta^2_{j_1 j_2}$, averaging $\delta G_{j_1 j_2}(t)$ would cancel such fluctuations.

The nature of the eigenfunctions (localized versus extended) plays a crucial role in Eq. (4.36). In App. D we prove that regardless of disorder, the $|G^0_{\mu_1 \mu_2}|^2$'s sum to the total number of fermions N_F in the initial state:

$$\sum_{\mu_1 \mu_2} |\langle \psi_0 | \hat{c}^\dagger_{\mu_1} \hat{c}_{\mu_2} | \psi_0 \rangle|^2 = N_F \, . \tag{4.37}$$

2 Using a non-degeneracy condition for the gaps, while often reasonable for single-particle energies, is dangerous for many-body energies. This would lead to the incorrect result that fluctuations are always negligibly small, as discussed in P. Reimann, Phys. Rev. Lett. **101**, 190403 (2008).

Therefore, if the final eigenstates are extended, $|u_{j_1\mu_1}|^2|u_{j_2\mu_2}|^2 \sim 1/L^2$, then $\delta^2_{j_1j_2}$ in Eq. (4.36) scales to zero as $N_F/L^2 \sim 1/L$ for a system with a finite density of fermions. If $\hat{H}$ is non-disordered we have to take care of the degeneracy $\epsilon_k = \epsilon_{-k}$ and also of particle-hole symmetry, but still, we can prove (see App. D) a bound $\delta^2_{j_1j_2} \leqslant 8N_F/L^2$, indicating that fluctuations vanish for $L \to \infty$. This is in perfect agreement with what we have obtained in App. B for fully-localized initial states and generalizes the result to any disordered initial state $|\Psi_0\rangle$.

When the final $\hat{H}$ is disordered (i.e. $W > 0$), by analyzing many realizations of the final Hamiltonian, we have seen that $x = \delta^2_{jj}$ strongly deviates from a Gaussian distribution, and is nearly (although not precisely) log-normal, i.e., $\ln(x)$ is approximately Gaussian distributed, see Fig. 4.2. For this set of quenches we will therefore compute and plot the median (i.e., the geometric mean) $[x]^G_{av} \equiv \exp([\ln(x)]_{av})$ and the geometric standard deviation $\exp(\sigma[\ln x])$, rather than the usual (arithmetic) mean $[x]_{av}$, and its standard deviation $\sigma[x]$ (in the plots, the error bars will then go from $[x]^G_{av}\exp(-\sigma[\ln x])$ to $[x]^G_{av}\exp(\sigma[\ln x])$).

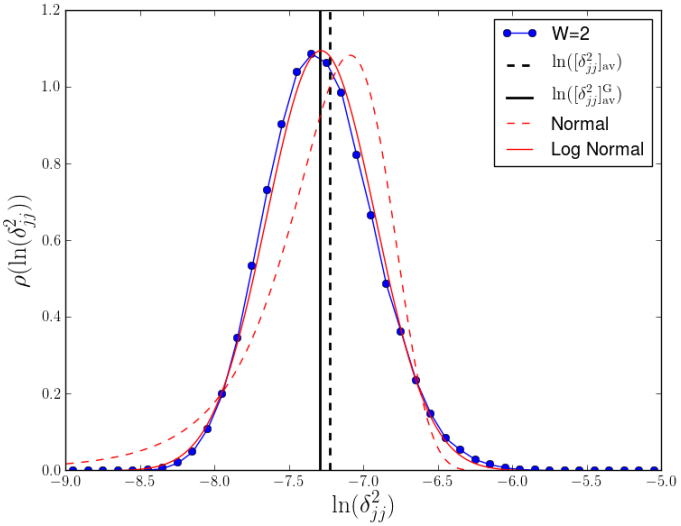

Figure 4.2.: Probability distribution of $\ln(\delta^2_{jj})$ for quenches with a clean initial Hamiltonian and a disordered final one with $W = 2$. The solid curve is the best log-normal distribution for δ^2_{jj} (i.e. Gaussian for $\ln(\delta^2_{jj})$), while the dashed curve is the best Gaussian distribution for δ^2_{jj}. The vertical lines are the logarithm of the geometric mean $[\delta^2_{jj}]^G_{av}$ (solid line), and the logarithm of the arithmetic mean $[\delta^2_{jj}]_{av}$ (dashed line). The distribution of δ^2_{jj} shows small fluctuations from a log-normal distribution. We used $j = L/2$, $L = 512$ and 10^5 different realizations.

Figure 4.3 shows the disorder average $[\delta^2_{jj}]_{av}$ (or $[\delta^2_{jj}]^G_{av}$) as a function of L in two opposite situations, quenches from a disordered $\hat{H}_0$ to a clean $\hat{H}$ (D $\to$ C), or vice-versa (C $\to$ D). In order to get small fluctuations for different sizes, and to focus on the thermodynamic limit of single realizations, disorder realizations for the smaller L chain are obtained, here and in the following, by removing the same amount of sites from the right and left edges of the largest chain. In all cases δ^2_{jj} is calculated from Eq. (4.36) (with the extra terms due to degeneracies in the D $\to$ C case). When $\hat{H}$ is clean (D $\to$ C data), $[\delta^2_{jj}]_{av}$ scales to 0 as $1/L$, as expected from the bound discussed below Eq. (4.37). On the contrary, when $\hat{H}$ is disordered (C $\to$ D data), $[\delta^2_{jj}]^G_{av}$ converges unambiguously to a non-vanishing quantity for $L \to \infty$: time fluctuations survive at all times when the final Hamiltonian $\hat{H}$ is disordered. Notice that, due to the Jensen's inequality (see App. C), namely $[\delta^2_{jj}]_{av} \geqslant [\delta^2_{jj}]^G_{av}$, for these quenches also $[\delta^2_{jj}]_{av}$ is finite

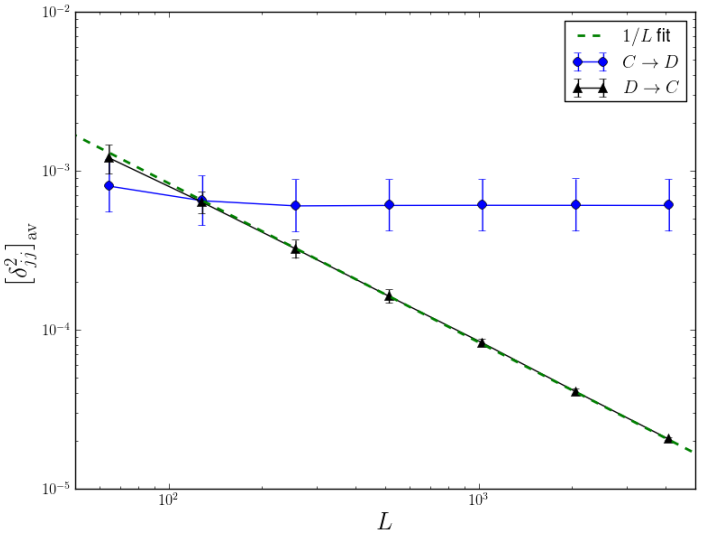

Figure 4.3.: Average values of δ^2_{jj} with $j = L/2$, Eqs. (4.34) and (4.36), for quenches with Anderson chains when $|\psi_0\rangle$ is the ground state of a disordered $\hat{H}_0$ (with $W = 2$), while $\hat{H}$ is clean with $W = 0$ (triangles D $\to$ C), or the opposite case (circles C $\to$ D), see text for details. The averages are taken over 20 different disordered realizations, and for the D $\to$ C points we used the arithmetic mean, while for C $\to$ D points the geometric mean (see text for details). The error bar is the standard deviation (or the geometric standard deviation) of the distributions (not the error on the average).

in the thermodynamic limit. For smaller disorder amplitude W, the situation is similar, except that the large-L plateau occurs for larger L, due to larger localization lengths.

To better gauge the role of the localized eigenfunctions in making $\delta^2_{j_1 j_2}$ finite for $L \to \infty$, we have analyzed histograms of the quantities appearing in Eq. (4.36). A histogram of $|G^0_{\mu_1\mu_2}|^2$ shows that while the average of $|G^0_{\mu_1\mu_2}|^2$ scales to zero as $1/L$, see Eq. (4.37), the distribution of its values has large tails. To analyze these tails, we work with logarithmic distributions, and define

$$P^w_{j_1 j_2}(x) \equiv \sum_{\mu_1 \neq \mu_2} \frac{|u_{j_1\mu_1}|^2 |u_{j_2\mu_2}|^2}{\mathcal{N}_{j_1 j_2}} \delta\left(x - \ln\left|G^0_{\mu_1\mu_2}\right|^2\right) , \tag{4.38}$$

where $\mathcal{N}_{j_1 j_2} \equiv \sum_{\mu_1 \neq \mu_2} |u_{j_1\mu_1}|^2 |u_{j_2\mu_2}|^2 = 1 - \sum_\mu |u_{j_1\mu}|^2 |u_{j_2\mu}|^2$ is a normalization constant, $0 < \mathcal{N}_{j_1 j_2} < 1$, related to the inverse participation ratio (see Eq. (3.14)) when $j_1 = j_2$. Figure 4.4 shows $P^w_{jj}(x)$ for two different sizes, and compares it with the unweighted distribution

$$P(x) \equiv \frac{1}{L(L-1)} \sum_{\mu_1 \neq \mu_2} \delta\left(x - \ln\left|G^0_{\mu_1\mu_2}\right|^2\right) . \tag{4.39}$$

We plot both single-instance distributions (solid points) as well as disorder average distributions $[\cdots]_{av}$, denoted by lines. The unweighted distribution $P(x)$ is smooth, and self-averaging, and moves towards smaller mean values when L increases. On the contrary, $P^w_{jj}(x)$ is more structured (single-instance distributions depend on the details of the weights $|u_{j_1\mu_1}|^2 |u_{j_2\mu_2}|^2$), but its mean does not decrease with L, due to an eigenfunction reweighting of rare events with large values of $|G^0_{\mu_1\mu_2}|^2$. Physically, this is quite transparent: similarly to what happens for the inverse participation ratio, localized eigenstates are rather insensitive to the size, while extended states are (see Sec. 3.1). The fact that the mean $\int dx\, x P^w_{j_1 j_2}(x)$, remains finite for $L \to \infty$ for almost all realiza-

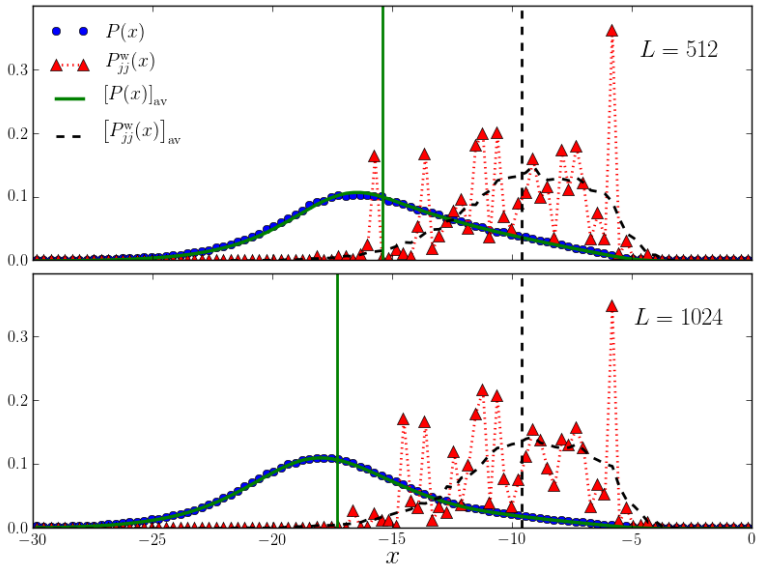

Figure 4.4.: Plot of $P^{w}_{jj}(x)$, Eq. (4.38) with $j = L/2$ (triangles), and $P(x)$, Eq. (4.39) (circles), for quenches from a clean $\hat{H}_0$ (with $W = 0$) to a disordered $\hat{H}$ (with $W = 2$), for two values of the chain length L. $[P^{w}_{j_1 j_2}(x)]_{av}$ and $[P(x)]_{av}$ (dashed and solid lines) are the distributions obtained averaging over different realizations of disorder, with the corresponding vertical lines indicating their mean values $\int dx\, x[P^{w}_{j_1 j_2}(x)]_{av}$ and $\int dx\, x[P(x)]_{av}$.

tions, is enough to conclude that $\delta^2_{j_1 j_2}$ stays finite in the disordered $\hat{H}$ case. Indeed, $\mathcal{N}_{j_1 j_2}$ remains finite when $L \to \infty$, and by Jensen's inequality (see App. C) we have:

$$\delta^2_{j_1 j_2} = \mathcal{N}_{j_1 j_2} \langle e^{x} \rangle_{P^{w}_{j_1 j_2}} \geqslant \mathcal{N}_{j_1 j_2} e^{\langle x \rangle_{P^{w}_{j_1 j_2}}} . \tag{4.40}$$

We have shown that $G_{j_1 j_2}(t)$ has persistent fluctuations after a quench to a final disordered $\hat{H}$. From the discussion of Sec. 4.2 we can conclude that, for these quenches and for any operator with a finite expansion over $\hat{c}^{\dagger}_{j_1} \hat{c}_{j_2}$, the time fluctuations don't vanish as well and, if the operator is many body, the GGE is not guaranteed to work. In the next section we will show an example in which the GGE fails on estimating the time average of the density-density correlations $\hat{\rho}_{j_1 j_2} \equiv \hat{n}_{j_1} \hat{n}_{j_2}$, with $j_1 \neq j_2$. The long-time fluctuations could be averaged out if one considers extensive operators involving sums over all sites. We will see later that, for instance, in a quench to a final disordered Ising chain, while the local transverse magnetization $\sigma^z_j(t) = 2G_{jj}(t) - 1$ has persistent fluctuations, the corresponding extensive operator, the total transverse magnetization (per site) $\hat{m}_z = L^{-1} \sum_j \hat{\sigma}^z_j$, has fluctuations which decrease to 0 as L is increased. Physically, extensive operators effectively perform a self-averaging of the fluctuations $\delta A(t)$, which then vanish in the $L \to \infty$ limit.

4.5 QUENCHES WITH 1D SPINLESS FERMIONS WITH LONG-RANGE HOPPING

In this section we consider quenches in which the initial state $|\Psi_0\rangle$ is the ground-state of the non-disordered tight-binding chain $\hat{H}_{hom}$, and the final Hamiltonian is $\hat{H}_{lrh}$, Eq. (3.20), i.e., a disordered one-dimensional (spinless) fermions with long-range hopping. The reason behind this simple choice for $|\Psi_0\rangle$ is that, as seen in the previous section, the long-time fluctuation properties do not depend, qualitatively, on the initial

Hamiltonian being ordered or not. Computations and results shown in this section are published in Ref. [90].

We will consider observables $\hat{A}$ with a finite expansion in real space and in momentum space, and hence we will need to ascertain the time dependence of both real-space and momentum-space Green's functions:

$$\begin{aligned} G_{j_1 j_2}(t) &= \langle \Psi(t)|\hat{c}^\dagger_{j_1}\hat{c}_{j_2}|\Psi(t)\rangle \,, \\ G^k_{k_1 k_2}(t) &= \langle \Psi(t)|\hat{c}^\dagger_{k_1}\hat{c}_{k_2}|\Psi(t)\rangle \end{aligned} \tag{4.41}$$

and the associated mean long-time squared fluctuations are:

Mean squared fluctuations

$$\begin{aligned} \delta^2_{j_1 j_2} &\equiv \lim_{t\to\infty}\frac{1}{t}\int_0^t dt' \, \left|\delta G_{j_1 j_2}(t')\right|^2 \,, \\ \delta^2_{k_1 k_2} &\equiv \lim_{t\to\infty}\frac{1}{t}\int_0^t dt' \, \left|\delta G^k_{k_1 k_2}(t')\right|^2 \,. \end{aligned} \tag{4.42}$$

To unify the treatment of both cases, we will consider a general fermionic operator $\hat{f}_n = \sum_\mu z_{n\mu}\hat{c}_\mu$ obtained by applying a unitary transformation z (of matrix elements $z_{n\mu}$, with $z^\dagger z$ the identity) to the $\hat{c}_\mu$'s which diagonalize $\hat{H}_{lrh}$: for the original real-space fermions $\hat{c}_j$, $z_{j\mu} = u_{j\mu}$ is the real-space wavefunction of the μ eigenstate, while for the momentum space fermions $\hat{c}_k$, $z_{k\mu} = \sum_j e^{-ikj}u_{j\mu}/\sqrt{L}$. We define $G_{ml}(t) \equiv \langle\Psi(t)|\hat{f}^\dagger_m\hat{f}_l|\Psi(t)\rangle$ the associated Green's function and δ^2_{ml} the associated mean squared fluctuations. The anomalous Green's functions associated to the operators $\hat{f}^\dagger_m\hat{f}^\dagger_l$ are zero because $\hat{H}_{lrh}$ conserves the total number of fermions. As discussed in Subsecs. 4.2.1 and 4.2.2, if the Green's functions $G_{ml}(t)$ have vanishing long-time fluctuations, then also the long-time fluctuations of $\hat{A}$ disappear and $\overline{A} = \langle\hat{A}\rangle_{GGE}$. In agreement with what we have seen in Sec. 4.4, we will show the crucial role played by the localization of the eigenfunctions. When quenching to a final Hamiltonian $\hat{H}_{lrh}$ with α (we recall that α is setting how fast the hoppings' variance decays with distance in $\hat{H}_{lrh}$, see Eq. (3.20)) in the localized phase ($\alpha > 1$), the real-space Green's functions $G_{j_1 j_2}(t)$ will be shown to have persistent time fluctuations, i.e., $\delta^2_{j_1 j_2} > 0$ in the thermodynamic limit $L \to \infty$, while quenching with α in the extended phase ($\alpha < 1$) leads to vanishing time fluctuations, $\delta^2_{j_1 j_2} \to 0$. In both cases, however, the eigenfunctions appear to be extended when analyzed in momentum space (see Sec. 3.2), which results in momentum space Green's functions with vanishing time fluctuations, $\delta^2_{k_1 k_2} \to 0$. We will then explicitly discuss (see Sec. 4.5.2) the discrepancy between time averages and GGE averages for real-space many-body operators, such as density-density spatial correlations, when quenching to the localized phase.

4.5.1 One-body Green's function fluctuations

As discussed in Subsec. 4.2.1, GGE correctly predicts the infinite-time average of any one-body operator, and hence, in particular, of the one-body Green's functions. The plot in Fig. 4.5 exemplifies this by showing the time evolution of $G_{jj}(t)$, the expectation value of the fermion density at site j, for two sizes and two values of α, one in the extended phase ($\alpha = 0.5$) and one in the localized phase ($\alpha = 2$). We now address in a more general way the question of the time fluctuations of the one-body Green's functions. Using the expansion $\hat{f}_n = \sum_\mu z_{n\mu}\hat{c}_\mu$ we can express $G_{ml}(t)$ as:

$$G_{ml}(t) = \sum_{\mu_1\mu_2} z^*_{m\mu_1} z_{l\mu_2} e^{i(\epsilon_{\mu_1}-\epsilon_{\mu_2})t} G^0_{\mu_1\mu_2} \,, \tag{4.43}$$

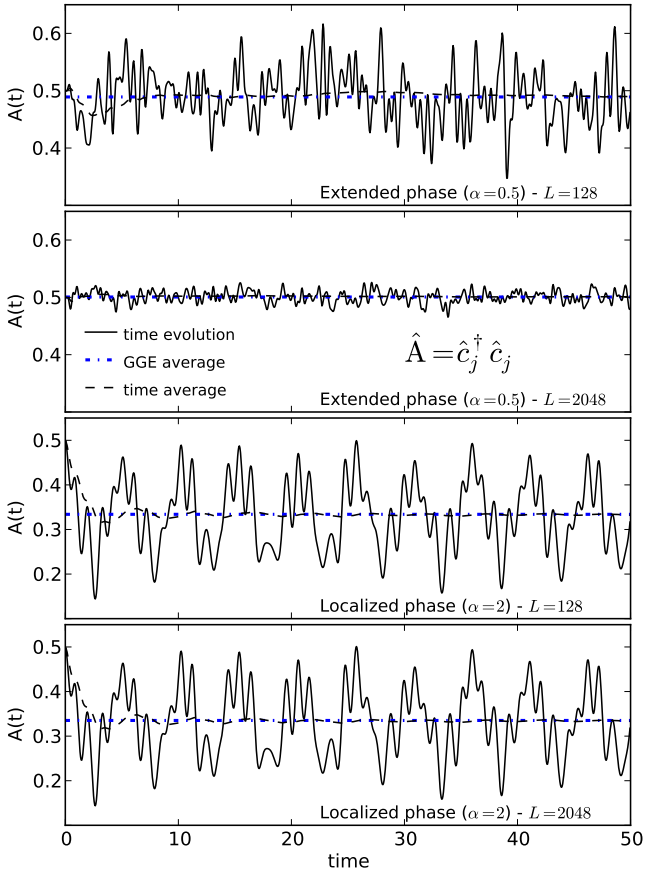

Figure 4.5.: Time evolution of $G_{jj}(t)$, with $j = L/2$ (solid line), and its running-time average $t^{-1}\int_0^t dt'\, G_{jj}(t')$ (dashed line). The initial state is the ground state of $\hat{H}_{hom}$ and the time evolution is performed with $\hat{H}_{lrh}$ with two different values of α and two different sizes. The horizontal dash-dotted line is the GGE average of $\hat{n}_j$. The data are obtained using a single realization, with $\alpha = 0.5$ for the extended case, and $\alpha = 2$ for the localized one (which shows no size effects). Disorder realizations for the smaller L chain are obtained, here and in the following, by removing sites from the right and left edges of the larger chain.

where $G^0_{\mu_1\mu_2} \equiv \langle\Psi_0|\hat{c}^\dagger_{\mu_1}\hat{c}_{\mu_2}|\Psi_0\rangle$. Assuming the model has no single-particle energy degeneracy (i.e., if $\epsilon_{\mu_1} = \epsilon_{\mu_2}$ then $\mu_1 = \mu_2$), only the diagonal terms with $\mu_1 = \mu_2$ will contribute to the infinite-time average of $G_{ml}(t)$:

$$\overline{G_{ml}} = \langle\hat{f}^\dagger_m\hat{f}_l\rangle_{GGE} = \sum_\mu z^*_{m\mu}z_{l\mu}G^0_{\mu\mu}\,. \tag{4.44}$$

Hence, the time fluctuations of $G_{ml}(t)$ will be given by:

$$\delta G_{ml}(t) = \sum_{\mu_1\neq\mu_2} z^*_{m\mu_1}z_{l\mu_2}e^{i(\epsilon_{\mu_1}-\epsilon_{\mu_2})t}G^0_{\mu_1\mu_2}\,. \tag{4.45}$$

Now we calculate δ^2_{ml} by squaring the previous expression and taking the infinite-time average. If we assume there is no gap degeneracy (i.e., if $\epsilon_{\mu_1} - \epsilon_{\mu_2\neq\mu_1} = \epsilon_{\mu_3} - \epsilon_{\mu_4\neq\mu_3}$ then $\mu_1 = \mu_3$ and $\mu_2 = \mu_4$) we arrive at:

$$\delta^2_{ml} = \sum_{\mu_1\neq\mu_2} \left|z_{m\mu_1}\right|^2 \left|z_{l\mu_2}\right|^2 \left|G^0_{\mu_1\mu_2}\right|^2\,, \tag{4.46}$$

which generalizes Eq. (4.36), obtained with real-space Green's functions, to general Green's functions. We will study it in various situations (different quenches and different choices of the fermionic operators $\hat{f}_n$) to understand when and why δ^2_{ml}, which is

always finite for any finite L (due to revivals), goes to zero in the thermodynamic limit. We will see, in perfect agreement with what we have seen for the Anderson model in Sec. 4.4, the crucial role played by the weights $|z_{m\mu_1}|^2|z_{l\mu_2}|^2$ and by localization.

Let us consider first real-space Green's functions $G_{j_1 j_2}(t)$, which for $j_1 = j_2 = j$, have a simple physical meaning: the expectation value at time t of the local density at the site j. From Eq. (4.46) we get:

$$\delta^2_{j_1 j_2} = \sum_{\mu_1 \neq \mu_2} \left|u_{j_1\mu_1}\right|^2 \left|u_{j_2\mu_2}\right|^2 \left|G^0_{\mu_1\mu_2}\right|^2 , \tag{4.47}$$

where $u_{j\mu}$ is the real-space wavefunction of the eigenstate μ. Depending on α, the eigenfunctions $u_{j\mu}$ are either localized (for $\alpha > 1$) or extended (for $\alpha < 1$), see Sec. 3.2. The main panel of Fig. 4.6 (top) shows the average value of δ^2_{jj} as a function of the chain size L for both choices of α. As we have shown for quenches in the Anderson model (Sec. 4.4), when eigenstates are extended, the weights $\left|u_{j_1\mu_1}\right|^2 \left|u_{j_2\mu_2}\right|^2 \sim 1/L^2$ in Eq. (4.47) can be essentially taken out of the sum. Then, without weights, it is a simple matter to show that:

$$\frac{1}{L^2} \sum_{\mu_1 \neq \mu_2} \left|G^0_{\mu_1\mu_2}\right|^2 \leqslant \frac{1}{L^2} \sum_{\mu_1\mu_2} \left|G^0_{\mu_1\mu_2}\right|^2 = \frac{N_F}{L^2} , \tag{4.48}$$

where N_F is the total number of fermions in the initial state (see App. D for the proof of the last equality). Hence, $\delta^2_{j_1 j_2}$ is expected to go to zero as $1/L$ when quenching towards a phase with extended eigenstates ($\alpha < 1$), as indeed found numerically. On the contrary, weights are of paramount importance when quenching to a phase with localized eigenstates ($\alpha > 1$), because they move the important contributions to $\delta^2_{j_1 j_2}$ from the average $|G^0_{\mu_1\mu_2}|^2$, which is of order $1/L$, to rare large values, leading to a finite $\delta^2_{j_1 j_2}$ which is rather insensitive to the size L (see discussion in Sec. 4.4).

Consider now the Green's functions in momentum space $G^k_{k_1 k_2}(t)$ representing, for $k_1 = k_2 = k$, the expectation value at time t of the momentum distribution. Since $\hat{c}^\dagger_k = \sum_j e^{ikj}\hat{c}^\dagger_j/\sqrt{L}$, the $G^k_{k_1 k_2}(t)$'s are straightforwardly related to the $G_{j_1 j_2}(t)$'s through a double summation on j_1 and j_2 with oscillating phase factors $e^{i(k_1 j_1 - k_2 j_2)}$. However, for $L \to \infty$ these are infinite sums, and this might change the behavior of the time fluctuations. We now show that, even when $G_{j_1 j_2}(t)$ has persistent time fluctuations, the corresponding $G^k_{k_1 k_2}(t)$ averages them out, and $\delta^2_{k_1 k_2} \to 0$ for $L \to \infty$. Indeed, using Eq. (4.46),

$$\delta^2_{k_1 k_2} = \sum_{\mu_1 \neq \mu_2} \left|u_{k_1\mu_1}\right|^2 \left|u_{k_2\mu_2}\right|^2 \left|G^0_{\mu_1\mu_2}\right|^2 , \tag{4.49}$$

where $u_{k\mu} = \sum_j e^{-ikj} u_{j\mu}/\sqrt{L}$ are the Fourier transforms of the real-space wavefunctions $u_{j\mu}$. Figure 4.6 (bottom) shows that $\delta^2_{kk} \to 0$ for $L \to \infty$, regardless of the value of α. This is in agreement with the fact that the eigenstates of $\hat{H}_{lrh}$ are delocalized both in real and reciprocal space (see Sec. 3.2 for details). Effectively, therefore, going to momentum space averages out persistent time-fluctuations which are seen in real space when eigenstates are localized, an effect akin to self-averaging of extensive quantities in disordered systems [100].

4.5.2 Many-body observables and failure of GGE

From the general analysis of Subsecs. 4.2.1 and 4.2.2 and the study of the one-body Green's functions of Sec. 4.5.1, we can conclude that many-body operators involving a finite expansion in terms of momentum space operators $\hat{c}_k$, such as correlations $\hat{c}^\dagger_{k_1}\hat{c}_{k_1}\hat{c}^\dagger_{k_2}\hat{c}_{k_2}$, will have time averages which coincide with GGE averages, regardless the value of α. The same is true in the delocalized phase ($\alpha < 1$) for many-body operators with a finite expansion in real space, because the time fluctuations of $G_{j_1 j_2}(t)$

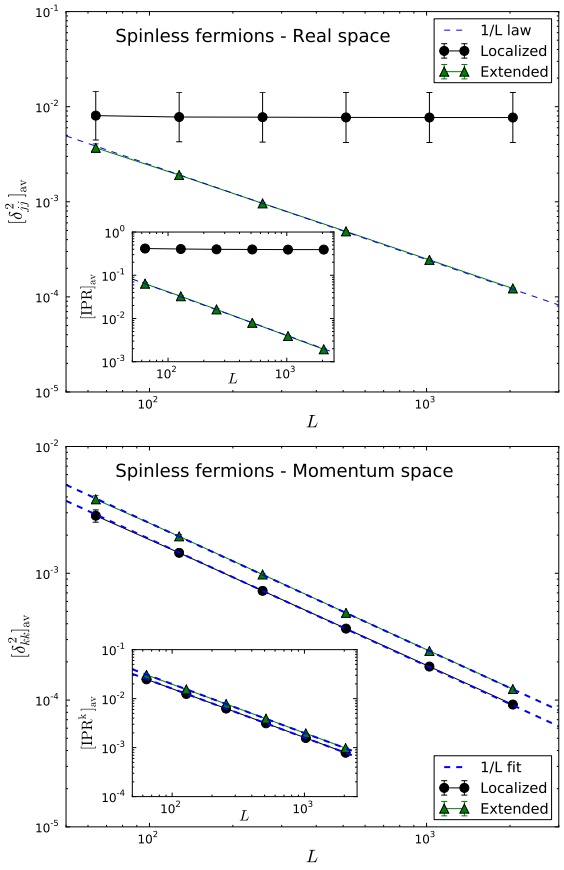

Figure 4.6.: Average value of δ^2_{jj} (top), with $j = L/2$, and δ^2_{kk} (bottom), with $k = 0$, for the disordered long-range hopping model $\hat{H}_{lrh}$ as a function of the chain size L for different values of α. The data are obtained starting from the ground state of a clean fermionic chain with nearest-neighbor hopping and quenching to $\hat{H}_{lrh}$ with different values of α. The "Localized" points are for $\alpha = 2$, while the "Extended" points are for $\alpha = 0.5$. We used 50 realizations of disorder. In all cases we report the usual (arithmetic) mean (the error bar, when visible, is the standard deviation), except for δ^2_{jj} in the localized phase, where we plot the median (the geometric mean, see Sec. 4.4 for details). In the inset, the IPR (see Eqs. (3.14) and (3.17)) as a function of size. Notice how for all cases ("Localized" and "Extended" quenches) the eigenstates of the final Hamiltonian are "extended" in reciprocal space and consequently $\delta^2_{k_1 k_2}$ goes to zero for $L \to \infty$. For a smoother size scaling, each disorder realization of the largest L generated is employed, by removing the same amount of sites from the two edges, to generate realizations for smaller L.

vanish. When $\alpha > 1$ (localized phase) the GGE ability in describing time averages of many-body operators is not guaranteed, because $G_{j_1 j_2}(t)$ have persistent time fluctuations and Wick's theorem is of no help. Here we will show that, when $\alpha > 1$, GGE fails in predicting the spatial density-density correlations $\hat{\rho}_{j_1 j_2} \equiv \hat{n}_{j_1}\hat{n}_{j_2}$. To see this, we compare, see Eqs. (4.24) and (4.25), the time average of $\rho_{j_1 j_2}(t)$ (i.e., a time average of a sum of products of G's) with the corresponding GGE average (a sum of products of time averages). In Fig. 4.7 we plot $\rho_{j_1 j_2}(t)$, together with its running-time average (i.e., $t^{-1}\int_0^t dt'\, \rho_{j_1 j_2}(t')$) and the GGE average for two chain sizes and two values of α. First we notice that, as in the case of $G_{j_1 j_2}(t)$, increasing the size L in the delocalized phase ($\alpha < 1$) strongly decreases the time fluctuations, which are, on the contrary, unaffected by L in the localized phase ($\alpha > 1$). The second feature emerging from Fig. 4.7 is that, while in the delocalized phase the time average tends to the GGE value, there is a marked and clear discrepancy between the two in the localized phase.

GGE error

The difference between the GGE average and the time average can be explicitly computed using the same strategy (and assumptions) of Sec. 4.5.1:

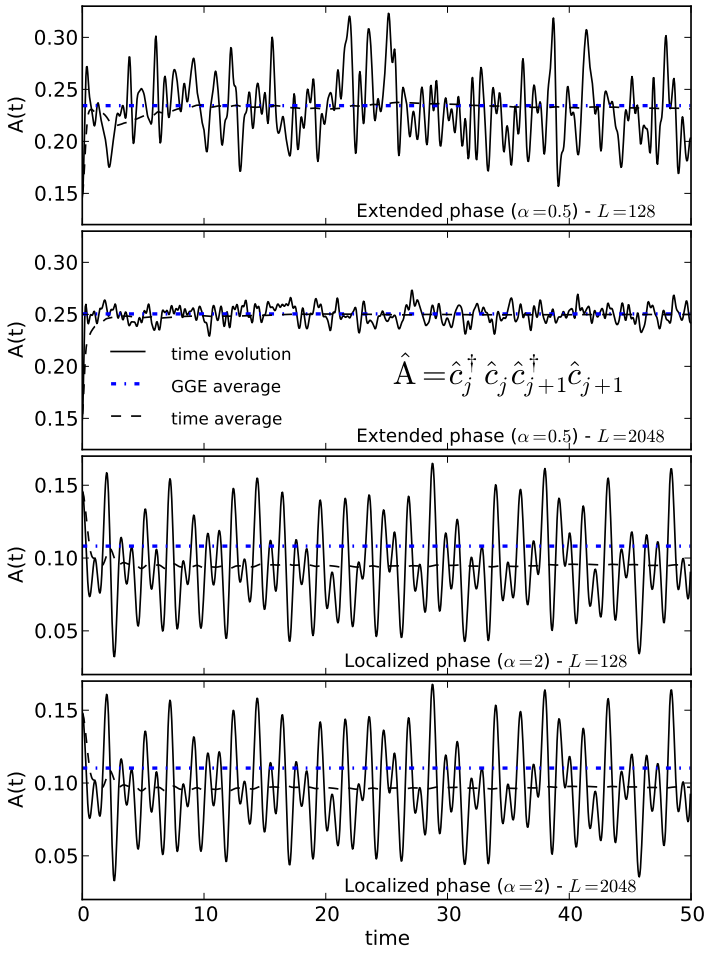

Figure 4.7.: Time evolution of $\rho_{j_1 j_2}(t)$, with $j_1 = L/2$ and $j_2 = j_1 + 1$ (solid line), and its running-time average $t^{-1}\int_0^t dt'\, \rho_{j_1 j_2}(t')$ (dashed line), for two different values of α and two different sizes. The horizontal dash-dotted line is the GGE average for $\hat{\rho}_{j_1 j_2}$. The data are obtained using a single realization (see caption of Fig. 4.5 for details).

$$
\begin{aligned}
\Delta_{j_1 j_2} &\equiv \langle \hat{\rho}_{j_1 j_2} \rangle_{\mathrm{GGE}} - \overline{\rho_{j_1 j_2}} \\
&= \langle \hat{c}^\dagger_{j_1} \hat{c}_{j_1} \rangle_{\mathrm{GGE}} \langle \hat{c}^\dagger_{j_2} \hat{c}_{j_2} \rangle_{\mathrm{GGE}} - \left| \langle \hat{c}^\dagger_{j_1} \hat{c}_{j_2} \rangle_{\mathrm{GGE}} \right|^2 - \\
&\qquad - \lim_{t\to\infty} \frac{1}{t} \int_0^t dt' \, \left[G_{j_1 j_1}(t') G_{j_2 j_2}(t') - |G_{j_1 j_2}(t')|^2 \right] \\
&= \lim_{t\to\infty} \frac{1}{t} \int_0^t dt' \, \left[|\delta G_{j_1 j_2}(t')|^2 - \delta G_{j_1 j_1}(t') \delta G_{j_2 j_2}(t') \right] \\
&= \sum_{\mu_1 \mu_2} \left(|u_{j_1 \mu_1}|^2 |u_{j_2 \mu_2}|^2 - u^*_{j_1 \mu_1} u_{j_1 \mu_2} u_{j_2 \mu_1} u^*_{j_2 \mu_2} \right) \left| G^0_{\mu_1 \mu_2} \right|^2 , \qquad (4.50)
\end{aligned}
$$

where we first used the Wick's expansions of $\langle \hat{\rho}_{j_1 j_2} \rangle_{\mathrm{GGE}}$ and $\langle \Psi(t) | \hat{\rho}_{j_1 j_2} | \Psi(t) \rangle$, then used the relationships $\delta G_{j_1 j_2}(t) = G_{j_1 j_2}(t) - \langle \hat{c}^\dagger_{j_1} \hat{c}_{j_2} \rangle_{\mathrm{GGE}}$ and $\overline{G_{j_1 j_2}} = \langle \hat{c}^\dagger_{j_1} \hat{c}_{j_2} \rangle_{\mathrm{GGE}}$ (since GGE works for one-body averages), and finally made use of Eq. (4.45) and of the no-gap-degeneracy assumption. The result is closely reminiscent of Eq. (4.47) for $\delta^2_{j_1 j_2}$, except

that now the weights have two contributions. Using the relation $|G^0_{\mu_1\mu_2}|^2 = |G^0_{\mu_2\mu_1}|^2$ we can finally re-express $\Delta_{j_1j_2}$ as an explicitly positive quantity as follows:

$$\begin{aligned}\Delta_{j_1j_2} &= \frac{1}{2}\sum_{\mu_1\mu_2}\Big[|u_{j_1\mu_1}|^2|u_{j_2\mu_2}|^2 + |u_{j_1\mu_2}|^2|u_{j_2\mu_1}|^2 - \\ &\qquad - \left(u^*_{j_1\mu_1}u_{j_1\mu_2}u_{j_2\mu_1}u^*_{j_2\mu_2} + \text{c.c.}\right)\Big]\left|G^0_{\mu_1\mu_2}\right|^2 \\ &= \frac{1}{2}\sum_{\mu_1\mu_2}\left|u_{j_1\mu_1}u_{j_2\mu_2} - u_{j_1\mu_2}u_{j_2\mu_1}\right|^2\left|G^0_{\mu_1\mu_2}\right|^2 \geqslant 0\,. \end{aligned} \tag{4.51}$$

This explicitly shows that, apart from the trivial cases in which all the terms in the sum are zero (e.g., $j_1 = j_2 = j$, when $\hat\rho_{jj} = \hat n_j\hat n_j = \hat n_j$ becomes a one-body operator for which GGE works and $\Delta_{jj} = 0$), the GGE average overestimates the time average of $\hat\rho_{j_1j_2}(t)$, as exemplified in Fig. 4.7 for a single realization. The question now is whether or not $\Delta_{j_1j_2}$ goes to zero for $L\to\infty$. In Fig. 4.8 we plot the average value of $\Delta_{j_1j_2}$ as a function of L for the same set of quenches presented before. $[\Delta_{j_1j_2}]_{\rm av}$ goes to zero in the thermodynamic limit in the "Extended" phase, and this confirms our general analysis: the real-space Green's functions have vanishing fluctuations in the extended phase, and GGE works for many-body observables with a finite expansion. On the contrary, in the "Localized" phase, $[\Delta_{j_1j_2}]^{\rm G}_{\rm av} = \exp([\ln\Delta_{j_1j_2}]_{\rm av})$ remains finite even in thermodynamic limit, and since $[\Delta_{j_1j_2}]_{\rm av} \geqslant [\Delta_{j_1j_2}]^{\rm G}_{\rm av}$ (by Jensen's inequality, see App. C), this ensures that also $[\Delta_{j_1j_2}]_{\rm av}$ is finite for $L\to\infty$. Clearly, the persistent time fluctuations of the Green's functions lead to time correlations between the $G_{j_1j_2}(t)$ appearing in the expansion of $\rho_{j_1j_2}(t)$, see Eq. (4.24), which reduce the time average with respect to the corresponding "sum of products" of time averages.

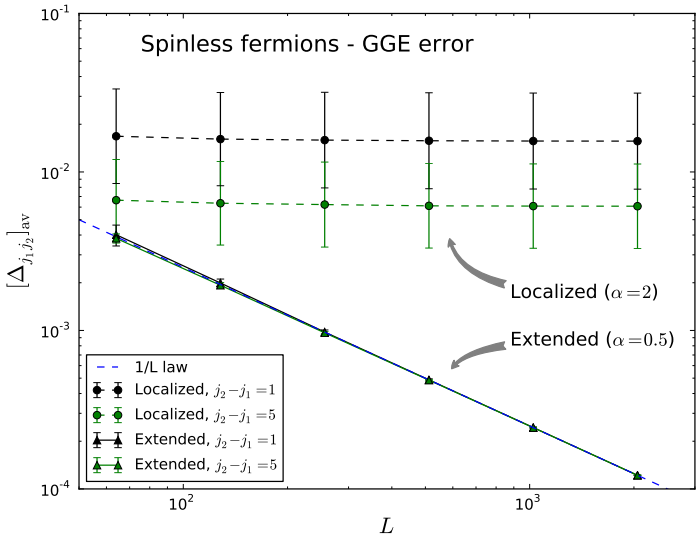

Figure 4.8.: Average value of $\Delta_{j_1j_2} = \langle\hat\rho_{j_1j_2}\rangle_{\rm GGE} - \overline{\rho_{j_1j_2}}$, the discrepancy between the GGE average and the time average, for the density-density correlation $\hat\rho_{j_1j_2} = \hat n_{j_1}\hat n_{j_2}$, as a function of the chain size, for with $j_1 = L/2$ and two values of $j_2 - j_1$. The data are obtained using the same quenches of Fig. 4.6 (see its caption for details). In the localized phase ($\alpha = 2$) we plot the median $[\Delta_{j_1j_2}]^{\rm G}_{\rm av} = \exp([\ln\Delta_{j_1j_2}]_{\rm av})$ because $\Delta_{j_1j_2}$ is there roughly log-normal distributed.

4.6 QUENCHES WITH ISING CHAINS IN TRANSVERSE FIELD

Let us now consider quenches with disordered Ising chains in transverse field, whose Hamiltonian and properties are described in Sec. 3.3. The most important difference

with respect to the tight-binding chains used in the previous sections is the presence of particle non-conserving (BCS-like) terms, which mix particles and holes. Because of that, it is convenient to work with Nambu vectors, see Sec. 3.3, which make the algebra similar to the previous one, with very similar results. In particular, we will show that, due to disorder and localization of eigenstates, the time fluctuations of the local magnetization $\hat{\sigma}^z_j = 2\hat{c}^\dagger_j \hat{c}_j - 1$ remain finite; however, considering for instance, the total magnetization $\hat{m}_z = \sum_j \hat{\sigma}^z_j / L$ which is extended over the whole chain, introduces an infinite summation which effectively leads to a self-averaging of time fluctuations. Computations and results shown in this section are published in Ref. [90].

Starting from Eq (4.11), assuming no energy degeneracy, the time fluctuations of $\mathcal{G}_{j_1 j_2}(t)$ read:

$$\delta\mathcal{G}_{j_1 j_2}(t) = \sum_{\mu_1 \neq \mu_2} U^*_{j_1 \mu_1} U_{j_2 \mu_2} e^{2i(\tilde{\epsilon}_{\mu_1} - \tilde{\epsilon}_{\mu_2})t} \mathcal{G}^0_{\mu_1 \mu_2} \,. \tag{4.52}$$

In computing the time-averaged squared fluctuations of $\mathcal{G}_{j_1 j_2}(t)$:

$$\delta^2_{j_1 j_2} \equiv \lim_{t\to\infty} \frac{1}{t} \int_0^t dt' \, \left|\delta\mathcal{G}_{j_1 j_2}(t')\right|^2 \,, \tag{4.53}$$

we have to take care of gap degeneracies due to the particle-hole symmetry of the spectrum $\tilde{\epsilon}_\mu$. To get compact equations we associate to every index $\mu \in [1, L]$ (such that $\hat{\Gamma}_\mu = \hat{\gamma}_\mu$, with energy $\tilde{\epsilon}_\mu > 0$) an index $\bar{\mu} = \mu + L \in [L+1, 2L]$ (associated to $\hat{\Gamma}_{\mu+L} = \hat{\gamma}^\dagger_\mu$, and with energy $-\tilde{\epsilon}_\mu$); similarly, for every $\mu \in [L+1, 2L]$ we define $\bar{\mu} = \mu - L \in [1, L]$. Using this notation and taking due care of the particle-hole symmetry, the value of $\delta^2_{j_1 j_2}$ turns out to be:

$$\begin{aligned}
\delta^2_{j_1 j_2} &= \sum_{\mu_1 \neq \mu_2} \sum_{\nu_1 \neq \nu_2} \overline{e^{i(\tilde{\epsilon}_{\mu_1} - \tilde{\epsilon}_{\mu_2} - \tilde{\epsilon}_{\nu_1} + \tilde{\epsilon}_{\nu_2})t}} U^*_{j_1 \mu_1} U_{j_2 \mu_2} U_{j_1 \nu_1} U^*_{j_2 \nu_2} \mathcal{G}^0_{\mu_1 \mu_2} \mathcal{G}^0_{\nu_2 \nu_1} \\
&= \sum_{\mu_1 \neq \mu_2} \left|U_{j_1 \mu_1}\right|^2 \left|U_{j_2 \mu_2}\right|^2 \left|\mathcal{G}^0_{\mu_1 \mu_2}\right|^2 - \sum_{\substack{\mu_1 \neq \mu_2 \\ \mu_1 \neq \bar{\mu}_2}} U^*_{j_1 \mu_1} U_{j_2 \mu_2} U_{j_1 \bar{\mu}_2} U^*_{j_2 \bar{\mu}_1} \left|\mathcal{G}^0_{\mu_1 \mu_2}\right|^2 \,,
\end{aligned} \tag{4.54}$$

where the over-line denotes the infinite-time average, and we used the relation $\hat{\Gamma}_\mu = \hat{\Gamma}^\dagger_{\bar{\mu}}$. The first term is due to the cases in which $\mu_1 = \nu_1$ and $\mu_2 = \nu_2$, similarly to what is found in Eq. (4.46). The second term originates from particle-hole symmetry (present even when the system is disordered) and occurs when $\mu_1 = \bar{\nu}_2$ and $\mu_2 = \bar{\nu}_1$. Similar to what we have done for the tight-binding Hamiltonians, one can show that (the proof is in App. D):

$$\sum_{\mu_1 \mu_2} |\langle \Psi_0 | \hat{\Gamma}^\dagger_{\mu_1} \hat{\Gamma}_{\mu_2} | \Psi_0 \rangle|^2 = L \,. \tag{4.55}$$

Moreover, using the fact that $U^\dagger U = 1$ we can repeat the same observations presented in Sec. 4.4 and Subsec. 4.5.1: if the eigenstates are delocalized (clean chain case) $\delta^2_{j_1 j_2}$ goes to zero for $L \to \infty$, while $\delta^2_{j_1 j_2}$ remains finite when the eigenstates are localized. For any finite disorder amplitude ϵ, the Hamiltonian $\hat{H}_{XY}$ has always localized states (see Sec. 3.3). This localization leads to persistent time fluctuations: $\delta^2_{j_1 j_2} > 0$ in the thermodynamic limit. This is shown in Fig. 4.9 where we plot the average value of $\delta^2_{\sigma^z_j} = 4\delta^2_{jj}$ (where $\delta^2_{\sigma^z_j}$ is the mean squared fluctuation associated to the observable σ^z_j) for a quench from the ground state of a clean Ising chain at the critical point ($\epsilon = 0$, $\gamma = 1$, $J_j = 1$, and $h_j = 1$) to a disordered Ising chain at the infinite randomness critical point ($\epsilon = 1$, $\gamma = 1$, $J_j \in [0, 2]$, and $h_j \in [0, 2]$) [76].

We now show that, while each $\hat{c}^\dagger_j \hat{c}_j$ has non-vanishing time fluctuations, the average magnetization per site $\hat{m}_z = \sum_j \hat{\sigma}^z_j / L = 2 \sum_{j=1}^L \hat{\Psi}^\dagger_j \hat{\Psi}_j / L - 1$ has vanishing time

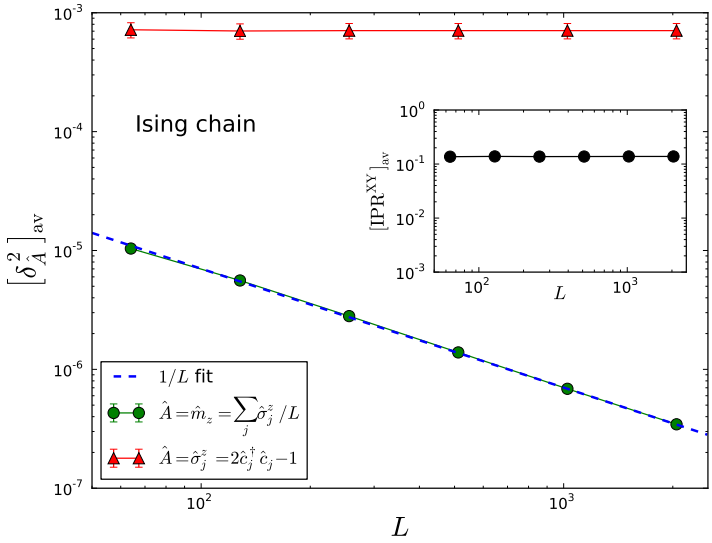

Figure 4.9.: Value of the mean squared fluctuation $\delta^2_{\hat{A}}$, with $\hat{A}$ the local transverse magnetization $\hat{\sigma}^z_j$ or the average magnetization per site $\hat{m}_z$, as a function of the chain size. The initial state is the ground state of a clean Ising chain at the critical point ($\epsilon = 0$, $\gamma = 1$, $J_j = 1$, and $h_j = 1$) and the final Hamiltonian is a disordered Ising chain at the infinite-randomness critical point ($\epsilon = 1$, $\gamma = 1$, $J_j \in [0, 2]$, and $h_j \in [0, 2]$). Data obtained with 50 disorder realizations. For a smoother size scaling, each disorder realization of the largest L generated is employed, by removing the same amount of sites from the two edges, to generate realizations for smaller L. For $\hat{A} = \hat{\sigma}^z_j$ we plot the median $[\delta^2_{\sigma^z_j}]^{G}_{av} = \exp([\ln \delta^2_{\sigma^z_j}]_{av})$ because $\delta^2_{\sigma^z_j}$ is roughly log-normal distributed.

fluctuations for large L, due to cancellations reminiscent of self-averaging in extensive observables [100]. Indeed, $\delta m_z(t) = 2\sum_{j=1}^{L} \delta G_{jj}(t)/L$, which implies that:

$$\delta m_z(t) = \sum_{\mu_1 \neq \mu_2} \left(\frac{2}{L} \sum_{j=1}^{L} U^*_{j\mu_1} U_{j\mu_2} \right) e^{2i(\tilde{\epsilon}_{\mu_1} - \tilde{\epsilon}_{\mu_2})t} \mathcal{G}^0_{\mu_1\mu_2} \, ,$$

i.e., an expression entirely similar to Eq. (4.52) for $\delta G_{j_1 j_2}(t)$ except for the weight $U^*_{j_1\mu_1} U_{j_2\mu_2}$ which is now replaced by the averaged weight $w_{\mu_1\mu_2} = 2\sum_j U^*_{j\mu_1} U_{j\mu_2}/L$. With the same steps done to obtain Eq. (4.54), we finally get that the mean squared long-time fluctuations of $\hat{m}_z$ are:

$$\delta^2_{\hat{m}_z} = \sum_{\mu_1 \neq \mu_2} |w_{\mu_1\mu_2}|^2 \left|\mathcal{G}^0_{\mu_1\mu_2}\right|^2 - \sum_{\substack{\mu_1 \neq \mu_2 \\ \mu_1 \neq \overline{\mu_2}}} w_{\mu_1\mu_2} w^*_{\overline{\mu_1}\mu_2} \left|\mathcal{G}^0_{\mu_1\mu_2}\right|^2 , \tag{4.56}$$

which is definitely different from Eq. (4.54), the site average having been performed before taking the squared time fluctuations. In Fig. 4.9 we plot $\delta^2_{\hat{m}_z}$, i.e. the mean squared fluctuation associated to $\hat{m}_z$, averaged over disorder realizations, as a function of the chain size L: we clearly see that, even if the eigenstates of $\hat{H}_{XY}$ are localized, the time fluctuations of $\hat{m}_z$ decay, and $\delta^2_{\hat{m}_z} \to 0$ in the thermodynamic limit. This behavior for $\hat{m}_z$ is similar to that of the Green's functions $G_{k_1 k_2}(t)$ for the disordered long-range hopping fermions analyzed in Sec. 4.5.1, where the infinite site summations lead to a cancellation of the time fluctuations of the various terms.

4.7 DISCUSSION OF THE RESULTS

Let us discuss some of the most relevant recent papers appeared in the literature, in the light of what we have presented in this chapter.

A detailed analysis of the validity of GGE averages for quantum quenches where the final Hamiltonian is integrable, disorder-free, and translationally invariant (the 1D quantum Ising/XX spin chains and the Luttinger model) has been made by Cazalilla *et al.* [23], showing that, for a general class of initial states $|\Psi_0\rangle$, the time fluctuations of the one-body Green's functions vanish and the GGE averages are correct, in the thermodynamic limit, for both local and nonlocal observables. These results are in complete agreement with what we have shown here, since homogeneous Hamiltonians have extended eigenstates and the time fluctuations of the one-body Green's functions decay for $t \to \infty$. In our study, we have extended the analysis of Ref. [23] to quantum quenches with a final Hamiltonian $\hat{H}$ which is disordered: we have shown that the localization properties of $\hat{H}$ are crucial for the relaxation of time fluctuations and, ultimately, also for the validity of the GGE. In particular, we showed that, for one-body operators, infinite-time averages are always reproduced by GGE, while for many-body operators, the localization of eigenstates of $\hat{H}$ and the ensuing absence of relaxation of one-body real-space Green's functions are, in principle, dangerous for the validity of GGE.

Given a finite-size system and an observable $\hat{A}$, we can think of the expectation value $A(t)$ as a random variable. Its probability distribution $P(A)$ is the probability density to find $A(t)$ equal to A at any time t from $t = 0$ to $t \to \infty$. [3] For integrable Hamiltonians, Venuti *et al.* [101] have conjectured that, in most cases, for the time fluctuations of a finite system of size L a central limit theorem can be formulated, leading to what they call "Gaussian equilibration": $P(A)$ displays a Gaussian distribution with a standard deviation $\sigma_A/\overline{A}$ which decreases as $1/\sqrt{L}$ for large L. They corroborated this conjecture with numerical computations using clean XY and tight-binding models, and extensive observables: the total magnetization in the XY model and the number of particles in a portion of the chain in the tight-binding model. If we take $\hat{A} = \hat{c}^\dagger_{j_1}\hat{c}_{j_2}$, we have that $A(t) = G_{j_1 j_2}(t)$, and the mean squared fluctuation $\delta^2_{j_1 j_2}$, defined in Eq. (4.34), is exactly the variance σ^2_A of $P(A)$ just introduced. In our results, in agreement with the "Gaussian equilibration" conjecture, $\delta^2_{j_1 j_2}$ goes like $1/L$ when the long-time fluctuations vanish in the thermodynamic limit (i.e., when the final Hamiltonian has extended eigenstates). We have also seen that this is not true for all observables and quenches: $\delta^2_{j_1 j_2}$ doesn't vanish when the single-particle eigenstates of the after-quench Hamiltonian are localized. Notice however that, unlike the observables considered in Ref. [101], the operator $\hat{c}^\dagger_{j_1}\hat{c}_{j_2}$ is local in space. For instance, in the Ising/XY chain, we have seen that the mean squared fluctuation $\delta^2_{\hat{m}_z}$ of the total magnetization (i.e., the sum of all the local magnetizations), vanishes as $1/L$, even in presence of disorder. This is in agreement with the "Gaussian equilibration" conjecture for extensive observables.

Quantum quenches with integrable Hamiltonians having a transition between extended and localized states have been analyzed in two recent works, by Gramsch *et al.* [102] and Kay *et al.* [103]. They have studied the Aubry-André model [85] for fermions [103] and hard-core bosons [102, 103] in a one-dimensional quasiperiodic potential. For fermions, the Hamiltonian is

$$\hat{H}_f = \sum_{j=1}^{L-1} (\hat{c}^\dagger_j \hat{c}_{j+1} + \text{h.c.}) + \lambda \sum_{j=1}^{L} \cos(2\pi\sigma j)\hat{n}^f_j \,, \tag{4.57}$$

where $\hat{c}^\dagger_j$ ($\hat{c}_j$) creates (annihilates) a fermion at site j, $\hat{n}^f_j \equiv \hat{c}^\dagger_j \hat{c}_j$, while for bosons:

$$\hat{H}_b = \sum_{j=1}^{L-1} (\hat{b}^\dagger_j \hat{b}_{j+1} + \text{h.c.}) + \lambda \sum_{j=1}^{L} \cos(2\pi\sigma j)\hat{n}^b_j \,, \tag{4.58}$$

where $\hat{b}^\dagger_j$ ($\hat{b}_j$) creates (annihilates) a hard-core boson at site j, $\hat{n}^b_j \equiv \hat{b}^\dagger_j \hat{b}_j$; in both cases σ is an irrational number, and λ is the strength of the quasiperiodic potential. For these

3 $P(A)$ is a Dirac delta if the fluctuations of $A(t)$ vanishes at long times, but here we are considering finite systems, for which time fluctuations do not vanish.

Hamiltonians the quasiperiodic on-site potential is able to induce a transition to a phase with localized eigenstates [85] at a finite strength of $\lambda = 2$.

Let us first focus on the fermionic Hamiltonian $\hat{H}_f$. Ref. [103] [4] considers two one-body operators, the local density $\hat{n}^f_j$, and the momentum distribution

$$\hat{m}^f_k = \frac{1}{L}\sum_{j_1 j_2} e^{ik(j_1-j_2)}\hat{c}^\dagger_{j_1}\hat{c}_{j_2} \, .$$

The time evolutions of these operators coincide exactly with the diagonal Green's functions $G_{jj}(t)$ and $G^k_{kk}(t)$ defined in Eqs. (4.41). Ref. [103] shows that, when the single-particle eigenstates of the final Hamiltonian are extended ($\lambda < 2$), independently from the initial value of λ, the long-time fluctuations of $\hat{n}^f_j$ vanishes in the thermodynamic limit, while the long-time fluctuations of $\hat{m}_k$ remain finite. The opposite situation is found when the single-particle eigenstates are localized ($\lambda > 2$). For quenches with the Hamiltonian $\hat{H}_{lrh}$, we have seen that the long-time fluctuations of $G^k_{kk}(t)$ always vanish in the thermodynamic limit, both when the after-quench Hamiltonian is in the extended phase (i.e., $\alpha < 1$) and in the localized phase (i.e., $\alpha > 1$). This difference is due to the self-duality of the Aubry-André model [104]: for $\hat{H}_f$, single-particle extended states in real space are localized in momentum space, and localized states in real space are extended in momentum space. For $\hat{H}_{lrh}$, on the contrary, the states are extended in momentum space in both phases. Therefore, the results for $G_{jj}(t)$ and $G^k_{kk}(t)$ presented in Ref. [103] are in perfect agreement with the analysis of the present chapter.

Let us now focus on the results for the bosonic Hamiltonian $\hat{H}_b$. This Hamiltonian can be diagonalized by mapping it, through the usual Jordan-Wigner transformation [77], onto the fermionic version of the same Hamiltonian $\hat{H}_f$. The difference between the two models arises from the non-local nature of the Jordan-Wigner transformation: in the bosonic Hamiltonian, one-body operators in term of bosons, may become many-body operators when rewritten in terms of fermions, due to the so-called Jordan-Wigner string [77]. Ref. [102] considered, among others, the bosonic local density $\hat{n}^b_j$, which remains a one-body operator even in terms of fermions, and the momentum distribution for bosons $\hat{m}^b_k = \sum_{j_1 j_2} e^{ik(j_1-j_2)}\hat{b}^\dagger_{j_1}\hat{b}_{j_2}/L$, a many-body operator when written in terms of fermions. Since $\hat{n}^b_j = \hat{n}^f_j$, as just discussed, the results for $\hat{n}^b_j$ are in agreement with what we have shown in this chapter. Concerning $\hat{m}^b_k$, the numerical results of Ref. [102] show that, when the eigenstates of the final Hamiltonian are extended ($\lambda < 2$), the long-time fluctuations vanish, and GGE predicts the time averages quite well, consistently with our analysis; when the eigenstates of the final Hamiltonian are localized ($\lambda > 2$), the situation is more complex: the time fluctuations of $\hat{m}^b_k$ appear to vanish, but GGE seems to fail. The failure of GGE in predicting time averages of a many-body observable like $\hat{m}^b_k$ when persistent time fluctuations of the one-body Green's functions are at play (localized phase, $\lambda > 2$) is perfectly in line with our results (see Sec. 4.5.2). What is definitely beyond our analysis, but not in contradiction with it, is the fact that the time fluctuations of $\hat{m}^b_k$ relax for large t: this is likely an effect of cancellation of fluctuations due to the summation of many terms, similar to what we have found for extensive operators (see Sec. 4.6) or for momentum space Green's functions (see Sec. 4.5.1).

Another paper quite relevant for our study is that of Khatami *et al.* [29], where they analyze quenches with a final Hamiltonian similar to our $\hat{H}_{lrh}$, Eq. (3.20), supplemented by an interaction term $V\sum_i(\hat{n}_i - 1/2)(\hat{n}_{i+1} - 1/2)$ which in principle makes the problem non-integrable. Two comments are in order here. First, as shown in Ref. [29], interactions do not change the picture dramatically: numerically, a metal-insulator transition occurs around $\alpha \sim 1 \div 1.2$, with a quite clear metallic phase for $\alpha \lesssim 1$, and an

4 Ref. [103] also proves that the GGE describes the time averages of any one-body observables, the same relation we have shown in Sec 4.2.1 and published in Ref. [90] before Ref. [103] appeared. The proof given is slightly different from ours: one projects the operator $\hat{\rho}(t) \equiv |\Psi(t)\rangle\langle\Psi(t)|$ onto the single-particle sector of the Hilbert space, and then shows that its time average is equal to corresponding single-particle density matrix predicted by the GGE.

insulating one for $\alpha \gtrsim 1.2$. Second, by comparing after-quench time averages with the microcanonical average for the momentum distribution function $\hat{c}_k^\dagger \hat{c}_k$ and the density-density structure factor $\sum_{ml} e^{ik(l-m)} \hat{n}_l \hat{n}_m / L$, Ref. [29] shows that quenches in the metallic phase ($\alpha \lesssim 1$) are well described by the microcanonical ensemble, while thermalization appears to break down when quenching to the insulating phase ($\alpha \gtrsim 1.2$). These results are definitely in line with what we have found, and suggest that, independently of the integrability of the Hamiltonian, the localization properties of $\hat{H}$ are crucial for the after-quench thermalization.

Quenches with disordered spin-1/2 quantum Ising chain with random on-site disorder both in the longitudinal couplings and in the transverse field are studied in Ref. [28]. They examine the behavior of the two-point correlator of the order parameter $\hat{\sigma}^x$, i.e., $C_t^{xx}(t', r) \equiv \langle \Psi(t)|\hat{\sigma}^x_{L/2}(t')\hat{\sigma}^x_{L/2+r}|\Psi(t)\rangle$. We focus here on their results for the equal-time correlation $C_t^{xx}(r) \equiv C_t^{xx}(t' = 0, r)$, and we denote by $C^{xx}_{GGE}(r)$ the corresponding GGE value. The observable $\hat{\sigma}^x_{L/2}\hat{\sigma}^x_{L/2+r}$ is, in terms of Jordan-Wigner fermions, a r-body operator involving $\hat{c}_j$ and $\hat{c}_j^\dagger$ with $j = L/2, \ldots, L/2 + r$. This means that, at any fixed value of r, the Wick's expansions of $C_t^{xx}(r)$ and $C^{xx}_{GGE}(r)$ have a finite number of terms and can be written, apart for a sign, as the Pfaffian of a $2r \times 2r$ matrix [77]. Therefore, in the light of what we have seen in this chapter, we can expect two things: i) the time fluctuations of $C_t^{xx}(r)$ do not vanish in the long-time limit, and ii) the GGE averages might fail in estimating its time average. For any finite value of disorder Caneva *et al.* [28] show that the disorder average of $|C^{xx}_{GGE}(r)|$ is different from the disorder average of $|C_t^{xx}(r)|$ (notice that the latter value is computed at a given time t, and it is not a time average). They also show that while the average value of $|C_t^{xx}(r)|$ tends to a constant value for $r \to \infty$, the GGE average decays exponentially. [5]

Finally, let us mention a technical point related to the relaxation of time fluctuations of general many-body operators for non-integrable models [105, 106]. In principle, with the technique we have used for one-body Green's functions of free-particle models, one could compute the time-averaged squared fluctuation $\lim_{t\to\infty} 1/t \int_0^{t'} dt' \, |\delta A(t')|^2$ for a general operator $\hat{A}$, starting from Eq. (2.23). However, to make progress, one would need to stipulate something about gap degeneracies in the many-body spectrum, i.e., $E_\alpha - E_\beta = E_{\alpha'} - E_{\beta'}$ with $\alpha \neq \alpha'$ and $\beta \neq \beta'$ (apart from the trivial case $\alpha = \beta$ and $\alpha' = \beta'$). (The assumption of the absence of gap degeneracies is often used in the literature, and dates back to the original paper of von Neumann [2, 3], who, however, carefully stipulates it to hold only within each microcanonical energy shell, and not for the many-body spectrum at large.) The condition of absence of gap degeneracies [105] is clearly untenable for models with non-interacting quasiparticles: you can produce an exponentially large number of many-body states $|\alpha'\rangle$ and $|\beta'\rangle$ whose spectral gap $E_{\alpha'} - E_{\beta'}$ coincides exactly with $E_\alpha - E_\beta$: simply operate on $|\alpha\rangle$ and $|\beta\rangle$ by applying, in identical fashion, an arbitrary number of particles and/or holes, $|\alpha'\rangle = \hat{\gamma}^\dagger_{\mu_1}\hat{\gamma}^\dagger_{\mu_2}\cdots\hat{\gamma}^\dagger_{\mu_n}|\alpha\rangle$, and $|\beta'\rangle = \hat{\gamma}^\dagger_{\mu_1}\hat{\gamma}^\dagger_{\mu_2}\cdots\hat{\gamma}^\dagger_{\mu_n}|\beta\rangle$. Then $E_{\alpha'} - E_\alpha = E_{\beta'} - E_\beta = \epsilon_{\mu_1} + \epsilon_{\mu_2} + \cdots \epsilon_{\mu_n}$ because quasiparticles do not interact, and therefore $E_{\alpha'} - E_{\beta'} = E_\alpha - E_\beta$. One might argue that this proliferation of exactly degenerate gaps is a peculiarity of models with non-interacting quasiparticles [106]: interaction effects might change the picture completely. This is definitely an interesting point, which deserves further studies, but certainly also a very hard one, because the combination of disorder and interactions makes the analysis highly non-trivial. Nevertheless, let us mention the following simple argument. Suppose that quasiparticles interact, but there is still an exponentially large (in the number of particles N) number of states with very small spectral gap differences Δ: $E_\alpha - E_\beta = E_{\alpha'} - E_{\beta'} + \Delta$. Then, all these spectral gap quasi-degeneracies will appear,

5 Even thought this might be a signature of the fact that GGE is failing, as we indeed expect, there is a technical issue to point out, related to the presence of an absolute value before taking the disorder average: from our analysis, we expect that the time fluctuations of $C_t^{xx}(r)$ do not vanish, but there is no reason to expect that $[|C_t^{xx}(r)|]_{av}$, at any fixed t, should coincide with $[|\overline{C_t^{xx}(r)}|]_{av}$, even if $[\overline{C_t^{xx}(r)}]_{av} = [C^{xx}_{GGE}(r)]_{av}$.

effectively, as true degeneracies until a time $t \sim \hbar/\Delta$ is reached, and that time might indeed be very large.

5 WEIGHTED WANG-LANDAU ALGORITHM

As seen in the previous chapters, interesting quantities often involve a sum over the Hilbert space basis set which can be a source of some difficulty, even when considering quadratic fermionic models, as we have restricted to. Consider, for instance, the diagonal average of an observable $\hat{A}$ after a quench of the Hamiltonian from $\hat{H}_0$, with initial state $|\Psi_0\rangle$, to $\hat{H}$:

$$\langle \hat{A} \rangle_D \equiv \sum_\alpha |c_\alpha|^2 A_{\alpha\alpha} \, . \tag{5.1}$$

Here, in principle, we should take the sum over all the (many-body) eigenstates $|\alpha\rangle$ of $\hat{H}$, an exponentially large number of states, calculating for each of them $c_\alpha \equiv \langle \alpha | \Psi_0 \rangle$ and the associated matrix element $A_{\alpha\alpha} \equiv \langle \alpha | \hat{A} | \alpha \rangle$. The quadratic nature of the problem will make life easy because we can avoid the exponentially large Hilbert space sum by switching to a dynamical time-dependent quantity which can be easily expressed in terms of single-particle Green's functions. [1] But suppose that you want to know more than just the diagonal average $\langle \hat{A} \rangle_D$, and pretend to have information on the whole distribution of the values of $A_{\alpha\alpha}$ accessed after the quench [8, 52], i.e.,

$$\rho_D(A) \equiv \sum_\alpha |c_\alpha|^2 \, \delta(A - A_{\alpha\alpha}) \, , \tag{5.2}$$

of which $\langle \hat{A} \rangle_D$ is just the average: $\langle \hat{A} \rangle_D = \int dA \, \rho_D(A) \, A$. Here there is, evidently, a problem: knowing the distribution of A requires exploring the full many-body Hilbert space, summing over the eigenstates $|\alpha\rangle$, and this exhaustive enumeration would restrict our calculations to exceedingly small sample sizes, although all information on c_α and $A_{\alpha\alpha}$ can be calculated by just solving one-body problems (hence, for much larger sizes). A similar problem occurs in considering, for instance, the corresponding generalized Gibbs ensemble (GGE) average: [2]

$$\langle \hat{A} \rangle_{GGE} \equiv \sum_\alpha \frac{e^{-\sum_\mu \lambda_\mu n_\mu^\alpha}}{Z_{GGE}} A_{\alpha\alpha} \, , \tag{5.3}$$

where μ labels the quasiparticle modes of $\hat{H}$, $n_\mu^\alpha \equiv \langle \alpha | \hat{c}_\mu^\dagger \hat{c}_\mu | \alpha \rangle = 0, 1$ are the fermionic occupations of state $|\alpha\rangle$, Z_{GGE} is the GGE partition function, and the Lagrange multipliers λ_μ are fixed by requiring $\langle \Psi_0 | \hat{c}_\mu^\dagger \hat{c}_\mu | \Psi_0 \rangle = \langle \hat{c}_\mu^\dagger \hat{c}_\mu \rangle_{GGE}$. Once again, this average is rather trivially calculated in terms of single-particle quantities, for the quadratic problems we are dealing with, but the corresponding distribution [3]

$$\rho_{GGE}(A) \equiv \sum_\alpha \frac{e^{-\sum_\mu \lambda_\mu n_\mu^\alpha}}{Z_{GGE}} \delta(A - A_{\alpha\alpha}) \, , \tag{5.4}$$

1 If $\hat{A}$ is a one-body operator we can use Eq. (4.20), while if it is many-body we have $\langle \hat{A} \rangle_D = \overline{A} = \lim_{t\to\infty} 1/t \int_0^t dt' \, A(t')$, where $A(t') \equiv \langle \Psi(t) | \hat{A} | \Psi(t) \rangle$ can be expanded with the Wick's theorem. A practical example is the $\overline{\rho_{j_1 j_2}}$ computed in Eq. (4.50).

2 The generalized Gibbs ensemble is the relevant ensemble for quenches with quadratic fermionic models, but a similar situation occurs for the usual statistical ensembles, i.e., microcanonical, canonical and grand-canonical.

3 Concerning the issue of thermalization after a quench, we might indeed expect that, if $\hat{A}$ thermalizes, not only the mean values of $\rho_D(A)$ and $\rho_{GGE}(A)$ are equal, i.e., $\langle \hat{A} \rangle_D \equiv \int dA \, \rho_D(A) A = \langle \hat{A} \rangle_{GGE} \equiv \int dA \, \rho_{GGE}(A) A$, but also the two distributions should have a somewhat "similar look" in the thermodynamic limit; at least this is what a good statistical ensemble should do.

requires a difficult sum over the Hilbert space. [4]

Quite generally, we might summarize the problem as follows: how can we obtain information on weighted distributions (or density of states)

$$\rho_w(A) \equiv \sum_\alpha w_\alpha \delta(A - A_\alpha) \,, \tag{5.5}$$

with positive weights [5] w_α, when both w_α and A_α are "easily calculated" but the sum over α runs over an exponentially large "configurations space"?

In this chapter we will introduce a Monte Carlo method — obtained by a rather natural extension of the Wang-Landau algorithm (WLA) [41–43] — which will allow us to compute weighted distributions of the form of Eq. (5.5). The WLA, proposed in 2001 by F. Wang and D.P. Landau, is a Monte Carlo method designed to compute the density of states of a classical statistical mechanics problem. The algorithm performs a non-Markovian random walk to build the density of states by overcoming the prohibitively long time scales typically encountered near phase transitions or at low temperatures. Besides the classical Ising and Potts models studied in the original papers [41–43], the method has been applied to the solution of numerical integrals [107], folding of proteins [108] and many other problems.

Here is the plan of the chapter. In Sec. 5.1 we briefly summarize the WLA. In Sec. 5.2 we show how this algorithm can be extended to compute weighted densities of states. In Sec. 5.3 we apply this algorithm, for illustration purposes, to the computation of the free energy as a function of magnetization for the classical two-dimensional Ising model. Finally in Sec. 5.4 we show how the weighted-WLA can be used to compute distributions related to quantum quenches with quadratic fermionic models.

5.1 WANG–LANDAU ALGORITHM

In this section we briefly overview the Wang-Landau algorithm (WLA) by describing the method, with a few useful remarks.

Let us consider a classical system with a discrete configuration space (for instance, the two-dimensional Ising model). Let us denote with α a configuration (state) of the system and with A_α the value that a given physical quantity assumes on such a state. The distribution function of the values of A_α is defined as:

$$\rho(A) \equiv \frac{1}{N} \sum_\alpha \delta_{A A_\alpha} \,, \tag{5.6}$$

where δ_{xy} is the Kronecker delta (for real variables) and N is the total number of states. [6] When an exhaustive enumeration is not feasible (the configuration space usually increases exponentially with the system size) the computation of $\rho(A)$ requires an approximate numerical approach. The WLA is a powerful Monte Carlo algorithm to compute $\rho(A)$. The idea behind the algorithm originates from the following observation: Let us consider a Monte Carlo procedure where, from an initial state α we generate a new α' with probability $T(\alpha'|\alpha)$, which we assume to be ergodic (i.e., any state can

4 In some cases, for the GGE ensemble, some analytical progress might follow from appropriately representing the Dirac's delta, for instance as:

$$\delta(x) = \frac{1}{2\pi i} \lim_{\epsilon \to 0} \left(\frac{1}{x - i\epsilon} - \frac{1}{x + i\epsilon} \right) .$$

(Private communication by Fabio Franchini.) Alternatively, one might try to compute the generating function of the distribution moments by taking the Fourier transform of $\rho_{GGE}(A)$. We have not explored these possibilities.

5 Evidently $w_\alpha = |c_\alpha|^2$ for the diagonal distribution above, while $w_\alpha = e^{-\sum_\mu \lambda_\mu n_\mu^\alpha} / Z_{GGE}$ for the GGE distribution.

6 The presence of the Kronecker delta, in place of the Dirac delta, is essentially due to the fact that to compute physical quantities we will use discrete sums over the possible values of A_α, rather than continuous integrals.

be reached from any other state in a finite number of steps), and we accept α' with probability:

$$R(\alpha'|\alpha) \equiv \text{Min}\left[1, \frac{\tilde{\rho}(A_\alpha)}{\tilde{\rho}(A_{\alpha'})}\frac{T(\alpha|\alpha')}{T(\alpha'|\alpha)}\right] , \tag{5.7}$$

where $\tilde{\rho}(A)$ is a given function of A. This is, in essence, a Metropolis Monte Carlo algorithm designed to converge towards an equilibrium distribution given by $P(\alpha) = c/\tilde{\rho}(A_\alpha)$, where c is a normalization constant. [7] Now suppose that at each Monte Carlo step we update a histogram $h(A)$ with the rule $h(A_\alpha) \to h(A_\alpha) + 1$, where α is the visited state (i.e., the new proposed state α' if accepted, the original α if α' is rejected). At equilibrium, after N_s steps, the mean histogram is:

$$\begin{aligned} h(A) = \sum_\alpha N_s P(\alpha)\delta_{AA_\alpha} = cN_s \sum_\alpha \frac{1}{\tilde{\rho}(A_\alpha)}\delta_{AA_\alpha} &= \frac{cN_s}{\tilde{\rho}(A)}\sum_\alpha \delta_{AA_\alpha} \\ &= cN_s N\frac{\rho(A)}{\tilde{\rho}(A)} , \end{aligned} \tag{5.8}$$

where we used the expression of $P(\alpha)$ and the definition of $\rho(A)$ in Eq. (5.6). Therefore, if $\tilde{\rho}(A)$ is a good approximation to $\rho(A)$, this random walk generates, apart for statistical fluctuations, a flat histogram $h(A)$. We have, in this way, a tool for checking if a proposed $\tilde{\rho}(A)$ is a good approximation for $\rho(A)$, but we still don't know how to generate it. The WLA is an algorithm in which $\tilde{\rho}(A)$ improves while the Monte Carlo walk is going on. The steps are the following:

Wang-Landau algorithm

(0) fix a modification factor $f > 1$, and set $\ln \tilde{\rho}(A) = 0$ and $h(A) = 0$ for all possible values of A;

(1) start the random walk using Eq. (5.7) and update at each step the histogram $h(A)$ and the density of states $\tilde{\rho}(A)$ with the rules $h(A_\alpha) \to h(A_\alpha) + 1$ and $\ln \tilde{\rho}(A_\alpha) \to \ln \tilde{\rho}(A_\alpha) + \ln f$;

(2) stop the random walk when $h(A)$ is almost flat (this condition can be implemented in many ways; here we require, as in the original papers, that $h(A) > 0.8\overline{h}$ for all values of A, where $\overline{h}$ is the mean histogram value). From the previous analysis, $\tilde{\rho}(A)$ is a good approximation of $\rho(A)$ (more precisely: $\ln \tilde{\rho}(A)$ is a good approximation of $\ln \rho(A)$ with a discrepancy of order $\ln f$);

(3) reduce the value of $f \to \sqrt{f}$, reset $h(A) = 0$ and restart from step (1). Stop the loop when $\ln f$ is smaller than the desired value of discrepancy ϵ.

A few important observations are in order: (i) With this procedure we violate the detailed balance because, at each step, we update the density of states $\tilde{\rho}(A)$ and this could, in principle, harm the convergence to a flat histogram $h(A)$. (ii) Why $\tilde{\rho}(A)$ should actually converge towards $\rho(A)$? The answer comes by looking at Eq. (5.8): if we accept too many times states with a given value of A (i.e., $h(A)$ is large for this value), this means that $\tilde{\rho}(A)$ is underestimated with respect to $\rho(A)$ and therefore increasing $\tilde{\rho}(A)$ we get closer to the true density. (iii) Why the density of states update is multiplicative, i.e. linear in logarithmic scale? This is due to the exponential behavior of the density of states: $\rho(A)$ in different histogram bins has usually differences of orders of magnitude and a linear update would slow down the convergence. (iv) At the end of the computation $\tilde{\rho}(A)$ is a good approximation of $\rho(A)$ up to a normalization factor (indeed any $\tilde{\rho}(A)$ proportional to $\rho(A)$ would produce a flat histogram, see Eq. (5.8)). This problem could be overcome by knowing the exact value of $\rho(A)$ at one value of A [41–43] or by normalizing the obtained $\tilde{\rho}(A)$ (which could be numerically dangerous

7 The equilibrium distribution of a Markov chain can be obtained by imposing the detailed balance condition: $P(\alpha)R(\alpha'|\alpha) = P(\alpha')R(\alpha|\alpha')$.

because $\tilde{\rho}(A)$, as mentioned above, usually spans many orders of magnitude [8]). (v) In general we don't know a priori the set of values which A_α can take, but only the range Δ_A in which A_α is defined. In these cases, as customary for histograms, we can split the domain Δ_A into an appropriate number of intervals and collect histograms for $\ln\tilde{\rho}(A)$ and $h(A)$ in those intervals. This is exactly equivalent to the replacement of the quantity A_α with a coarse-grained version of it, in which A_α is approximated to the central value of the nearest interval. Moreover, in general, we do not know if all the intervals can be visited. Therefore, in principle, we can not properly check if $h(A)$ is flat because there might be bins which are always empty. Practically, we overcome this issue with a Wang-Landau "zero run": fixing $\ln f$ to its initial value, we perform a fixed number of steps (proportional to the system size), without checking the flatness of $h(A)$ but updating $\ln\tilde{\rho}(A)$, and storing the list of intervals that are actually visited. After this preliminary run, we start the real WLA and we check the flatness of $h(A)$ in the accessible intervals. If, during the "main" run, we visit a new interval not contained in the list, we restart the WLA [9] adding the new interval to the list of those that have to be visited. (iv) Practically, we always store the more manageable $\ln\tilde{\rho}(A)$, rather than $\tilde{\rho}(A)$, often an astronomically large number which cannot be represented with a 64-bit double-precision number.

In Sec. 5.3 we will illustrate the application of this algorithm to the classical two-dimensional Ising model, one of the systems used by Wang and Landau to test the algorithm [41–43].

5.2 WEIGHTED WANG–LANDAU ALGORITHM

In this section we discuss an extension of the WLA which can be used to compute weighted density of states.

Let us consider again a system with a discrete configuration space, a given physical observable A, and define the weighted density of states:

$$\rho_w(A) \equiv \sum_\alpha w_\alpha \delta_{A A_\alpha} \,, \tag{5.9}$$

where w_α is a positive weight. We will now show how to modify Eq. (5.7) to compute $\rho_w(A)$ with a WLA-like procedure.

Consider a generic function $\tilde{\rho}_w(A)$ and set up a random walk in which, given a state α, a new state α' is generated with probability $T(\alpha'|\alpha)$ and accepted with probability:

$$R(\alpha'|\alpha) = \text{Min}\left[1, \frac{w_{\alpha'}}{w_\alpha}\frac{\tilde{\rho}_w(A_\alpha)}{\tilde{\rho}_w(A_{\alpha'})}\frac{T(\alpha|\alpha')}{T(\alpha'|\alpha)}\right] \,. \tag{5.10}$$

With this Metropolis Monte Carlo prescription the equilibrium distribution, which fulfills the detailed balance, is $P(\alpha) = c w_\alpha/\tilde{\rho}_w(A_\alpha)$. As in the WLA, while the random walk goes on, we collect an histogram $h(A)$, and at each visited state α we update $h(A_\alpha) \to h(A_\alpha) + 1$. At equilibrium, after N_s steps, the mean histogram is:

$$\begin{aligned} h(A) = \sum_\alpha N_s P(\alpha)\delta_{A A_\alpha} = c N_s \sum_\alpha \frac{w_\alpha}{\tilde{\rho}_w(A_\alpha)}\delta_{A A_\alpha} &= \frac{c N_s}{\tilde{\rho}_w(A)}\sum_\alpha w_\alpha \delta_{A A_\alpha} \\ &= c N_s \frac{\rho_w(A)}{\tilde{\rho}_w(A)} \,. \end{aligned} \tag{5.11}$$

8 The normalizations requires the computation of $\sum_A \tilde{\rho}(A) = \sum_A e^{\ln\tilde{\rho}(A)}$ ($\ln\tilde{\rho}(A)$ is the stored quantity), and to compute numerically this summation we can use the following trick: we find $\ln\tilde{\rho}_{max}$, the maximum value of $\ln\tilde{\rho}(A)$, and then $\ln[\sum_A \tilde{\rho}(A)] = \ln\tilde{\rho}_{max} + \ln[\sum_A e^{\ln\tilde{\rho}(A) - \ln\tilde{\rho}_{max}}]$, where the summation now contains only positive terms smaller or equal to 1.

9 We set $\ln f$ to its initial value, and reset $h(A) = 0$ but we do not erase $\ln\tilde{\rho}(A)$, in order not to lose the information accumulated so far.

Exactly as for the WLA, if $\tilde{\rho}_w(A)$ is a good approximation to $\rho_w(A)$ the histogram $h(A)$ is almost flat. Therefore, closely inspired by the WLA, we define the following algorithm:

Weighted Wang-Landau algorithm

(0) fix a modification factor $f > 1$, and set $\ln \tilde{\rho}_w(A) = 0$ and $h(A) = 0$ for all values of A;

(1) start the Monte Carlo procedure using Eq. (5.10) and update at each step the histogram and the weighted density of states with the rules $h(A_\alpha) \to h(A_\alpha) + 1$ and $\ln \tilde{\rho}_w(A_\alpha) \to \ln \tilde{\rho}_w(A_\alpha) + \ln f$;

(2) stop the random walk when $h(A)$ is almost flat (i.e., as before, $h(A) > 0.8\overline{h}$ for all values of A, where $\overline{h}$ is the mean histogram value). For the previous observations, at the end of this step $\ln \tilde{\rho}_w(A)$ is a good approximation to $\ln \rho_w(A)$ with a discrepancy of order $\ln f$;

(3) reduce the value of $f \to \sqrt{f}$, reset $h(A) = 0$ and restart the procedure from step (1) using the $\tilde{\rho}_w(A)$ just obtained. Stop this loop when $\ln f$ is smaller than the desired discrepancy ϵ.

After introducing this extension of the WLA, we have found a reference in the literature [109, 110] where the essence of the algorithm is presented for the case in which w_α is the Boltzmann distribution, with the aim of computing the free energy profile as a function of a reaction coordinate.

Let us return for a moment to the unweighted density of states and the original WLA. A first trivial observation is that, as it should be, the weighted-WLA with $w_\alpha = 1/N$ coincides with the WLA. In many situations, when the size of the configuration space is too big and the density of states ranges over too many orders of magnitude, it is convenient, in computing $\rho(A)$, to run many WLA over small domains $\Delta_A^{(i)} = [A_{min}^{(i)}, A_{max}^{(i)}]$. Indeed, the update rule of the WLA has to be changed to avoid that, during the random walk, A_α leaves the domain $\Delta_A^{(i)}$. This trick was already used in the first papers by Wang and Landau, when dealing with the largest sizes [41]. To avoid leaks from $\Delta_A^{(i)}$ the empirical solution was to reject any proposal to states α' with $A_{\alpha'} \notin \Delta_A^{(i)}$, without any update of $\tilde{\rho}(A)$ and $h(A)$. With this prescription, however, there are "boundary effects", actually a systematic underestimation of the density of states at the borders of the intervals [111]. [10] Schulz *et al.* [111] showed phenomenologically that such boundary effects are eliminated by using the rather obvious update rule: given a proposal α', if $A_{\alpha'}$ is outside the interval we remain in α and we update $h(A)$ and $\ln \tilde{\rho}(A)$ using the state α, otherwise we accept α' with the usual role. This update rule can be obtained rigorously by using our weighted-WLA. Indeed, the density of states in a restricted range $\Delta_A^{(i)}$ is proportional to a weighted density of states in which $w_\alpha = 1$ when $A_\alpha \in \Delta_A^{(i)}$, and zero otherwise. With these weights, the update rule of the weighted-WLA is exactly the one obtained phenomenologically by Schulz *et al.* [111].

5.3 THE ISING MODEL

One of the first systems in which the WLA was used is the two-dimensional Ising model [41–43]. The two-dimensional Ising model with nearest-neighbor interactions on a $L \times L$ square lattice is described by the Hamiltonian:

$$H = -J \sum_{\langle j_1 j_2 \rangle} s_{j_1} s_{j_2} \,, \tag{5.12}$$

10 Wang and Landau in Ref. [41] overcame this problem by allowing small overlaps between adjacent intervals, and then cutting away the bins affected by this "boundary effect".

where $s_j = \{-1, 1\}$ is the spin in site j, J is the coupling and the sum runs over nearest-neighbor sites. The phase diagram of this Hamiltonian is well known: there is a second-order phase transition at the critical temperature $T_c/J \approx 2.269$ (we fixed $k_B = 1$), separating the high-temperature disordered phase from the low temperature one, where ferromagnetic order (spontaneous magnetization) sets in. The number of states as a function of energy

$$g(E) \equiv \sum_{\alpha} \delta_{E E_\alpha} = 2^L \rho(E) \,, \tag{5.13}$$

is a very useful quantity. [11] Once $g(E)$ is computed, many thermodynamic properties can be obtained at any temperature T without performing other simulations. Some examples are: the partition function $Z(T) = \sum_\alpha e^{-\beta E_\alpha} = \sum_E g(E) e^{-\beta E}$ ($\beta \equiv 1/T$ and the last sum is over the allowed energies), the Gibbs free energy $F(T) = -T \ln Z(T)$, the entropy and the specific heat [41]. [12] In their first works, Wang and Landau used the WLA to compute $g(E)$ [41–43], and the Monte Carlo proposals were random spin flips. In Fig. 5.1 there is a plot of the density of states $g(E)$ they have obtained for $L = 256$. In this case the computed $\ln g(E)$ can be normalized using the relation $g(-2JL^2)[= g(2JL^2)] = 2$. Notice that the configuration space is in this case huge, $2^{256\times256} \approx 10^{19728}$ states, and an exhaustive enumeration is impossible. With the obtained $g(E)$ they were able to compute, for temperatures ranging from 0 to $8J$, the internal energy, with relative errors smaller than 0.09% [42], the entropy, with relative errors smaller than 1.2% [42], and the specific heat (see inset of Fig. 5.1), with relative errors smaller than 4% [41].

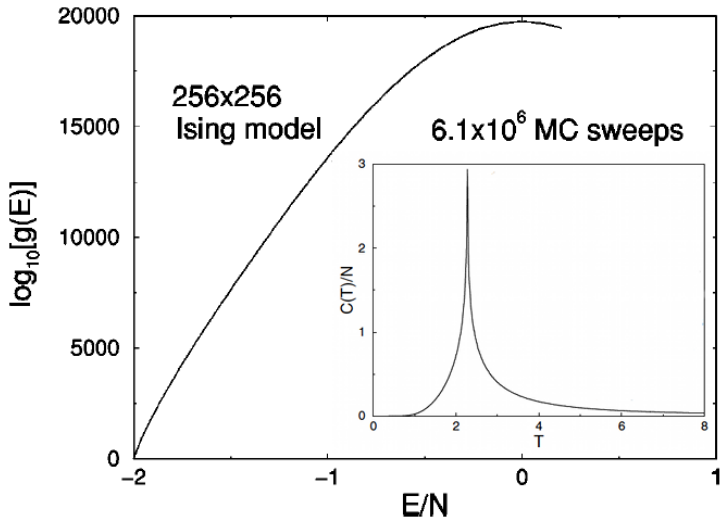

Figure 5.1.: Logarithm of the density of states $\log_{10} g(E)$ computed in Ref. [42] with the WLA for the two-dimensional Ising model. The parameters are $L = 256$, $J = 1$, $\epsilon = 10^{-7}$, and the computation reached convergence after $6.1 \cdot 10^6$ Monte Carlo sweeps of the whole lattice. To speed up the calculation, the allowed energy region has been divided into 15 energy intervals, and the density of states has been estimated for each interval with independent random walks. In the inset, taken from Ref. [41], a plot of the specific heat computed using the $g(E)$ obtained.

Not all the physically interesting quantities are directly accessible with $g(E)$ and a plain WLA. Consider, as an example, the free energy as function of the magnetization order parameter:

$$F(M) \equiv -\frac{1}{\beta} \ln Z(M) \,, \tag{5.14}$$

11 Notice that $g(E)$ is defined over a discrete set of energies, i.e., $E = -2J(L^2 - 2n)$ where $n = 0, \ldots, L^2$, with $n \neq 1$ and $n \neq L^2 - 1$.

12 Computing $g(E)$ not only drastically reduces the computational effort, by avoiding multiple simulations for different temperatures, but it also overcomes problems connected with the slow kinetics at low temperature or near T_c.

where:

$$Z(M) \equiv \sum_{\alpha} e^{-\beta E_\alpha} \delta_{M M_\alpha} \, , \tag{5.15}$$

and $M_\alpha = \sum_j s_j^\alpha$ is the total magnetization of the configuration α. In this case, the standard WLA cannot be directly used. The only way out would be to compute, with a WLA, the joined density of states $g(E, M)$, i.e., the number of states with energy E and magnetization M, and then trace over E to get $Z(M) = \sum_E e^{-\beta E} g(E, M)$. The drawback of this approach is that the computation of two-dimensional density of states has a slower convergence. An example of such a calculation for the three-dimensional Ising model can be found in Ref. [43]. The function $Z(M)$ has exactly the structure of a weighted density of states (see definition in Eq. (5.9)), and an alternative approach is to use the weighted WLA we have illustrated. In Fig. 5.2 we plot the free energy per site, i.e., $f(m) \equiv F(mL^2)/L^2$, for two temperatures, a $T > T_c$ and a $T < T_c$. This quantity illustrates the phase transition in a very direct way: For $T > T_c$, the free energy has a single minimum at $m = 0$ (the disordered phase), while for $T < T_c$, $f(m)$ displays two symmetric minima, separated by a barrier $f_b \equiv f(m = 0) - f_{min}$, where f_{min} is the minimum free energy. In the inset of Fig. 5.2 we show the barrier free-energy per site f_b as a function of L, and we see that it scales as $1/L$ as expected for the two-dimensional Ising model [112]. This power law comes from the fact that, in going from the minimum at $m < 0$ to the other minimum, at $m > 0$, the system has to pay for the creation of a domain wall separating two domains of opposite magnetization; the free energy for the formation of the domain wall scales as L, leading to the $1/L$ scaling in the barrier free-energy per site. With the weighted-WLA we were able to compute the free energy $F(M)$ for sizes up to $L = 256$, without splitting the magnetic domain (which would speedup the calculation). The drawback of this algorithm to compute $F(M)$ is that we have to perform a calculation for every fixed temperature we are interested in, losing one of the benefits of the plain WLA.

5.4 QUANTUM QUENCHES

In this section we come back to the initial problem of computing the distributions $\rho_D(A)$ and $\rho_{GGE}(A)$ related to quantum quenches. We will show that with the weighted-WLA we can compute these distributions for sizes inaccessible with an exhaustive enumeration.

Let us consider the set of Hamiltonians introduced in Chap. 3, and for reasons of simplicity, let us focus on the tight-binding chains. After the diagonalization, these Hamiltonians, can always be written as:

$$\hat{H} = \sum_{\mu=1}^{L} \epsilon_\mu \hat{c}_\mu^\dagger \hat{c}_\mu \, , \tag{5.16}$$

where $\hat{c}_\mu$ ($\hat{c}_\mu^\dagger$) is the annihilation (creation) fermionic operator associated to the single-particle eigenstate μ, and ϵ_μ is the associated single-particle energy. For the numerical computations of this section we used three different quenches in which the initial state is always the ground state of a clean chain [13], and the final Hamiltonian is the Anderson model $\hat{H}_A$ with $W = 2$, or the long-range hopping chain $\hat{H}_{lrh}$ with $\alpha = 0.5$ or 2 (see Chap. 3 for the details on these Hamiltonians). To get a smoother size dependence of the computed quantities, the smaller size realizations are obtained by cutting an equal amount of sites at the two edges of the largest realization.

13 The initial clean chain has the same boundary conditions of the final Hamiltonian. Namely, periodic boundary conditions when quenching to $\hat{H}_A$ and open boundary conditions when quenching to $\hat{H}_{lrh}$.

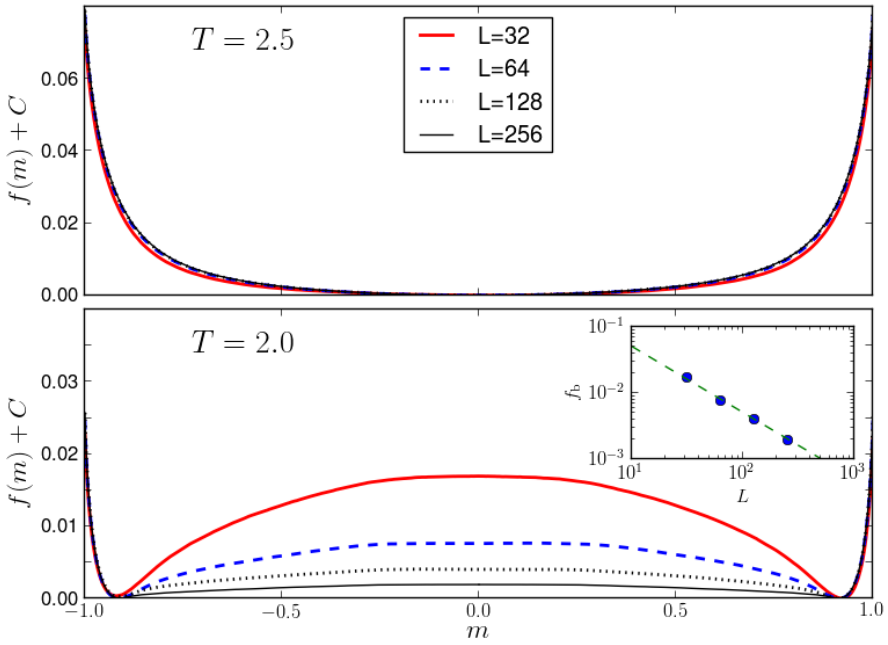

Figure 5.2.: Plot of the free energy per site $f(m)$ as a function of the magnetization per site m for the two-dimensional Ising model. The curves are obtained with the weighted-WLA. In the two panels we use two different temperatures, $T = 2 < T_c$ in the upper panel, and $T = 2.5 > T_c$ in the lower panel. In the inset the free energy barrier $f_b = f(m = 0) - f_{min}$ as a function of L. The dashed line is proportional to $1/L$. For the calculation we used $\epsilon = 10^{-6}$ and, for $L = 256$ we have performed the computation only in the $m \leqslant 0$ domain (the $m > 0$ part is obtained plotting $f(-m)$). With $L = 256$ we reached convergence after $1.6 \cdot 10^7$ and $5.7 \cdot 10^6$ Monte Carlo sweeps for $T = 2$ and $T = 2.5$. The constant C is taken in such a way that $f(M) + C$ has minimum in 0.

Given an observable $\hat{A}$, consider the two distributions discussed in the introduction, which we report here for the reader's convenience:

$$\rho_D(A) \equiv \sum_\alpha |c_\alpha|^2 \delta(A - A_{\alpha\alpha})$$
$$\rho_{GGE}(A) \equiv \sum_\alpha \frac{e^{-\sum_\mu \lambda_\mu n_\mu^\alpha}}{Z_{GGE}} \delta(A - A_{\alpha\alpha}) \,, \tag{5.17}$$

where $\delta(x)$ is the Dirac's delta, $\{|\alpha\rangle\}$ are the many-body eigenstates of $\hat{H}$, $A_{\alpha\beta} \equiv \langle\alpha|\hat{A}|\beta\rangle$, $c_\alpha \equiv \langle\alpha|\Psi_0\rangle$, and $n_\mu^\alpha = 0, 1$ is the occupation of the single-particle eigenstate μ in the many-body eigenstate $|\alpha\rangle$. These functions give the weighted distributions of $A_{\alpha\alpha}$ in the diagonal and GGE ensembles. Notice that the sum over α is effectively restricted to the canonical Hilbert space $\mathcal{H}_N$ with a fixed number of particles $N = N_F$ in the diagonal ensemble, since $c_\alpha \equiv \langle\alpha|\Psi_0\rangle = 0$ if $N_\alpha \neq N_F$. No such restriction is in principle present in the GGE case, where the sum over α runs over the grand-canonical Hilbert space. By definition, the distributions are such that $\langle\hat{A}\rangle_D = \int dA\, \rho_D(A) A$ and $\langle\hat{A}\rangle_{GGE} = \int dA\, \rho_{GGE}(A) A$, where the integration is over the domain of $A_{\alpha\alpha}$. As customary in any numerical finite-size study, one really needs to consider a coarse-grained (cg) version of these distributions, obtained by splitting the domain of A into small domains $\Delta^{(i)}$ of amplitude Δ. For instance, we might define:

$$\rho_D^{cg}(A) \equiv \frac{\int_{\Delta^{(i)}} dA'\, \rho_D(A')}{\Delta} = \sum_\alpha \frac{|c_\alpha|^2}{\Delta} \delta_{\Delta^{(i)}}(A_{\alpha\alpha}) \,, \tag{5.18}$$

where $\Delta^{(i)}$ is the interval containing A, and $\delta_{\Delta^{(i)}}(x)$ is 1 if $x \in \Delta^{(i)}$, and zero otherwise. (A similar coarse graining can be applied to the GGE case as well.) Such a coarse-grained distribution has exactly the form of a weighted density of states, see Eq. (5.9), in which $w_\alpha = |c_\alpha|^2 / \Delta$ in the diagonal case, and $w_\alpha = e^{-\sum_\mu \lambda_\mu n_\mu^\alpha}/(\Delta\, Z_{GGE})$ in the GGE case. The configuration space $\{|\alpha\rangle\}$ (i.e.,the canonical Hilbert space $\mathcal{H}_N$ for the diagonal distribution and the full Hilbert space for the GGE) over which the two weighted distributions are defined is discrete and grows exponentially with the system size. The weighted-WLA is therefore a good candidate for the numerical computation of $\rho_D^{cg}(A)$ and $\rho_{GGE}^{cg}(A)$. To simplify the notation we drop hereafter the superscript cg.

The eigenstates $|\alpha\rangle$ which appear in the definition of $\rho_D(A)$ have a fixed number of fermions N_F (the same of the initial state), while in $\rho_{GGE}(A)$ the number of particles can change. In the weighted-WLA, for the diagonal ensemble, we use therefore a "particle conserving" proposal scheme: given a state $|\alpha\rangle$, the state $|\alpha'\rangle$ is given by moving at random a fermion in one of the unoccupied single-particle eigenstates. In this case, the ratio $w_{\alpha'}/w_\alpha$ which appears in Eq. (5.10), is equal to:

$$\frac{w_{\alpha'}}{w_\alpha} = \frac{|c_{\alpha'}|^2}{|c_\alpha|^2}\,, \tag{5.19}$$

where the coefficient $|c_\alpha|^2$ is the square of the determinant of a $N_F \times N_F$ matrix (see App. D for the explicit expression of $|c_\alpha|^2$). For the GGE case, instead, we do not have restrictions on the number of fermions and, given a state $|\alpha\rangle$, we generate a state $|\alpha'\rangle$ by changing the occupation of a randomly selected single-particle eigenstate μ. In this case:

$$\frac{w_{\alpha'}}{w_\alpha} = e^{\pm\lambda_\mu}\,, \tag{5.20}$$

where the $+$ ($-$) sign appears when the mode μ is initially occupied (empty). Let us recall that the λ_μ's are obtained by requiring $\langle\Psi_0|\hat{c}_\mu^\dagger\hat{c}_\mu|\Psi_0\rangle = \langle\hat{c}_\mu^\dagger\hat{c}_\mu\rangle_{GGE}$. This condition, written explicitly, reads:

$$e^{\lambda_\mu} = \frac{1}{\sum_\nu n_\nu^0 \left|\left[u^{0\dagger}u\right]_{\nu\mu}\right|^2} - 1\,, \tag{5.21}$$

where u^0 and u are $L \times L$ matrices whose elements $u^0_{j\nu}$ and $u_{j\mu}$ are the single-particle wavefunctions of the initial Hamiltonian $\hat{H}_0$ and the final one $\hat{H}$, and $n_\nu^0 = 0, 1$ is the occupation of the mode ν of $\hat{H}_0$ in the initial state. The difference in the computational effort on computing the ratio $w_{\alpha'}/w_\alpha$ in the two ensembles is evident: in the diagonal case at each step we have to compute the determinant of a $N_F \times N_F$ matrix, while in the GGE we have just to recover the value of e^{λ_μ} (they can be computed and stored before the Monte Carlo calculation because their number is L). Here we will show results for sizes up to $L = 256$, where both $\rho_D(A)$ and $\rho_{GGE}(A)$ can be computed and compared. In the GGE ensemble, we can anyhow reach $L = 1024$.

In the next two subsections we show the results obtained with the weighted-WLA for the calculation of $\rho_D(A)$ and $\rho_{GGE}(A)$ for two observables, the total energy and the local density. In the numerical computations we used $\epsilon = 10^{-6}$ and we split the domain of A in L bins. Notice that the domain of A in $\rho_{GGE}(A)$ is always larger than the domain of $\rho_D(A)$ because, in the GGE, the many-body eigenstates do not have a restriction on the number N_F of fermions.

5.4.1 Probability distributions of the energy

The first observable we consider is the total energy, and in this case $A_{\alpha\alpha} = E_\alpha = \sum_\mu \epsilon_\mu n_\mu^\alpha$, where $n_\mu^\alpha = \langle\alpha|\hat{c}_\mu^\dagger\hat{c}_\mu|\alpha\rangle = 0, 1$ are the single-particle occupations of the eigenstate $|\alpha\rangle$. In Fig. 5.3 we show the values of $\ln[\rho_D(E)]$ and $\ln[\rho_{GGE}(E)]$ divided by the size L, computed for $L = 128$ and $L = 256$. We see that, when the after-quench

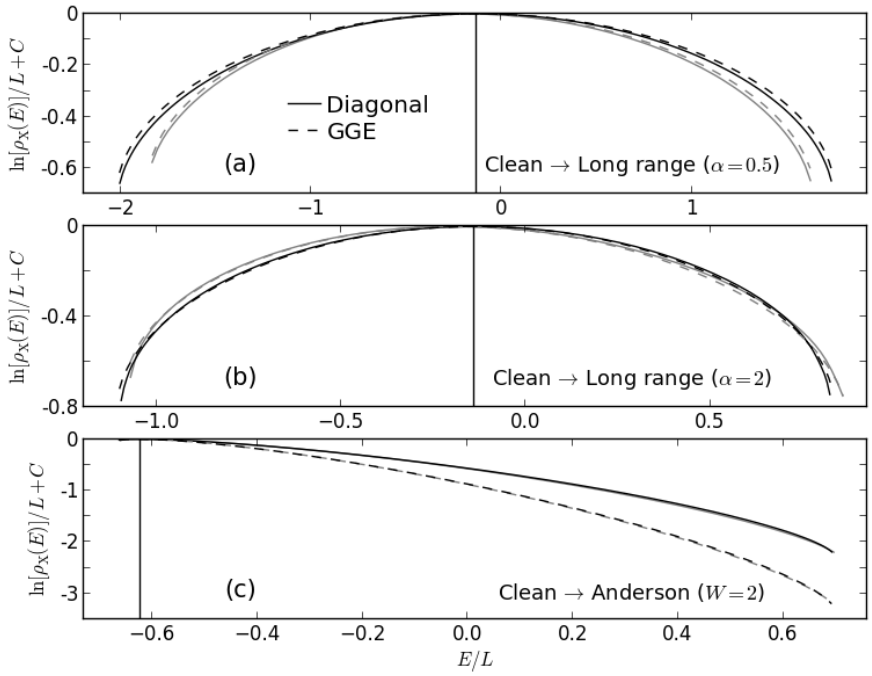

Figure 5.3.: Value of $\ln[\rho_D(E)]/L$ and $\ln[\rho_{GGE}(E)]/L$ computed with the weighted-WLA. The gray curves are obtained with $L = 128$, while the black ones with $L = 256$. The vertical lines are the energy after the quench, i.e. $\langle\Psi_0|\hat{H}|\Psi_0\rangle$, for $L = 256$. The three panels are obtained starting from the ground states of clean chains and quenching to different disordered Hamiltonians: panel (a) long-range hopping with $\alpha = 0.5$, panel (b) long-range hopping with $\alpha = 2.0$ and panel (c) Anderson model with $W = 2$. For the computations we used a single disorder realization and, to get a smoother size dependence, the smaller size realization is obtained by cutting an equal amount of sites at the two edges of the larger realization.

Hamiltonian is the Anderson model, $\rho_D(E)$ has both mode (i.e., maximum value) and average very close to the ground state energy: the quench excites mostly the low-energy part of the many-body spectrum. On the contrary, for both the quenches towards $\hat{H}_{lrh}$, mode and average are almost in the middle of the many-body spectrum. There, indeed, the quench is more dramatic: we are going from the ground state of a chain with nearest-neighbor hopping to a disordered chain with long-range hopping. This is evident by looking at the occupations $n^0_\mu \equiv \langle\Psi_0|\hat{c}^\dagger_\mu\hat{c}_\mu|\Psi_0\rangle$ as a function of the single-particle energy ϵ_μ, shown in Fig. 5.5a. By definition, in $|\Psi_0\rangle$, only the eigenstates of $\hat{H}_0$ with $\epsilon^0_\nu < 0$ are occupied. The quench to $\hat{H}_A$ only slightly modifies the initial occupations: n^0_μ, apart for fluctuations due to disorder, goes smoothly from 1, in the lower part of the single-particle spectrum, to 0, in the highest part of the spectrum. On the contrary, for the quenches towards $\hat{H}_{lrh}$, the single-particle spectrum is entirely excited, both the positive and the negative part. This explains why, for these quenches, the after-quench energy $\langle\Psi_0|\hat{H}|\Psi_0\rangle = \sum_\mu \epsilon_\mu n^0_\mu$ is near the center of the many-body spectrum.

Returning to the distributions $\rho_D(E)$ and $\rho_{GGE}(E)$ shown in Fig. 5.3, we observe that their average values coincide:

$$\langle\hat{H}\rangle_D = \int dE\, \rho_D(E)E = \int dE\, \rho_{GGE}(E)E = \langle\hat{H}\rangle_{GGE}\,. \tag{5.22}$$

This result comes directly from the fact that the energy does not fluctuate in time (i.e., the diagonal energy coincides with the energy $\langle\Psi_0|\hat{H}|\Psi_0\rangle$) and GGE fixes the occupation of the fermionic eigenstates in such a way as to exactly reproduce the energy. [14] Let

14 As we have proved in Chap. 4, the same statement holds for any one-body operator.

us now consider the fluctuations of the energies in both distributions. In the diagonal ensemble the variance is:

$$\sigma^2_{E,D} = \int dE\, \rho_D(E) E^2 - \langle \hat{H} \rangle^2_D = \langle \hat{H}^2 \rangle_D - \langle \hat{H} \rangle^2_D \,, \tag{5.23}$$

where the expression on the right-hand side holds only for the Hamiltonian (it would not apply to arbitrary operators, because $A^2_{\alpha\alpha} \neq \langle \alpha | \hat{A}^2 | \alpha \rangle$). An entirely similar expression applies to the GGE case. Since the energy is an extensive operator, it is reasonable to ask what happens to the fluctuations in the energy-per-site $e = E/L$, which are simply given by $\sigma^2_{e,D} = \sigma^2_{E,D}/L^2$, and $\sigma^2_{e,GGE} = \sigma^2_{E,GGE}/L^2$. On pretty general grounds, for quenches of local non-integrable Hamiltonians, one can show [8, 52] that $\sigma^2_{e,D} \to 0$ in the thermodynamic limit, $L \to \infty$. Indeed, as shown in Fig. 5.4 both $\sigma^2_{e,D}$ and $\sigma^2_{e,GGE}$ decrease to 0 for $L \to \infty$ for the three considered set of quenches. For our quadratic problems, we can say a bit more. First of all, from the explicit expression in Eq. (5.23) after very simple algebra (mainly using Wick's theorem), we arrive at: *Energy variances*

$$\begin{aligned} \sigma^2_{e,GGE} &= \frac{1}{L^2} \sum_\mu \epsilon^2_\mu n^0_\mu \left(1 - n^0_\mu\right) \,, \\ \sigma^2_{e,D} &= \sigma^2_{e,GGE} - \frac{1}{L^2} \sum_{\mu_1 \neq \mu_2} \epsilon_{\mu_1} \epsilon_{\mu_2} \left| G^0_{\mu_1 \mu_2} \right|^2 \,, \end{aligned} \tag{5.24}$$

where $G^0_{\mu_1\mu_2} \equiv \langle \Psi_0 | \hat{c}^\dagger_{\mu_1} \hat{c}_{\mu_2} | \Psi_0 \rangle$ is the $t = 0$ one-body Green's function introduced in Chap. 4 (see Eq. (4.6)). The off-diagonal elements of $G^0_{\mu_1\mu_2}$ play again (see Secs. 4.4, 4.5) an important role, and the correction in $\sigma^2_{e,D}$ originates from the fact that, by definition, GGE does not include correlations between different modes, i.e., $\langle \hat{c}^\dagger_{\mu_1} \hat{c}_{\mu_2} \rangle_{GGE} = 0$, when $\mu_1 \neq \mu_2$.

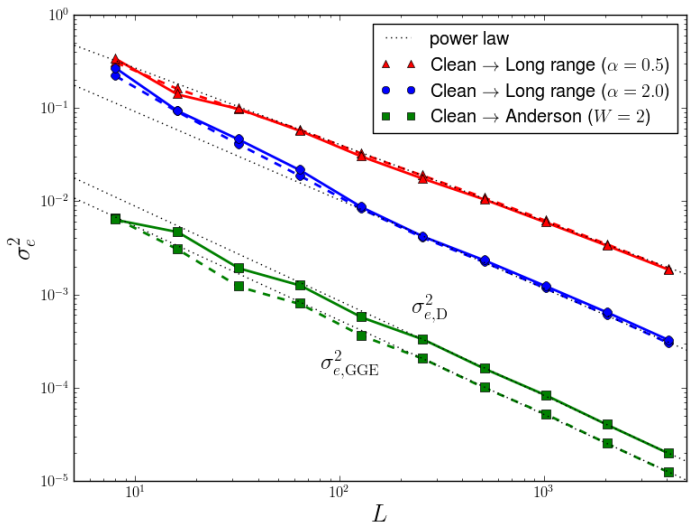

Figure 5.4.: Variances $\sigma^2_{e,D} = \sigma^2_{E,D}/L^2$ (solid lines) and $\sigma^2_{e,GGE} = \sigma^2_{E,GGE}/L^2$ (dashed lines) as a function of the size L. The data are obtained using the same set of quenches used in Fig. 5.3 and the values are computed using Eqs. (5.24). The dotted lines are power law fits $\sigma^2_e \sim L^{-s}$, where $s \approx 1$ for the Anderson case, while, for the quench to $\hat{H}_{lrh}$, $s \approx 0.82$ when $\alpha = 0.5$, and $s \approx 0.95$ when $\alpha = 2.0$.

Let us first consider the Anderson model case. Assuming, as we have done so far, a bounded distribution of disorder, we are guaranteed that a finite bound ϵ_{max} exists such that $|\epsilon_\mu| \leqslant \epsilon_{max}$ for any size. With this assumption, it is easy show that $\sigma^2_{e,GGE}$

has to go to zero at least as $1/L$ for $L \to \infty$. Indeed, the occupation factors appearing in $\sigma^2_{e,GGE}$ are such that $0 \leqslant n^0_\mu \left(1 - n^0_\mu\right) \leqslant 1$. Hence:

$$\sigma^2_{e,GGE} \leqslant \frac{\epsilon^2_{max}}{L^2} \sum_\mu n^0_\mu \left(1 - n^0_\mu\right) \leqslant \frac{\epsilon^2_{max}}{L} \,. \tag{5.25}$$

The same statement can be made for $\sigma^2_{e,D}$, because the difference between the two variances has a similar upper bound:

$$\begin{aligned} |\sigma^2_{e,D} - \sigma^2_{e,GGE}| \leqslant \frac{1}{L^2} \sum_{\mu_1 \neq \mu_2} |\epsilon_{\mu_1}||\epsilon_{\mu_2}| \left|G^0_{\mu_1\mu_2}\right|^2 \leqslant \frac{\epsilon^2_{max}}{L^2} \sum_{\mu_1 \neq \mu_2} \left|G^0_{\mu_1\mu_2}\right|^2 \\ \leqslant \epsilon^2_{max} \frac{N_F}{L^2} \leqslant \frac{\epsilon^2_{max}}{L} \,, \end{aligned} \tag{5.26}$$

where we used the fact that $\sum_{\mu_1\mu_2} \left|G^0_{\mu_1\mu_2}\right|^2 = N_F$ (see App. D). Nevertheless, although both $\sigma^2_{e,D}$ and $\sigma^2_{e,GGE}$ indeed appear to go to 0 as $1/L$ for the Anderson model, they do so with a different prefactor, see Fig. 5.4 and comments below.

For the quenches to $\hat{H}_{lrh}$, a bound ϵ_{max} for the single-particle spectrum is in principle not defined: one can think of rare realizations in which the hopping is large at arbitrarily large distances, which would give an unbounded distribution of eigenvalues ϵ_μ. Indeed, the behavior of both $\sigma^2_{e,D}$ and $\sigma^2_{e,GGE}$ suggest, see Fig. 5.4, that the power-law approach to 0 might be slower than $1/L$, i.e., as L^{-s} with $s < 1$ (we find $s \approx 0.82$ for the case $\alpha = 0.5$ and $s \approx 0.95$ for $\alpha = 2$). While this might be a finite-size artifact, we find it intriguing that such deviations are quite clearly seen in all cases in which a simple analytic bound appears to fail.

Concerning the similarity between $\sigma^2_{e,D}$ and $\sigma^2_{e,GGE}$, we observe that the two essentially coincide for the case of quenches to $\hat{H}_{lrh}$, whereas there is a clearly different prefactor in the $1/L$ approach, $\sigma^2_{e,D} \sim C_D/L$ and $\sigma^2_{e,GGE} \sim C_{GGE}/L$ with $C_{GGE} < C_D$, for the Anderson model case. The different prefactor can be understood by analyzing the term $\sum_{\mu_1 \neq \mu_2} \epsilon_{\mu_1}\epsilon_{\mu_2}|G^0_{\mu_1\mu_2}|^2$ which appears in Eq. (5.24). In Fig. 5.5b we show the structure of the matrix $|G^0_{\mu_1\mu_2}|^2$ for the three set of quenches. We divide this matrix into four sectors, one for each sign of the single particle energies ϵ_{μ_1} and ϵ_{μ_2}: in two of these quadrants the product $\epsilon_{\mu_1}\epsilon_{\mu_2}$ is positive (top-right and bottom-left), and in the others is negative. For quenches to $\hat{H}_{lrh}$ this matrix is almost equally distributed in all the four sectors: the sum $\sum_{\mu_1 \neq \mu_2} \epsilon_{\mu_1}\epsilon_{\mu_2}|G^0_{\mu_1\mu_2}|^2$ has a cancellation effects, leading to $\sigma^2_{e,GGE} \approx \sigma^2_{e,D}$ for large sizes. For quenches to $\hat{H}_A$, on the contrary, the matrix $|G^0_{\mu_1\mu_2}|^2$ is mainly concentrated in the sectors in which $\epsilon_{\mu_1}\epsilon_{\mu_2} < 0$, leading to $\sigma^2_{e,GGE} < \sigma^2_{e,D}$. [15]

5.4.2 Probability distributions of the local density

Let us now consider the local density $\hat{n}_j \equiv \hat{c}^\dagger_j \hat{c}_j$, perhaps the simplest intensive few-body (indeed, one-body) observable. For definiteness, we concentrate on $j = L/2$, i.e., in the middle of the chain. It is important to stress that we are going to consider the fluctuations of this quantity before any possible average over the sites j: averaging over the sites j an intensive local operator would effectively send to zero the fluctuations in the thermodynamic limit [52], while we will show that, for a fixed j, finite fluctuations survive in the thermodynamic limit when the eigenstates are localized, due to disorder.

15 Notice that, in general, GGE and diagonal ensemble are bound to show different fluctuations of the energy, a fact that is in some way related to the issue of the GGE ensemble being grand-canonical in nature. If you imagine quenching towards a final Hamiltonian in which all eigenvalues are shifted up by a common energy h, i.e., the single-particle energies become $\epsilon_\mu \to \epsilon_\mu + h$, then one can easily verify that $\sigma^2_{e,GGE}$ would be greatly affected, while $\sigma^2_{e,D}$ is totally unchanged, due to cancellations with the extra term $\sum_{\mu_1 \neq \mu_2} (\epsilon_{\mu_1} + h)(\epsilon_{\mu_2} + h)|G^0_{\mu_1\mu_2}|^2$ (see Eq. (5.24)).

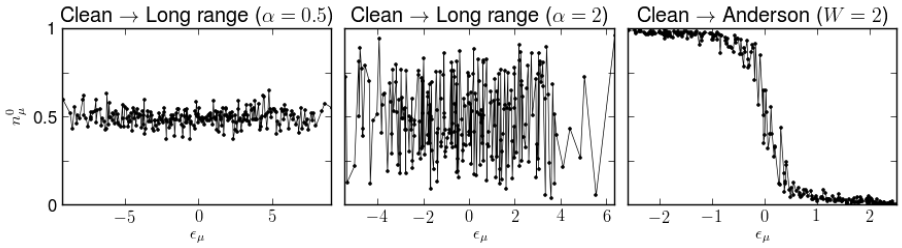

(a) Single particle occupations $n^0_\mu = \langle\Psi_0|\hat{c}^\dagger_\mu \hat{c}_\mu|\Psi_0\rangle$

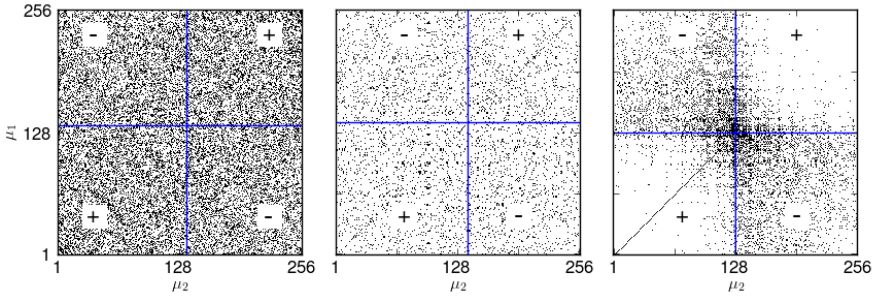

(b) Representation of the matrix $\left|G^0_{\mu_1\mu_2}\right|^2 = \left|\langle\Psi_0|\hat{c}^\dagger_{\mu_1}\hat{c}_{\mu_2}|\Psi_0\rangle\right|^2$ for $L = 256$

Figure 5.5.: Panel (a): occupations $n^0_\mu = \langle\Psi_0|\hat{c}^\dagger_\mu\hat{c}_\mu|\Psi_0\rangle$ as a function of the single-particle energy ϵ_μ. Panel (b): representation of the matrix $|G^0_{\mu_1\mu_2}|^2$. For the diagonal and off-diagonal elements we add a black pixel when the value exceeds their mean value. For the diagonal elements the mean value is $x \equiv \sum_\mu (n^0_\mu)^2/L$, while for the off-diagonal elements the mean value is $(N_F - xL)/L(L-1)$, where N_F is the number of fermions in the initial state, and we used the relation $\sum_{\mu_1\mu_2}|G^0_{\mu_1\mu_2}|^2 = N_F$ (see App. D). The vertical and horizontal lines indicate the indexes at which the single-particle energies ϵ_{μ_1} and ϵ_{μ_2} change sign, and the signs shown in the four quadrants are those of the product $\epsilon_{\mu_1}\epsilon_{\mu_2}$. For the two panels we used $L = 256$ and the same quenches used in Fig. 5.3 and Fig. 5.4.

The diagonal and GGE distributions are $\rho_D(n)$ and $\rho_{GGE}(n)$, where n can go from 0 to 1, and $n_{\alpha\alpha} \equiv \langle\alpha|\hat{n}_j|\alpha\rangle = \sum_\mu |u_{j\mu}|^2 n^\alpha_\mu$, where $n^\alpha_\mu = 0, 1$ are the occupations of the eigenstate $|\alpha\rangle$. In Fig. 5.6 we plot $\ln[\rho_D(n)]$ and $\ln[\rho_{GGE}(n)]$, computed with the three quenches used before. (Notice that for the quench to $\hat{H}_{lrh}$ with $\alpha = 0.5$ (extended single-particle eigenstates) we plotted the rescaled distribution $\ln[\rho_D(n)]/L$ and $\ln[\rho_{GGE}(n)]/L$.)

The case of a quench to $\hat{H}_{lrh}$ with $\alpha = 2.0$ (localized eigenstates) is quite peculiar. The values that n can assume is actually split in two separated domains, one just above $n = 0$ and one just below $n = 1$, and the mean value is exactly in the middle, where no values of $n_{\alpha\alpha}$ happen to fall. This is due to the strong localization which is at play for this Hamiltonian. As we show in Fig. 5.7, at fixed j, the value of $|u_{j\mu}|^2$ is strongly localized in a single mode $\tilde{\mu}$. This implies that the value $n_{\alpha\alpha} = \sum_\mu |u_{j\mu}|^2 n^\alpha_\mu$ has a strong jump when we go from a state $|\alpha\rangle$ in which the mode $\tilde{\mu}$ is unoccupied, to the state $|\alpha\rangle$ in which the mode $\tilde{\mu}$ is occupied. For the quench to $\hat{H}_A$, with $W = 2$, the localization is not strong enough to produce such a gap: we however expect this to happen for larger values of the disorder amplitude W.

Since $\hat{n}_j$ is a one-body operator, the diagonal and GGE averages coincide (see Subsec. 4.2.1), and therefore, the mean value of the two distributions is the same:

$$\int dn\, \rho_D(n) n = \int dn\, \rho_{GGE}(n) n\,. \tag{5.27}$$

We moreover note that, for this observable, $(\hat{n}_j)^m = \hat{n}_j$ for any positive integer m, and therefore $\langle(\hat{n}_j)^m\rangle_D = \langle(\hat{n}_j)^m\rangle_{GGE}$. However, this does not allow us to conclude that the

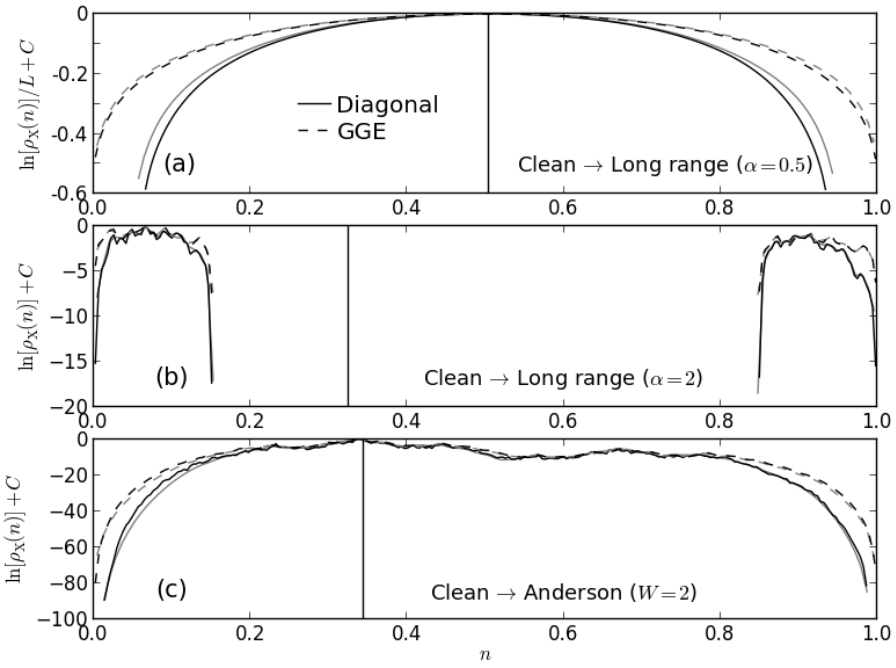

Figure 5.6.: In panel (a), values of $\ln[\rho_D(n)]/L$ and $\ln[\rho_{GGE}(n)]/L$, while in panels (b) and (c), values of $\ln[\rho_D(n)]$ and $\ln[\rho_{GGE}(n)]$. The distributions are computed with the weighted-WLA and we have taken the local density at the middle of the chain, i.e., $j = L/2$. The vertical lines are the diagonal and GGE average of $\hat{n}_j$, which coincide for the local density. The three panels are obtained, using the same quenches used in Fig. 5.3.

two distributions $\rho_D(n)$ and $\rho_{GGE}(n)$ are the same. Indeed, in this case, unlike the case of the total energy, we have that:

$$\int dn\, \rho_D(n) n^2 \neq \langle \hat{n}_j^2 \rangle_D \qquad \int dn\, \rho_{GGE}(n) n^2 \neq \langle \hat{n}_j^2 \rangle_{GGE} \,. \tag{5.28}$$

Local-density variances

The variance of the two distributions can be computed by exploiting again Wick's theorem. We find that:

$$\begin{aligned} \sigma^2_{n,GGE} &= \sum_\mu |u_{j\mu}|^4 \, n^0_\mu \left(1 - n^0_\mu\right) \\ \sigma^2_{n,D} &= \sigma^2_{n,GGE} - \sum_{\mu_1 \neq \mu_2} |u_{j\mu_1}|^2 \, |u_{j\mu_2}|^2 \left| G^0_{\mu_1\mu_2} \right|^2 \,. \end{aligned} \tag{5.29}$$

In Fig. 5.8 we plot $\sigma^2_{n,GGE}$ and $\sigma^2_{n,D}$ as a function of size. We see that, in both ensembles, the variances vanish as $1/L$ when quenching to $\hat{H}_{lrh}$ with $\alpha = 0.5$ (extended eigenstates) while they are finite when quenching to $\hat{H}_A$, and to $\hat{H}_{lrh}$ with $\alpha = 0.5$ (i.e., when the final Hamiltonian has localized eigenstates). These results agree with the findings of Ref. [103], who show that, for large L, the variance of few-body intensive (but not site-averaged) observables remains finite both in the microcanonical ensemble and in the diagonal ensemble for the Aubry-André model.

From the equation for $\sigma^2_{n,GGE}$, we see that it is related to an inverse participation ratio (IPR): the sum is over the eigenmodes μ, [16] each μ weighted with the corresponding

16 The usual $IPR_\mu \equiv \sum_j |u_{j\mu}|^4$, fixes an eigenstate and sums over the sites. However, one can define an $IPR_j \equiv \sum_\mu |u_{j\mu}|^4$ by summing over eigenstates at fixed j. As for the usual IPR_μ, if the eigenstates are all localized (extended), the IPR_j remains finite (vanishes) in the thermodynamic limit.

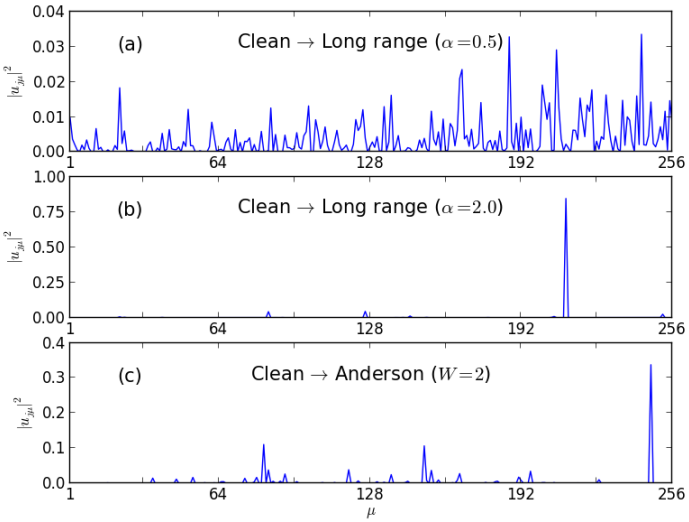

Figure 5.7.: Squared single-particle wavefunction $|u_{j\mu}|^2$ as a function of the eigenstates index μ, at fixed site $j = L/2$. We have taken $L = 256$ and the three panels are obtained using the same quenches of Fig. 5.3.

occupation factor $0 \leqslant n^0_\mu \left(1 - n^0_\mu\right) \leqslant 1$ depending on the initial state. It is therefore easy to realize that:

$$\sigma^2_{n,\mathrm{GGE}} \leqslant \sum_\mu \left|u_{j\mu}\right|^4 = \mathrm{IPR}_j \,, \tag{5.30}$$

where in the last equation we have defined the IPR at fixed site j. This shows that, whenever the IPR goes to zero, i.e., when the final Hamiltonian has delocalized eigenstates, $\sigma^2_{n,\mathrm{GGE}}$ goes to zero as well. For a final Hamiltonian with localized eigenstates we have instead the opposite. Indeed, there is at least one mode $\tilde{\mu}$ localized around j, and therefore there is a single-particle wavefunction $u_{j\tilde{\mu}}$ which does not vanish in the thermodynamic limit. Now, if the initial occupation on this mode $n^0_{\tilde{\mu}}$ is finite, and smaller than 1, in the thermodynamic limit, $\sigma^2_{n,\mathrm{GGE}}$ is finite as well.

Concerning $\sigma^2_{n,D}$, Eq. (5.29) can be rewritten as:

$$\sigma^2_{n,D} = \sigma^2_{n,\mathrm{GGE}} - \delta^2_{jj} \,, \tag{5.31}$$

where δ^2_{jj} is the mean squared time-fluctuations we have introduced in Chap. 4, see Eq. (4.34). In that chapter we have seen that, if the final Hamiltonian has extended eigenstates, then $\delta^2_{jj} \approx 1/L$ for large sizes, while if it has localized eigenstates, then δ^2_{jj} stays finite. This explains all the features shown in Fig. 5.8, in particular the clear difference between $\sigma^2_{n,D}$ and $\sigma^2_{n,\mathrm{GGE}}$ in all cases.

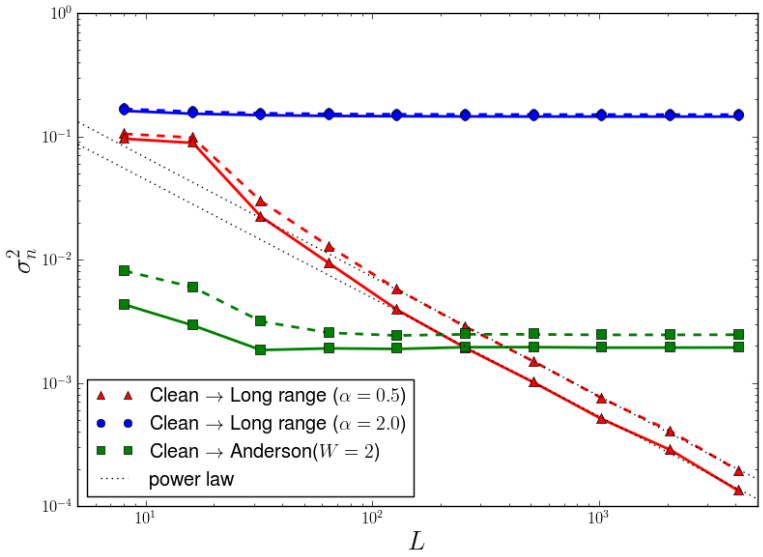

Figure 5.8.: Plot of the variances $\sigma^2_{n,D}$ (solid lines) and $\sigma^2_{n,GGE}$ (dashed lines) as a function of size. The data are obtained using the same set of quenches used in Fig. 5.6. The dotted lines are power-law fits $\sigma^2_n \sim L^{-s}$, where $s \approx 0.97$ in both cases. The values are computed using Eq. (5.29).

6 CONCLUSIONS

In the present thesis we have analyzed some issues related to the relaxation and thermalization of quenched closed quantum systems in presence of disorder. The analysis was carried out by studying, numerically and analytically, the long-time dynamics after a sudden quantum quench, where the initial state is the ground state of an initial Hamiltonian and the system then evolves with a different final Hamiltonian. We have considered three class of disordered one-dimensional chains which can be mapped to quadratic fermionic Hamiltonians: a tight-binding Anderson model, a tight-binding chain with long-range hopping, and the Ising/XY chain.

Concerning the issue of relaxation, we have shown that, when looking at local observables, the localization properties of the final Hamiltonian govern the long-time fluctuations of the observables. Indeed, in presence of localization, the long-time dynamics does not relax towards a stationary state, and time fluctuations generally persist in the expectation values of local operators, even in the thermodynamic limit (see Sec. 4.4). This is not the case for final Hamiltonian with extended states, even in presence of disorder (see Sec. 4.5). The crucial ingredient is, essentially, the presence of a pure-point spectrum of the final Hamiltonian associated to localized wave functions, as opposed to the smooth continuum of a system with extended states.

Concerning the issue of thermalization, we have compared the time averages with the generalized Gibbs ensemble (GGE), which is the relevant statistical ensemble for the free-fermion models we have considered. We have shown analytically that the GGE always predicts the time averages of one-body operators, even at finite sizes (see Subsec. 4.2.1). This is not true in general for many-body operators, where GGE may fail (see Subsec. 4.2.2): we have shown an explicit example (the density-density correlations in the long-range hopping Hamiltonians) in which the GGE average overestimates persistently the corresponding time average (see Subsec. 4.5.2). This failure derives from the non-vanishing of long-time fluctuations of one-body Green's functions. All these results are in perfect agreement with many of the recent results on quenches with similar Hamiltonians (see Sec. 4.7) and clarify the role and the validity of the GGE.

In the final part of the thesis we have introduced an extension of the Wang-Landau algorithm (see Sec. 5.2) which allows to compute weighted distributions associated to quantum quenches, in particular the diagonal and the GGE ensemble expectation-value distributions (see Sec. 5.4).

While we have analyzed systems which are perhaps hard to realize experimentally (for instance, the long-range hopping Hamiltonian), similar results and discussions can be extended to systems which are already been experimentally realized (see Sec. 3.4), like Aubry-André models, where an incommensurate external period potential is added to a one-dimensional chain, and an Anderson-like transition can be seen for a finite strength of the potential.

What is left completely untouched in the present thesis is understanding the role of interactions, possibly in combination with quenched disorder, in the out-of-equilibrium dynamics of closed quantum systems. This is of course a hard and long-standing problem, even at equilibrium, which has stimulated a recent interest in the issue of many-body localization [24, 26, 113–115]. This issue clearly call for future investigations.

ACKNOWLEDGEMENTS

My first thanks go to my supervisor Giuseppe E. Santoro. I am really grateful to Giuseppe for his patience, enthusiasm and continuous support during my Ph.D. at SISSA.

A special thanks go to Alessandro Silva for his suggestions that allowed to make progress in my research.

I would like to thank also Angelo, Giuseppe, Jamir, Pietro, and the whole "group meeting" team for the useful and pleasant discussions on the topic of out-of-equilibrium quantum physics.

Last but not the least, I am grateful to Elisa and my family, for their love, support and patience during the last four years.

A RIEMANN-LEBESGUE LEMMA

In this appendix we first show the proof of the Riemann-Lebesgue lemma and then we emphasize the link between this lemma and the long-time fluctuations of the expectation values after a quantum quench.

Let's take f a L^1 integrable function on $\mathbb{R}^d$. We recall that a L^1 integrable function is a function in which the Lebesgue integral [116] of $|f|$ is finite:

$$\int_{\mathbb{R}^d} d\mathbf{x}\,|f(\mathbf{x})| < \infty \,. \tag{A.1}$$

The Fourier transform of f is defined as:

$$F[f](\mathbf{z}) \equiv \int_{\mathbb{R}^d} d\mathbf{x}\, f(\mathbf{x}) e^{-i\mathbf{z}\cdot\mathbf{x}} \,. \tag{A.2}$$

The Riemann-Lebesgue lemma states that:

$$\lim_{|\mathbf{z}|\to\infty} |F[f](\mathbf{z})| = 0 \tag{A.3}$$

The mathematical proof of the general case can be found in Ref. [117]; here we focus on the one dimensional case $d = 1$ (the case we actually meet in the present thesis). We define the interval $I = [a, b[$ and its characteristic function

$$w_I(x) = \begin{cases} 1 & \text{if} \quad x \in I \\ 0 & \text{if} \quad x \notin I \end{cases} \,. \tag{A.4}$$

Its Fourier transform is:

$$F[w_I](z) = \int_a^b dx\, e^{-izx} = \frac{e^{-izb} - e^{-iza}}{-iz} \,, \tag{A.5}$$

and therefore

$$|F[w_I](z)| \leqslant \frac{2}{|z|} \,. \tag{A.6}$$

For the linearity of the Fourier transform this results holds for every step-function $f(x)$ which is constant on a finite number of (bounded) intervals and vanishes outside. For instance, if f is made by two step-functions, i.e. $f(x) = f_1 w_{I_1}(x) + f_2 w_{I_2}(x)$, its Fourier transform is:

$$|F[f](z)| = \left|f_1 F[w_{I_1}](z) + f_2 F[w_{I_2}](z)\right| \leqslant 2\frac{|f_1| + |f_2|}{|z|} \,. \tag{A.7}$$

These step-functions are dense in the space L^1, that is, for any $\epsilon > 0$, there exists a step function $f_\epsilon(x)$ such that:

$$\int_{-\infty}^{+\infty} dx\, |f(x) - f_\epsilon(x)| < \epsilon \,. \tag{A.8}$$

Again, for the linearity of the Fourier transform:

$$F[f](z) = F[f - f_\epsilon](z) + F[f_\epsilon](z) \,, \tag{A.9}$$

and:

$$|F[f](z)| \leqslant |F[f - f_\epsilon](z)| + |F[f_\epsilon](z)| \leqslant \epsilon + |F[f_\epsilon](z)| \,, \tag{A.10}$$

which results from the relation:

$$|F[f - f_\epsilon](z)| \leqslant \int_{-\infty}^{+\infty} dx\, \left|[f(x) - f_\epsilon(x)]\, e^{-izx}\right| \leqslant \epsilon \,. \tag{A.11}$$

Thus, for any ϵ we have:

$$\lim_{|z|\to\infty} |F[f](z)| \leqslant \epsilon + \lim_{|z|\to\infty} |F[f_\epsilon](z)| \ . \tag{A.12}$$

But the second term on the right-hand-side is zero for a step function $f_\epsilon(x)$ and therefore, for any $\epsilon > 0$ we have:

$$\lim_{|z|\to\infty} |F[f](z)| \leqslant \epsilon \ , \tag{A.13}$$

which obviously implies, since $\epsilon > 0$ is arbitrarily small, that:

$$\lim_{|z|\to\infty} |F[f](z)| = 0 \ . \tag{A.14}$$

Let us now return to the problem of time fluctuations after a quantum quench. The time fluctuation of the expectation value of an observable $\hat{A}$ can be written as:

$$\delta A(t) = \int_{-\infty}^{+\infty} d\Omega \, e^{-i\Omega t/\hbar} f_A(\Omega) = F[f_A](t/\hbar) \ . \tag{A.15}$$

where

$$f_A(\Omega) \equiv \sum_{\alpha\neq\beta} c_\beta^* c_\alpha A_{\beta\alpha} \delta\left(\Omega - E_\alpha + E_\beta\right) \tag{A.16}$$

is a weighted joint (many-body) density of states, $c_\alpha \equiv \langle\alpha|\psi_0\rangle$, $\{E_\alpha\}$ is the spectrum of the Hamiltonian after the quench, and $A_{\beta\alpha} \equiv \langle\beta|\hat{A}|\alpha\rangle$ (for the details see Chap. 2). $f_A(\Omega)$ is a sum of Dirac's deltas and the Fourier transform of any finite sum of Dirac's deltas leads to a non-vanishing limit for $t \to \infty$. This is not in contradiction with the Riemann-Lebesgue lemma, since the Dirac's delta is not Lebesgue integrable. The way to get vanishing fluctuations, i.e.,

$$\lim_{t\to\infty} \delta A(t) = 0 \ , \tag{A.17}$$

is that the sum has infinite terms and the Dirac's deltas smoothly merge in such a way that $f_A(\Omega)$ becomes an L^1 integrable function. In the thesis we show that when the spectrum has an important pure-point spectrum part, i.e., delta functions associated to localized eigenstates, then one should expect persistent time fluctuations for certain operators. On the contrary, when the eigenstates are extended, for some operators the $f_A(\Omega)$ is smooth and the long-time fluctuations vanish. See Chap. 4 for details.

B DISORDER IN THE INITIAL STATE: A TOY MODEL

In this appendix we consider a set of quenches in which the final Hamiltonian is a disorder-free tight-binding chain. We show analytically that for disordered fully-localized initial states the time fluctuations of the Green's functions vanish with a power law.

When the final Hamiltonian is $\hat{H}_{\text{hom}}$ the one-body Green's functions are:

$$G_{j_1 j_2}(t) = \frac{1}{L}\sum_{k_1 k_2} e^{-i(k_1 j_1 - k_2 j_2)} e^{-i(\epsilon_{k_2} - \epsilon_{k_1})t} G^0_{k_1 k_2} \,, \tag{B.1}$$

where we have used Eq. (4.6). From the definition of $\hat{c}^\dagger_k$ and $\hat{c}_k$ (see Eqs. (3.6)) we have:

$$G^0_{k_1 k_2} \equiv \langle \Psi_0 | \hat{c}^\dagger_{k_1} \hat{c}_{k_2} | \Psi_0 \rangle = \frac{1}{L}\sum_{l_1 l_2} e^{-i(k_2 l_2 - k_1 l_1)} \langle \Psi_0 | \hat{c}^\dagger_{l_1} \hat{c}_{l_2} | \Psi_0 \rangle \,. \tag{B.2}$$

Plugging this equation inside the expression of $G_{j_1 j_2}(t)$ and rearranging the summations we get:

$$G_{j_1 j_2}(t) = \sum_{l_1 l_2} g^*_{j_1 - l_1}(t) g_{j_2 - l_2}(t) \langle \Psi_0 | \hat{c}^\dagger_{l_1} \hat{c}_{l_2} | \Psi_0 \rangle \,, \tag{B.3}$$

where:

$$g_n(t) = \frac{1}{L}\sum_k e^{ikn} e^{-i\epsilon_k t} \,. \tag{B.4}$$

In the thermodynamic limit, switching the summation to an integration, and using the dispersion $\epsilon_k = -2J\cos k + h$, we have:

$$\begin{aligned} g_n(t) &= \int_{-\pi}^{\pi} \frac{dk}{2\pi} e^{ikn} e^{-i(-2J\cos k + h)t} \\ &= e^{-iht} i^n \int_{-\pi}^{\pi} \frac{dk'}{2\pi} e^{i(2Jt)\sin k'} e^{-ink'} \\ &= e^{-iht} i^n J_n(2Jt) \,, \end{aligned} \tag{B.5}$$

where in the first step we have done a change of variable $k' = \pi/2 - k$ and in the last step we used the integral representation of the Bessel functions of the first kind $J_n(x)$. For large values of x the $J_n(x)$ can be approximated as:

$$J_n(x) \sim \sqrt{\frac{2}{\pi x}} \cos\left(z - \frac{n\pi}{2} - \frac{\pi}{4}\right) \qquad \text{for} \quad x \gg \left| n^2 - \frac{1}{4} \right| \,. \tag{B.6}$$

Therefore each term $g^*_{j_1 - l_1}(t) g_{j_2 - l_2}(t) \langle \Psi_0 | \hat{c}^\dagger_{l_1} \hat{c}_{l_2} | \Psi_0 \rangle$ in Eq. (B.3) goes to zero as $1/t$ for large enough times. In other words, $G_{j_1 j_2}(t)$ vanishes as $1/t$ for large times when the initial state has a finite number of terms (even in the thermodynamic limit) with $\langle \Psi_0 | \hat{c}^\dagger_{l_1} \hat{c}_{l_2} | \Psi_0 \rangle \neq 0$. Indeed, in this case, we can define $n_{\max}$ as the maximum order of the Bessel functions which appear in the summation. Then, for $t \gg n^2_{\max}/2J$, the approximation in Eq. (B.6) is valid for any term and $G_{j_1 j_2}(t) \sim 1/t$. However we can't still say anything about quenches in which, in the thermodynamic limit, there are an infinite number of terms such that $\langle \Psi_0 | \hat{c}^\dagger_{l_1} \hat{c}_{l_2} | \Psi_0 \rangle \neq 0$. In this case in Eq. (B.3) there is a double infinite summation which could produce a non vanishing long-time limit and non-vanishing long-time fluctuations.

Now, to make progress, we restrict the initial state to ground states of $\hat{H}_A$ in which $J = 0$. The hopping term of the initial Hamiltonian is zero and the eigenstates are fully-localized fermions in each site. The state $|\Psi_0\rangle$ has a fermion in site j when $h_j < 0$, and therefore:

$$\langle\Psi_0|\hat{c}^\dagger_{j_1}\hat{c}_{j_2}|\Psi_0\rangle = n^0_{j_1}\delta_{j_1 j_2}\,, \tag{B.7}$$

where n^0_j is zero if $h_j > 0$ and one if $h_j < 0$. For this $|\Psi_0\rangle$ the number of terms for which $\langle\Psi_0|\hat{c}^\dagger_{j_1}\hat{c}_{j_2}|\Psi_0\rangle$ is non zero can be infinite in the thermodynamic limit and we can't use the approximation in Eq. (B.6). Let's take random initial Hamiltonians in which $h_j < 0$ with probability p, and $h_j \geqslant 0$ with probability $1-p$. With this set of initial states:

$$G^0_{k_1 k_2} = \frac{1}{L}\sum_l n^0_l e^{-i(k_2-k_1)l}\,, \tag{B.8}$$

and therefore $G^0_{kk} = N_F/L = p$. When we compute the time average of $G_{j_1 j_2}(t)$ starting starting from Eq. (B.1), the non zero terms are the one for which $\epsilon_{k_1} = \epsilon_{k_2}$ (namely $k_1 = k_2$ and, for the single-particle degeneracy, $k_1 = -k_2$) and therefore:

$$\overline{G_{j_1 j_2}} = \frac{1}{L}\sum_k e^{ik(j_2-j_1)}G^0_{kk} + \frac{1}{L}\sum_{k\neq 0} e^{-ik(j_1+j_2)}G^0_{k-k}\,. \tag{B.9}$$

In the thermodynamic limit the second term is zero because G^0_{k-k} goes to zero as $1/L$ for this set of initial states, and therefore $\overline{G_{j_1 j_2}} = p\delta_{j_1 j_2}$. The time fluctuations with respect to the time average are:

$$\begin{aligned}\delta G_{j_1 j_2}(t) &= G_{j_1 j_2}(t) - p\delta_{j_1 j_2}\\ &= \frac{1}{L}\sum_{k_1 k_2} e^{-i(k_1 j_1 - k_2 j_2)}e^{-i(\epsilon_{k_2}-\epsilon_{k_1})t}\left(G^0_{k_1 k_2} - p\delta_{k_1 k_2}\right)\,,\end{aligned} \tag{B.10}$$

where in the second step we used the orthonormality of planewaves. Since now we have different realizations of $|\Psi_0\rangle$ we can think at $\delta G_{j_1 j_2}(t)$ as a random variable with a given probability density at any fixed t. In Fig. B.1 we fix $j_1 = j_2 = j$ and we plot this probability density in the plane time-δG_{jj}, computed numerically using many realizations of $|\Psi_0\rangle$. The distribution shrinks for $t \to \infty$, suggesting that the long-time fluctuations of $G_{jj}(t)$ vanish. To characterize quantitatively this effect we compute analytically the moments of $\delta G_{j_1 j_2}(t)$ at any fixed time t. The average is easily:

$$\left[\delta G_{j_1 j_2}(t)\right]_{av} = \frac{1}{L}\sum_{k_1 k_2} e^{-i(k_1 j_1 - k_2 j_2)}e^{-i(\epsilon_{k_2}-\epsilon_{k_1})t}\left(\left[G^0_{k_1 k_2}\right]_{av} - p\delta_{k_1 k_2}\right) = 0\,, \tag{B.11}$$

where we have exploited the fact that:

$$\left[G^0_{k_1 k_2}\right]_{av} = \frac{1}{L}\sum_l \left[n^0_l\right]_{av} e^{-i(k_2-k_1)l} = \frac{p}{L}\sum_l e^{-i(k_2-k_1)l} = p\delta_{k_1 k_2}\,. \tag{B.12}$$

This is not surprising: averaging over the disorder directly $\delta G_{j_1 j_2}(t)$ there is a cancellation effect which gives an averaged time fluctuation equal to zero for any time. Evidently this doesn't prove that the fluctuations go to zero for $t \to \infty$. More interesting is the standard deviation:

$$\begin{aligned}\sigma_{j_1 j_2}(t) &\equiv \left[|\delta G_{j_1 j_2}(t)|^2\right]_{av}\\ &= \frac{1}{L^2}\sum_{k_1 k_2}\sum_{k_3 k_4} e^{-i((k_1-k_3)j_1-(k_2-k_4)j_2)}e^{-i(\epsilon_{k_2}-\epsilon_{k_1}-\epsilon_{k_4}+\epsilon_{k_3})t}\cdot\\ &\qquad\cdot\left(\left[G^0_{k_1 k_2}G^{0*}_{k_3 k_4}\right]_{av} - p^2\delta_{k_1 k_2}\delta_{k_3 k_4}\right)\\ &= \frac{p(1-p)}{L^3}\sum_{k_1 k_2}\sum_{k_3 k_4} e^{-i((k_1-k_3)j_1-(k_2-k_4)j_2)}e^{-i(\epsilon_{k_2}-\epsilon_{k_1}-\epsilon_{k_4}+\epsilon_{k_3})t}\cdot\\ &\qquad\cdot\delta_{k_2-k_1 k_4-k_3}\,,\end{aligned} \tag{B.13}$$

where $\delta_{k_2-k_1k_4-k_3}$ is a Kronecker's delta modulo 2π (i.e., $\delta_{xy} = 1$ only when $x = y + 2n\pi$, with n integer), and we used the relation:

$$\left[G^0_{k_1k_2} G^{0*}_{k_3k_4}\right]_{av} = \frac{p(1-p)}{L}\delta_{k_2-k_1k_4-k_3} + p^2\delta_{k_1k_2}\delta_{k_3k_4}\,, \tag{B.14}$$

which comes from the fact that the n^0_l's are uncorrelated for different sites. In Fig. B.1, superimposed to the density distribution, there is a plot of $\pm\sigma_{j_1j_2}(t)$, with $j_1 = j_2$. From the inset it is clear that $\sigma_{jj}(t)$ goes to zero with a power law for $t \to \infty$. We actually find $\sigma_{jj}(t) \sim A/t^\nu$ with $\nu \approx 0.44$, probably going to larger times we would get $\nu = 1/2$ (but notice that larger times means larger sizes, in order to avoid revival effects). This proves that, in average, the long-time fluctuations of $G_{j_1j_2}(t)$ go to zero for this set of quenches. This show the importance of the final Hamiltonian on the time fluctuations of $G_{j_1j_2}(t)$: even with disordered and localized initial states, the long-time fluctuations of $G_{j_1j_2}(t)$ vanish.

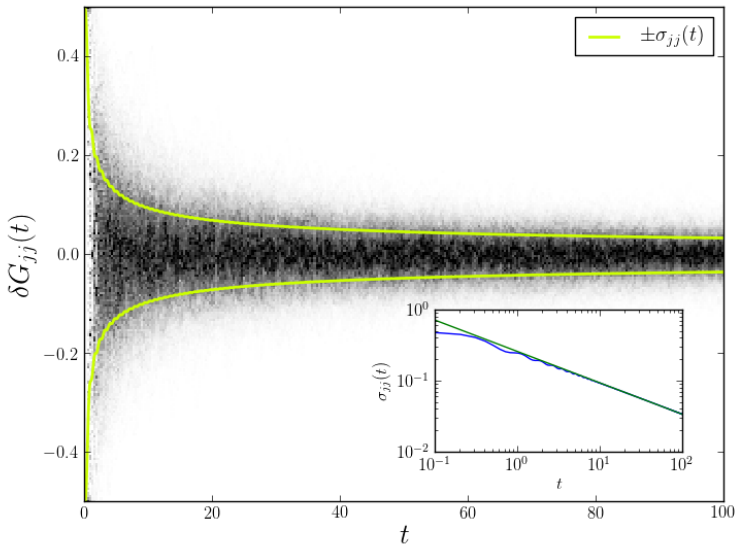

Figure B.1.: Probability density to find the value $\delta G_{jj}(t)$ at a fixed time t in quenches in which the initial state is a random disposition of localized fermion and the final Hamiltonian is $\hat{H}_{hom}$. The two lines are the standard deviation $\sigma_{jj}(t)$ computed using Eq. (B.13). In the inset a plot of $\sigma_{jj}(t)$ as a function of time in log scale. The line is a fit with the function $f(t) = A/t^\nu$, with $\nu \approx 0.44$. The probability density is obtained computing $\delta G_{jj}(t)$ for 2000 realizations of the initial state with $p = 1/2$ and $L = 500$.

In Ref. [23] was shown numerically that, starting with non-translationally invariant initial states and using an homogeneous final Hamiltonian, the fluctuations of $G_{j_1j_2}(t)$ go to zero for $t \to \infty$. It was argued that this happens because, in the thermodynamic limit, $|G^0_{k_1k_2}|^2 \to n^0_k\delta_{k_1k_2}$. This sounds reasonable because in this case the main contributions for $G_{j_1j_2}(t)$ in Eq. (B.1) come from the diagonal, time-independent, terms. This is for instance true for the set of quenches we have just considered with fully-localized random initial states. However, we are going to show that the fluctuations go to zero even for initial states in which $G^0_{k_1k_2}$ has important non-vanishing contributions for $k_1 \neq k_2$ in the thermodynamic limit. Let's consider again the fully-localized Hamiltonian where the local field h_j has regular repeated intervals of size M with positive and negative h_j (see sketch in the inset of Fig (B.2)). Calculating $G^0_{k_1k_2}$ we get:

$$G^0_{k_1k_2} = \frac{1}{L}\frac{\sin\left((k_1-k_2)L/2\right)}{\sin\left((k_1-k_2)M\right)}\frac{\sin\left(\frac{k_1-k_2}{2}M\right)}{\sin\left(\frac{k_1-k_2}{2}\right)}\,, \tag{B.15}$$

which is plotted in the inset of Fig. B.2 for $M = 2$ and two different sizes. Clearly, there are off-diagonal terms of $G^0_{k_1 k_2}$ which do not vanish in the thermodynamic limit, but reveal a well defined structure: a series of Kronecker's delta centered at $k_1 - k_2 = 2\pi m$ and $k_1 - k_2 = \pi(2m+1)/M$ with m a natural number. For $j_1 = j_2$ we can compute analytically $\delta G_{jj}(t)$ and we have found that it is proportional to $J_0(2\sqrt{2}Jt)$, where $J_0(x)$ is the Bessel function of order 0 which, as we have seen before, goes to zero as $1/\sqrt{t}$ for large times. In Fig. B.2 there is a plot of $\delta G_{j_1 j_2}(t)$ with $j_1 \neq j_2$ and also in this case the fluctuations go to zero with an envelope $1/\sqrt{t}$. This confirms that, while $G^0_{k_1 k_2}$ is not necessarily a simple delta-function $\delta_{k_1 k_2}$, the the long time fluctuations vanish. This emphasizes the importance of the final Hamiltonian with respect to the properties of the initial state, as we have shown and emphasized in Chap. 4.

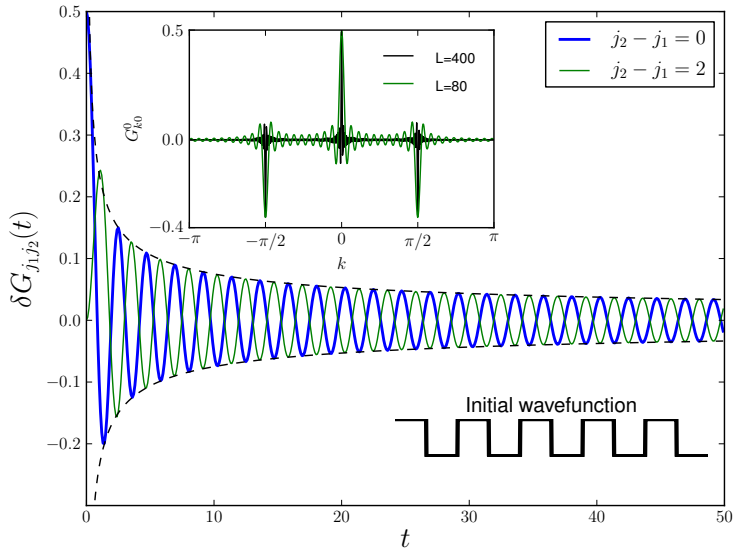

Figure B.2.: Time fluctuations of $G_{j_1 j_2}(t)$ for a quench with a tight-binding chain in which the final Hamiltonian is homogeneous and the initial $\hat{H}_0$ has $J = 0$ and h^0_i grater than zero only on consecutive intervals of amplitude 2 (square wave pattern). The data are obtained using $L = 2000$. The dashed line is the envelop $\pm 1/\sqrt{\sqrt{2}\pi Jt}$. In the inset there are two plots of $G^0_{k_1 k_2}$ with $k_2 = 0$, for the same quench, but two different sizes.

C JENSEN'S INEQUALITY

The Jensen's inequality can be stated in a discrete or continuous version. The discrete version states that, if $f(x)$ is a convex function, given the numbers x_i, where $i = 1, \dots, M$, and the positive normalized weights λ_i (i.e., $\sum_i \lambda_i = 1$), then:

$$f\left(\sum_{i=1}^{M} \lambda_i x_i\right) \leqslant \sum_{i=1}^{M} \lambda_i f(x_i) \,. \tag{C.1}$$

The inequality is reversed if $f(x)$ is concave. We are going to prove this inequality by induction. If $M = 2$, using that λ_1 and λ_2 are non-negative real numbers such that $\lambda_1 + \lambda_2 = 1$, from the definition of convexity:

$$f(\lambda_1 x_1 + \lambda_2 x_2) \leqslant \lambda_1 f(x_1) + \lambda_2 f(x_2) \,. \tag{C.2}$$

Suppose now that the inequality holds true also for $M = N - 1$: we then to prove it for $M = N$. Indeed:

$$\begin{aligned} f\left(\sum_{i=1}^{N} \lambda_i x_i\right) &\leqslant f(\lambda_1 x_1 + (1-\lambda_1) \sum_{i=2}^{N} \frac{\lambda_i}{1-\lambda_1} x_i) \\ &\leqslant \lambda_1 f(x_1) + (1-\lambda_1) f(\sum_{i=2}^{N} \frac{\lambda_i}{1-\lambda_1} x_i) \\ &\leqslant \sum_{i=1}^{N} \lambda_i f(x_i) \,, \end{aligned} \tag{C.3}$$

where we used twice the Jensen's inequality, in the first step for $M = 2$ and in the final step for $M = N - 1$.

A consequence of this inequality, obtained by just fixing $\lambda_i = 1/M$, is that:

$$f([x]_{av}) \leqslant [f(x)]_{av} \,, \tag{C.4}$$

where $[\cdot]_{av}$ indicates the standard arithmetic mean. Therefore, using the convex function $f(x) = e^x$, we have:

$$e^{[x]_{av}} \leqslant [e^x]_{av} \,. \tag{C.5}$$

We can also prove that the arithmetic mean is always greater than the geometric mean:

$$[x]_{av} = \frac{1}{M} \sum_{i=1}^{M} x_i \geqslant \sqrt[M]{\prod_{i=1}^{M} x_i} = [x]^G_{av} \,, \tag{C.6}$$

which is a straightforward consequence of Eq. (C.5):

$$\frac{1}{M} \sum_{i=1}^{M} x_i = \frac{1}{M} \sum_{i=1}^{M} e^{\ln x_i} = \left[e^{\ln x_i}\right]_{av} \geqslant e^{[\ln x]_{av}} = \sqrt[M]{e^{\sum_{i=1}^{M} \ln x_i}} = \sqrt[M]{\prod_{i=1}^{M} x_i} \,. \tag{C.7}$$

The continuous version of Jensen's inequality states that if $P(x)$ is a probability distribution, $g(x)$ any real-valued measurable function and $f(x)$ a convex function over the range of g, then:

$$f\left(\int dx\, g(x) P(x)\right) \leqslant \int dx\, f(g(x)) P(x) \,. \tag{C.8}$$

Taking $g(x) = x$ we obtain:

$$f\left(\int dx\, xP(x)\right) \leqslant \int dx\, f(x)P(x)\,, \tag{C.9}$$

which is the continuous counterpart of Eq. (C.4):

$$f\left(\langle x\rangle\right) \leqslant \langle f(x)\rangle\,, \tag{C.10}$$

where now the mean $\langle x\rangle \equiv \int dx\, xP(x)$ is the average over the probability distribution $P(x)$.

D SOME PROOFS

$|G^0_{\mu_1\mu_2}|^2$'S SUM FOR THE TIGHT-BINDING CHAIN

In this section we are going to show that, in the tight-binding class of Hamiltonians, we have:

$$\sum_{\mu_1\mu_2} |G^0_{\mu_1\mu_2}|^2 = \sum_{\mu_1\mu_2} |\langle\Psi_0|\hat{c}^\dagger_{\mu_1}\hat{c}_{\mu_2}|\Psi_0\rangle|^2 = N_F\,, \tag{D.1}$$

where $|\Psi_0\rangle$ is the ground state of an initial Hamiltonian $\hat{H}_0$, N_F the total number of fermions in this state, and $\hat{c}^\dagger_\mu$ and $\hat{c}_\mu$ are the fermionic operators associated to the modes of a different Hamiltonian $\hat{H}$. The proof start from the following relations:

$$\hat{c}_\mu = \sum_{j=1}^{L} u^*_{j\mu}\hat{c}_j \qquad\qquad \hat{c}^\dagger_\mu = \sum_{j=1}^{L} u_{j\mu}\hat{c}^\dagger_j \tag{D.2}$$

$$\hat{c}_j = \sum_{\nu=1}^{L} u^0_{j\nu}\hat{c}^0_\nu \qquad\qquad \hat{c}^\dagger_j = \sum_{j=\nu}^{L} u^{0*}_{j\nu}\hat{c}^\dagger_\nu\,, \tag{D.3}$$

where $u^0_{j\nu}$ are the single-particle eigenstates of $\hat{H}_0$, and $\hat{c}^{0\dagger}_\nu$ and $\hat{c}^0_{\nu_2}$ are the corresponding fermionic operators. Therefore:

$$\langle\Psi_0|\hat{c}^\dagger_{\mu_1}\hat{c}_{\mu_2}|\Psi_0\rangle = \sum_{j_1j_2}\sum_{\nu} u_{j_1\mu_1}u^{0*}_{j_1\nu}u^*_{j_2\mu_2}u^0_{j_2\nu}n^0_\nu\,, \tag{D.4}$$

where n^0_ν is 0 (or 1) if the mode ν is empty (or occupied) in the ground state $|\Psi_0\rangle$. Finally using the orthonormality of the wavefunctions $u_{j\mu}$ and $u^0_{j\nu}$ we get:

$$\begin{aligned}
\sum_{\mu_1\mu_2} |\langle\Psi_0|\hat{c}^\dagger_{\mu_1}\hat{c}_{\mu_2}|\Psi_0\rangle|^2 &= \sum_{\substack{\mu_1\mu_2\\ \nu_1\nu_2}}\sum_{\substack{j_1j_2\\ j_3j_4}} u_{j_1\mu_1}u^{0*}_{j_1\nu_1}u^*_{j_2\mu_2}u^0_{j_2\nu_1}u^*_{j_3\mu_1}u^0_{j_3\nu_2}u_{j_4\mu_2}u^{0*}_{j_4\nu_2}n^0_{\nu_1}n^0_{\nu_2}\\
&= \sum_{\substack{j_1j_2\\ j_3j_4}}\sum_{\nu_1\nu_2} \delta_{j_1j_3}\delta_{j_2j_4}u^{0*}_{j_1\nu_1}u^0_{j_2\nu_1}u^0_{j_3\nu_2}u^{0*}_{j_4\nu_2}n^0_{\nu_1}n^0_{\nu_2}\\
&= \sum_{j_1j_2}\sum_{\nu_1\nu_2} u^{0*}_{j_1\nu_1}u^0_{j_2\nu_1}u^0_{j_1\nu_2}u^{0*}_{j_2\nu_2}n^0_{\nu_1}n^0_{\nu_2}\\
&= \sum_{\nu_1\nu_2} \delta_{\nu_1\nu_2}n^0_{\nu_1}n^0_{\nu_2}\\
&= \sum_{\nu} n^0_\nu = N_F\,,
\end{aligned} \tag{D.5}$$

which had to be demonstrated.

$|\mathcal{G}^0_{\mu_1\mu_2}|^2$'S SUM FOR THE ISING/XY CHAIN

In this section we are going to show that, in the Ising/XY class of Hamiltonians, we have:

$$\sum_{\mu_1\mu_2} |\mathcal{G}^0_{\mu_1\mu_2}|^2 = \sum_{\mu_1\mu_2} |\langle\Psi_0|\hat{\Gamma}^\dagger_{\mu_1}\hat{\Gamma}_{\mu_2}|\Psi_0\rangle|^2 = L\,, \tag{D.6}$$

where $|\Psi_0\rangle$ is the ground state of an initial Ising/XY Hamiltonian $\hat{H}_0$, L is the chain size, and $\hat{\Gamma}^\dagger_\mu$ and $\hat{\Gamma}_{\mu_2}$ are the component of the Nambu vector associated to the modes of the final Hamiltonian $\hat{H}$ (see Sec. 3.3 for the details).

Defining $\hat{\Gamma}_0 \equiv U_0^\dagger \hat{\Psi}$ as the Nambu vector associated to the modes of $\hat{H}_0$, and using the relation $\hat{\Gamma} = U^\dagger \hat{\Psi}$, we have:

$$\hat{\Gamma} = U^\dagger U_0 \hat{\Gamma}_0 \,, \tag{D.7}$$

where U_0 and U are $2L \times 2L$ unitary transformations. Defining $R \equiv U^\dagger U_0$ we have:

$$\begin{aligned}\langle \Psi_0 | \hat{\Gamma}^\dagger_{\mu_1} \hat{\Gamma}_{\mu_2} | \Psi_0 \rangle &= \sum_{\nu_1 \nu_2} R^*_{\mu_1 \nu_1} R_{\mu_2 \nu_2} \langle \Psi_0 | \hat{\Gamma}^{0\dagger}_{\nu_1} \hat{\Gamma}^0_{\nu_2} | \Psi_0 \rangle \\ &= \sum_{\nu=L+1}^{2L} R^*_{\mu_1 \nu} R_{\mu_2 \nu} \,,\end{aligned} \tag{D.8}$$

where in the last step we exploited the fact that $|\Psi_0\rangle$ is the empty states with respect to the fermionic operators $\hat{\gamma}^0_\mu$ and $\hat{\gamma}^{0\dagger}_\mu$, and therefore the terms $\langle \Psi_0 | \hat{\Gamma}^{0\dagger}_{\nu_1} \hat{\Gamma}^0_{\nu_2} | \Psi_0 \rangle$ are one when $\nu_1 = \nu_2$ with $\nu_2 > L$, and zero otherwise. Finally we have:

$$\begin{aligned}\sum_{\mu_1 \mu_2} |\langle \Psi_0 | \hat{\Gamma}^\dagger_{\mu_1} \hat{\Gamma}_{\mu_2} | \Psi_0 \rangle|^2 &= \sum_{\mu_1 \mu_2} \sum_{\nu_1=L+1}^{2L} \sum_{\nu_2=L+1}^{2L} R^*_{\mu_1 \nu_1} R_{\mu_2 \nu_1} R_{\mu_1 \nu_2} R^*_{\mu_2 \nu_2} \\ &= \sum_{\nu_1=L+1}^{2L} \sum_{\nu_2=L+1}^{2L} \left[\sum_{\mu_1} R^*_{\mu_1 \nu_1} R_{\mu_1 \nu_2} \right] \left[\sum_{\mu_1} R_{\mu_2 \nu_1} R^*_{\mu_2 \nu_2} \right] \\ &= \sum_{\nu_1=L+1}^{2L} \sum_{\nu_2=L+1}^{2L} \delta_{\nu_1 \nu_2} = L \,,\end{aligned} \tag{D.9}$$

where we used the fact that R is unitary.

$\delta^2_{j_1 j_2}$ FOR A QUENCH TO A NON-DISORDERED TIGHT-BINDING CHAIN

When the final eigenstates are extended the value of $\delta^2_{j_1 j_2}$ goes to zero in the thermodynamic limit. In the particular case in which the final $\hat{H}$ is translationally invariant, we have to take care of the degeneracies k, $-k$, where k is the momentum, and of the particle-hole symmetry, which were not taken into account in the general derivation of the expression for $\delta^2_{j_1 j_2}$ in Eq. (4.36). In this case, starting from Eq. (4.6), the time-average of the single-fermion Green's functions is:

$$\overline{G_{j_1 j_2}} = \sum_k u^*_{j_1 k} u_{j_2 k} \langle \Psi_0 | \hat{c}^\dagger_k \hat{c}_k | \Psi_0 \rangle + u^*_{j_1 k} u_{j_2 -k} \langle \Psi_0 | \hat{c}^\dagger_k \hat{c}_{-k} | \Psi_0 \rangle \,, \tag{D.10}$$

where $u_{jk} = \exp(ikj)/\sqrt{L}$ is the plane wave with momentum k and the second term is due to the degeneracy k, $-k$. The time-fluctuations of $G_{j_1 j_2}(t)$ is then equal to:

$$G_{j_1 j_2}(t) - \overline{G_{j_1 j_2}} = {\sum_{k_1 k_2}}' e^{i\epsilon_{k_1} t} e^{-i\epsilon_{k_2} t} u^*_{j_1 k_1} u_{j_2 k_2} \langle \Psi_0 | \hat{c}^\dagger_{k_1} \hat{c}_{k_2} | \Psi_0 \rangle \,,$$

where the prime indicates that the summation is over all the k_1 and k_2 with $|k_1| \neq |k_2|$. Using this expression and the definition of $\delta^2_{j_1 j_2}$ (see Eq. 4.34) we have:

$$\delta^2_{j_1 j_2} = {\sum_{k_1 k_2}}' {\sum_{k_3 k_4}}' \Delta(k_1, k_2, k_3, k_4) u^*_{j_1 k_1} u_{j_2 k_2} u_{j_1 k_3} u^*_{j_2 k_4} \langle \Psi_0 | \hat{c}^\dagger_{k_1} \hat{c}_{k_2} | \Psi_0 \rangle \langle \Psi_0 | \hat{c}^\dagger_{k_3} \hat{c}_{k_4} | \Psi_0 \rangle^* \,, \tag{D.11}$$

where $\Delta(k_1,k_2,k_3,k_4) \equiv \overline{e^{i(\epsilon_{k_1}-\epsilon_{k_2}-\epsilon_{k_3}+\epsilon_{k_4})t}}$ is one when $\epsilon_{k_1}-\epsilon_{k_2}-\epsilon_{k_3}+\epsilon_{k_4}=0$ and zero otherwise. Using the fact that $|u_{jk}| = 1/\sqrt{L}$ we have:

$$\begin{aligned}
\delta^2_{j_1 j_2} &\leqslant \frac{1}{L^2}{\sum_{k_1 k_2}}' {\sum_{k_3 k_4}}' \Delta(k_1,k_2,k_3,k_4) \left|\langle\Psi_0|\hat{c}^\dagger_{k_1}\hat{c}_{k_2}|\Psi_0\rangle\right| \left|\langle\Psi_0|\hat{c}^\dagger_{k_3}\hat{c}_{k_4}|\Psi_0\rangle\right| \\
&\leqslant \frac{1}{2L^2}{\sum_{k_1 k_2}}' {\sum_{k_3 k_4}}' \Delta(k_1,k_2,k_3,k_4) \left(\left|\langle\Psi_0|\hat{c}^\dagger_{k_1}\hat{c}_{k_2}|\Psi_0\rangle\right|^2 + \left|\langle\Psi_0|\hat{c}^\dagger_{k_3}\hat{c}_{k_4}|\Psi_0\rangle\right|^2\right) \\
&\leqslant \frac{1}{L^2}{\sum_{k_1 k_2}}' \left(\left|\langle\Psi_0|\hat{c}^\dagger_{k_1}\hat{c}_{k_2}|\Psi_0\rangle\right|^2 {\sum_{k_3 k_4}}' \Delta(k_1,k_2,k_3,k_4)\right) ,
\end{aligned} \tag{D.12}$$

where (in the second inequality) we used that, if a and b are real numbers then $2ab \leqslant a^2+b^2$, and (in the third inequality) that $\Delta(k_1,k_2,k_3,k_4) = \Delta(k_3,k_4,k_1,k_2)$. Once k_1 and k_2 have been fixed, with $|k_1| \neq |k_2|$, the inner sum is 4 when $|k_1| = \pi - |k_2|$, and 8 in the other cases [1] and therefore:

$$\delta^2_{j_1 j_2} \leqslant \frac{8}{L^2}\sum_{k_1 k_2}\left|\langle\Psi_0|\hat{c}^\dagger_{k_1}\hat{c}_{k_2}|\Psi_0\rangle\right|^2 , \tag{D.13}$$

where we also added the (positive) terms $|k_1| = |k_2|$ to the sum. Using the relation proved in the first section of this appendix:

$$\delta^2_{j_1 j_2} \leqslant 8\frac{N_F}{L^2} , \tag{D.14}$$

where N_F is the total number of fermions in the initial state.

$|c_\alpha|^2$ IN A TIGHT-BINDING CHAIN

Let's take two Hamiltonian of the tight-binding class, $\hat{H}_0$ and $\hat{H}$, with their single-particle spatial eigenstates, $u^0_{j\mu}$ and $u_{j\mu}$. We define $|\Psi_0\rangle$ the ground state of $\hat{H}_0$, in which the N_F occupied modes are $\{\nu^0_i\}$, and $|\alpha\rangle$ an eigenstate of $\hat{H}$, with the same number of fermions, whose occupied modes are $\{\mu_i\}$. We are going to show that:

$$|c_\alpha|^2 \equiv |\langle\alpha|\Psi_0\rangle|^2 = \left|\det U[\{\mu_i\},\{\nu^0_i\}]\right|^2 , \tag{D.15}$$

where $U[\{\mu_i\},\{\nu^0_i\}]$ is the $N_F \times N_F$ submatrix of $U \equiv u^\dagger u^0$ in which we selected the rows $\{\mu_i\}$ and columns $\{\nu^0_i\}$. The equation can be easily extended to any eigenstate of $\hat{H}_0$.

To simplify the notation we start reshuffling the labels of the modes in such a way that the occupied modes in the states $|\Psi_0\rangle$ and $|\alpha\rangle$ are the first N_F indexes, i.e., $\nu^0_i = i$ and $\mu_i = i$, with $i = 1,\dots,N_F$. If $\hat{f}^0_\nu$ and $\hat{f}_\mu$ are the single-particle fermionic operators associated to the modes of $\hat{H}_0$ and $\hat{H}$ we have that:

$$\hat{f}_\mu = \sum_\nu U_{\mu\nu}\hat{f}^0_\nu , \tag{D.16}$$

where we used the relations $\hat{f}_\mu = \sum_j u^*_{j\mu}\hat{c}_j$ and $\hat{c}_j = \sum_\nu u^0_{j\nu}\hat{f}^0_\mu$. The two many-body eigenstates can be written as:

$$|\Psi_0\rangle = \hat{f}^{0\dagger}_{N_F}\cdots\hat{f}^{0\dagger}_1|0\rangle \qquad\qquad |\alpha\rangle = \hat{f}^\dagger_{N_F}\cdots\hat{f}^\dagger_1|0\rangle , \tag{D.17}$$

1 This is due to the fact that the condition $\epsilon_{k_1}-\epsilon_{k_2}-\epsilon_{k_3}+\epsilon_{k_4}=0$ is fulfilled only when $|k_3| = |k_1|$ and $|k_4| = |k_2|$ or when $|k_3| = \pi - |k_2|$ and $|k_4| = \pi - |k_1|$ (because of particle-hole symmetry). At fixed k_1 and k_2 there are 8 values of k_3 and k_4 with which $\Delta(k_1,k_2,k_3,k_4)$ is one. The cases in which the summation is 4 is instead due to the double counting happening when the two condition are both fulfilled.

in which $|0\rangle$ is the state without fermions, and therefore:

$$\begin{aligned} c_\alpha &= \langle 0|\hat{f}_1 \cdots \hat{f}_{N_F} \hat{f}^{0\dagger}_{N_F} \cdots \hat{f}^{0\dagger}_1|0\rangle \\ &= \langle 0| \left(\sum_{\nu_1} U_{1\nu_1} \hat{f}^0_{\nu_1} \right) \cdots \left(\sum_{\nu_{N_F}} U_{N\nu_{N_F}} \hat{f}^0_{\nu_{N_F}} \right) \hat{f}^{0\dagger}_{N_F} \cdots \hat{f}^{0\dagger}_1|0\rangle \, . \end{aligned} \tag{D.18}$$

In this expansion there is a huge number of terms, but only a small set is different from zero: the ones in which $\{\nu_i\}$ is a permutation of the set $\{1, \ldots, N_F\}$. Due to the anticommutation properties of the fermionic operators we have to take core of a sign, indeed if σ_i is the permutation we have:

$$\langle 0|\hat{f}^0_{\sigma_1} \cdots \hat{f}^0_{\sigma_{N_F}} \hat{f}^{0\dagger}_{N_F} \cdots \hat{f}^{0\dagger}_1|0\rangle = \text{sign}(\sigma) \, , \tag{D.19}$$

where $\text{sign}(\sigma)$ is the parity of the permutation σ. Finally we have:

$$c_\alpha = \sum_\sigma \text{sign}(\sigma) U_{1\sigma_1} \cdots U_{N_F\sigma_{N_F}} \, , \tag{D.20}$$

which is, by definition, the determinant of $U[\{1, \ldots N_F\}, \{1, \ldots N_F\}]$ and therefore:

$$|c_\alpha|^2 = |\det U[\{1, \ldots N_F\}, \{1, \ldots N_F\}]|^2 \, , \tag{D.21}$$

which had to be demonstrated.

$|c_\alpha|^2$ IN A ISING/XY CHAIN

The computation of $|c_\alpha|^2 \equiv |\langle \alpha|\emptyset_0\rangle|^2$, where $|\emptyset_0\rangle$ is the ground state of a Hamiltonian $\hat{H}_0$ and $|\alpha\rangle$ an eigenstate of a different Hamiltonian $\hat{H}$, in a Ising/XY chain is more elaborated than the case of tight-binding models (see previous section). This is essentially because, while in the latter case the modes do not mix holes and particles and hence the empty state is the same for any Hamiltonian, in the former the modes are given by mixing holes and particles (see Eq. (3.29)), and consequently changing basis set the empty state changes.

Let's start considering the two ground states $|\emptyset_0\rangle$ and $|\emptyset_1\rangle$ of $\hat{H}_0$ and $\hat{H}$. These two states are empty states with respect to the sets of fermionic operators $\hat{\gamma}_{0\mu}, \hat{\gamma}^\dagger_{0\mu}$ and $\hat{\gamma}_{1\mu}, \hat{\gamma}^\dagger_{1\mu}$, which are the normal modes of $\hat{H}_0$ and $\hat{H}$. We will first compute $|\langle \emptyset_1|\emptyset_0\rangle|^2$, and then we will extend the result to a general $|\langle \alpha|\emptyset_0\rangle|^2$. This computation can also be found in Ref. [118]. Using Eqs. (3.29) the two basis sets can be written as:

$$\hat{\gamma}^\dagger_{0\nu} = \sum_{j=1}^{L} \left(v_{0j\nu} \hat{c}_j + u_{0j\nu} \hat{c}^\dagger_j \right) \qquad \hat{\gamma}^\dagger_{1\mu} = \sum_{j=1}^{L} \left(v_{1j\mu} \hat{c}_j + u_{1j\mu} \hat{c}^\dagger_j \right) \, . \tag{D.22}$$

We can write the direct unitary transformation from the two basis sets as follow:

$$\hat{\gamma}^\dagger_{1\mu} = \sum_{\nu=1}^{L} \left(V_{\nu\mu} \hat{\gamma}_{0\nu} + U_{\nu\mu} \hat{\gamma}^\dagger_{0\nu} \right) \, , \tag{D.23}$$

where:

$$U = u_0^\dagger u_1 + v_0^\dagger v_1 \qquad V = v_0^T u_1 + u_0^T v_1 \, . \tag{D.24}$$

We will prove that, if $|\emptyset_0\rangle$ and $|\emptyset_1\rangle$ are not orthogonal, then:

$$|\langle \emptyset_1|\emptyset_0\rangle|^2 = |\det U| \, . \tag{D.25}$$

To prove this we will perform an intermediate canonical transformation which first allows to write an explicit equation for $|\emptyset_1\rangle$ in terms of $|\emptyset_0\rangle$, and then to compute easily $\langle\emptyset_1|\emptyset_0\rangle$. We introduce the following compact Nambu notation:

$$\begin{pmatrix}\hat{\gamma}_1\\ \hat{\gamma}_1^\dagger\end{pmatrix} = \mathcal{W}^\dagger \begin{pmatrix}\hat{\gamma}_0\\ \hat{\gamma}_0^\dagger\end{pmatrix} , \tag{D.26}$$

where $\mathcal{W}$ is the following $2L \times 2L$ matrix:

$$\mathcal{W} \equiv \begin{pmatrix} U & V^* \\ V & U^* \end{pmatrix} . \tag{D.27}$$

For a theorem proved by Bloch and Messiah [119], matrices with the structure of $\mathcal{W}$ can be decomposed into a product of three unitary transformations:

$$\mathcal{W} = \begin{pmatrix} D & 0 \\ 0 & D^* \end{pmatrix} \begin{pmatrix} \overline{U} & \overline{V} \\ \overline{V} & \overline{U} \end{pmatrix} \begin{pmatrix} C & 0 \\ 0 & C^* \end{pmatrix} , \tag{D.28}$$

where D, C are $L \times L$ unitary matrices and $\overline{U}$, $\overline{V}$ are $L \times L$ real matrices of the form:

$$\overline{U} = \begin{pmatrix} 0 & & & & & & & & & & \\ & \ddots & & & & & & & & & \\ & & 0 & & & & & & & & \\ & & & u_1 & 0 & & & & & & \\ & & & 0 & u_1 & & & & & & \\ & & & & & \ddots & & & & & \\ & & & & & & u_n & 0 & & & \\ & & & & & & 0 & u_n & & & \\ & & & & & & & & 1 & & \\ & & & & & & & & & \ddots & \\ & & & & & & & & & & 1 \end{pmatrix}$$

$$\overline{V} = \begin{pmatrix} 1 & & & & & & & & & & \\ & \ddots & & & & & & & & & \\ & & 1 & & & & & & & & \\ & & & 0 & v_1 & & & & & & \\ & & & -v_1 & 0 & & & & & & \\ & & & & & \ddots & & & & & \\ & & & & & & 0 & v_n & & & \\ & & & & & & -v_n & 0 & & & \\ & & & & & & & & 0 & & \\ & & & & & & & & & \ddots & \\ & & & & & & & & & & 0 \end{pmatrix} \tag{D.29}$$

in which $u_p > 0$, $v_p > 0$ and $u_p^2 + v_p^2 = 1$. From these relations we have:

$$U = D\overline{U}C \qquad\qquad V = D^*\overline{V}C . \tag{D.30}$$

To simplify the presentation we use the following notation for the indexes: k are the indexes in which there is a pure particle-hole transformation (the zeros in the $\overline{U}$ diagonal), $(p, \overline{p})$ are the indexes which are paired with the u_p and v_p coefficients, and l the indexes in which there is no transformation (the ones in the diagonal of $\overline{U}$). We now introduce two new sets of fermionic operators:

$$\hat{\alpha}_{0n}^\dagger = \sum_\nu D_{\nu n}\hat{\gamma}_{0\nu}^\dagger \qquad\qquad \hat{\alpha}_{1m}^\dagger = \sum_\mu C_{m\mu}^*\hat{\gamma}_{1\mu}^\dagger \tag{D.31}$$

and, using Eq. (D.26) and the Nambu notation, we have:

$$\begin{pmatrix} \hat{\alpha}_1 \\ \hat{\alpha}_1^\dagger \end{pmatrix} = \begin{pmatrix} \overline{U} & -\overline{V} \\ -\overline{V} & \overline{U} \end{pmatrix} \begin{pmatrix} \hat{\alpha}_0 \\ \hat{\alpha}_0^\dagger \end{pmatrix} , \tag{D.32}$$

or equivalently:

$$\begin{aligned} \hat{\alpha}_{1p}^\dagger &= u_p \hat{\alpha}_{0p}^\dagger - v_p \hat{\alpha}_{0\overline{p}} \\ \hat{\alpha}_{1\overline{p}}^\dagger &= u_p \hat{\alpha}_{0\overline{p}}^\dagger + v_p \hat{\alpha}_{0p} \\ \hat{\alpha}_{1k}^\dagger &= \hat{\alpha}_{0k} \\ \hat{\alpha}_{1l}^\dagger &= \hat{\alpha}_{0l}^\dagger . \end{aligned} \tag{D.33}$$

In the definitions of the sets $\hat{\alpha}_{0n}$,$\hat{\alpha}_{0n}^\dagger$, and $\hat{\alpha}_{1m}$, $\hat{\alpha}_{1m}^\dagger$ we don't mix at all particles and holes (see Eqs. (D.31)), therefore the states $|\emptyset_0\rangle$ and $|\emptyset_1\rangle$ are empty states also for the new sets of fermions. Since $|\emptyset_1\rangle$ is the state which is annihilated for any $\hat{\alpha}_{1n}$ we can write it as:

$$|\emptyset_1\rangle = \mathcal{N} \prod_m \hat{\alpha}_{1m} |\emptyset_0\rangle = \prod_k \hat{\alpha}_{0k} \prod_p \left(u_p + v_p \hat{\alpha}_{0p}^\dagger \hat{\alpha}_{0\overline{p}}^\dagger \right) |\emptyset_0\rangle , \tag{D.34}$$

where $\mathcal{N}$ is a normalization constant and the first product is not over the l indexes since $|\emptyset_0\rangle$ is already empty with respect to these fermions. In the second step we used Eqs. (D.33) and we have properly normalized the state. Since, by hypothesis the two states $|\emptyset_0\rangle$ and $|\emptyset_1\rangle$ are not orthogonal we don't have pure particles-holes transformations (i.e. no k indexes) and therefore:

$$\langle \emptyset_0 | \emptyset_1 \rangle = \langle \emptyset_0 | \prod_p \left(u_p + v_p \hat{\alpha}_{0p}^\dagger \hat{\alpha}_{0\overline{p}}^\dagger \right) |\emptyset_0\rangle = \prod_p u_p = \sqrt{\prod_p u_p^2} = \sqrt{\det \overline{U}} . \tag{D.35}$$

Finally, since $\overline{U} = D^\dagger U C^\dagger$, and D, C are unitary transformations:

$$|\langle \emptyset_0 | \emptyset_1 \rangle|^2 = |\det D^\dagger U C^\dagger| = |\det U| , \tag{D.36}$$

which had to be demonstrated.

The extension to any eigenstate $|\alpha\rangle = \prod_{\mu \in I} \hat{\gamma}_{1\mu} |\emptyset_1\rangle$, where I is the set of occupied modes, is straightforward. This state can be thought as an empty set with respect to the following new set of fermions:

$$\hat{\beta}_\mu^\dagger = \hat{\gamma}_\mu^\dagger \quad \text{if } \mu \notin I \qquad\qquad \hat{\beta}_\mu^\dagger = \hat{\gamma}_\mu \quad \text{if } \mu \in I , \tag{D.37}$$

in which we have performed a particle-hole transformation for the occupied modes. Now we can use the equation obtained for the scalar product between empty states, i.e., $|c_\alpha|^2 = |\det U'|$, where the matrix U' is:

$$U' = u_0^\dagger u_1' + v_0^\dagger v_1' , \tag{D.38}$$

in which:

$$\begin{aligned} u'_{1j\mu} &= u_{1j\mu} \quad \text{if } \mu \notin I \qquad & u'_{1j\mu} &= v^*_{1j\mu} \quad \text{if } \mu \in I \\ v'_{1j\mu} &= v_{1j\mu} \quad \text{if } \mu \notin I \qquad & u'_{1j\mu} &= u^*_{1j\mu} \quad \text{if } \mu \in I . \end{aligned} \tag{D.39}$$

BIBLIOGRAPHY

[1] K. Huang, *Statistical Mechanics* (John Wiley & Sons, 1987).

[2] J. von Neumann, Zeitschrift für Physik **57**, 30 (1929).

[3] J. von Neumann, Eur. Phys. J. H **35**, 201 (2010).

[4] I. Bloch, J. Dalibard, and W. Zwerger, Rev. Mod. Phys. **80**, 885 (2008).

[5] M. Lewenstein, A. Sanpera, V. Ahufinger, B. Damski, A. Sen(De), and U. Sen, Advances in Physics **56**, 243 (2007).

[6] J. M. Deutsch, Phys. Rev. A **43**, 2046 (1991).

[7] M. Srednicki, Phys. Rev. E **50**, 888 (1994).

[8] M. Rigol, V. Dunjko, and M. Olshanii, Nature **452**, 854 (2008).

[9] J. José and E. Saletan, *Classical Dynamics: A Contemporary Approach* (Cambridge University Press, 1998).

[10] E. Fermi, J. Pasta, and S. Ulam, Los Alamos Report No. LA-1940 (1955).

[11] A. Kolmogorov, Dokl. Akad. Nauk SSSR (N.S.) **98**, 527 (1954).

[12] V. Arnold, Russ. Math. Surveys **18**, 9 (1963).

[13] J. Moser, Nachr. Akad. Wiss. Göttingen Math.-Phys. Kl. II **1962**, 1 (1962).

[14] G. Biroli and M. Mézard, Phys. Rev. Lett. **88**, 025501 (2001).

[15] G. Parisi, M. Mézard, and M. Virasoro, *Spin Glass Theory and Beyond* (World Scientific, 1987).

[16] M. Rigol, Phys. Rev. Lett. **103**, 100403 (2009).

[17] M. Rigol, Phys. Rev. A **80**, 053607 (2009).

[18] E. T. Jaynes, Phys. Rev. **108**, 171 (1957).

[19] M. Rigol, A. Muramatsu, and M. Olshanii, Phys. Rev. A **74**, 053616 (2006).

[20] M. Rigol, V. Dunjko, V. Yurovsky, and M. Olshanii, Phys. Rev. Lett. **98**, 050405 (2007).

[21] T. Barthel and U. Schollwöck, Phys. Rev. Lett. **100**, 100601 (2008).

[22] P. Calabrese, F. H. L. Essler, and M. Fagotti, Phys. Rev. Lett. **106**, 227203 (2011).

[23] M. A. Cazalilla, A. Iucci, and M.-C. Chung, Phys. Rev. E **85**, 011133 (2012).

[24] G. Carleo, F. Becca, M. Schirò, and M. Fabrizio, Scientific Reports **2**, 243 (2012).

[25] P. W. Anderson, Physical Review **109**, 1492 (1958).

[26] D. Basko, I. Aleiner, and B. Altshuler, Ann. Phys. **321**, 1126 (2006).

[27] D. M. Gangardt and M. Pustilnik, Phys. Rev. A **77**, 041604 (2008).

[28] T. Caneva, E. Canovi, D. Rossini, G. E. Santoro, and A. Silva, Journal of Statistical Mechanics: Theory and Experiment **2011**, P07015 (2011).

[29] E. Khatami, M. Rigol, A. Relaño, and A. M. Garcia-Garcia, Phys. Rev. E **85**, 050102 (2012).

[30] V. Oganesyan and D. A. Huse, Phys. Rev. B **75**, 155111 (2007).

[31] A. Pal and D. A. Huse, Phys. Rev. B **82**, 174411 (2010).

[32] E. Canovi, D. Rossini, R. Fazio, G. E. Santoro, and A. Silva, New J. Phys. **14**, 095020 (2012).

[33] E. Canovi, D. Rossini, R. Fazio, G. E. Santoro, and A. Silva, Phys. Rev. B **83**, 094431 (2011).

[34] M. Cramer, C. M. Dawson, J. Eisert, and T. J. Osborne, Phys. Rev. Lett. **100**, 030602 (2008).

[35] M. Cramer, A. Flesch, I. P. McCulloch, U. Schollwöck, and J. Eisert, Phys. Rev. Lett. **101**, 063001 (2008).

[36] M. Cramer and J. Eisert, New J. Phys. **12**, 055020 (2010).

[37] A. Flesch, M. Cramer, I. P. McCulloch, U. Schollwöck, and J. Eisert, Phys. Rev. A **78**, 033608 (2008).

[38] A. J. Daley, C. Kollath, U. Schollwöck, and G. Vidal, JSTAT **2004**, P04005 (2004).

[39] S. R. White and A. E. Feiguin, Phys. Rev. Lett. **93**, 076401 (2004).

[40] S. Trotzky, Y.-A. Chen, A. Flesch, I. P. McCulloch, U. Schollwöck, J. Eisert, and I. Bloch, Nature Phys. **8**, 325 (2012).

[41] F. Wang and D. P. Landau, Phys. Rev. Lett. **86**, 2050 (2001).

[42] F. Wang and D. P. Landau, Phys. Rev. E **64**, 056101 (2001).

[43] D. Landau and F. Wang, Computer Physics Communications **147**, 674 (2002).

[44] A. I. Khinchin, *Mathematical Foundations of Statistical Mechanics* (Dover Publications, 1949).

[45] J. L. Lebowitz and O. Penrose, Phys. Today **26**, 23 (1973).

[46] R. Balescu, *Equilibrium and Non-Equilibrium Statistical Mechanics* (John Wiley & Sons, 1975).

[47] A. Patrascioi, Los Alamos Science **15**, 263 (1987).

[48] J. G. Sinai, in *Statistical Mechanics: Foundations and Applications*, edited by T. A. Bak (1967) p. 559.

[49] Y. G. Sinai, Russian Mathematical Surveys **25**, 137 (1970).

[50] T. Erber, B. Schweizer, and A. Sklar, Communications in Mathematical Physics **29**, 311 (1973).

[51] A. Messiah, *Quantum mechanics*, Quantum Mechanics No. v. 1 (North-Holland, 1965).

[52] G. Biroli, C. Kollath, and A. M. Läuchli, Phys. Rev. Lett. **105**, 250401 (2010).

[53] G. Gallavotti, *Statistical Mechanics: A Short Treatise*, Texts and Monographs in Physics (Springer, 1999).

[54] G. Mahan, *Many Particle Physics*, Physics of Solids and Liquids (Springer, 2000).

[55] T. D. Kühner and H. Monien, Phys. Rev. B **58**, R14741 (1998).

[56] A. R. Kolovsky and A. Buchleitner, EPL (Europhysics Letters) **68**, 632 (2004).

[57] C. Kollath, G. Roux, G. Biroli, and A. M. Luchli, Journal of Statistical Mechanics: Theory and Experiment **2010**, P08011 (2010).

[58] A. Polkovnikov, K. Sengupta, A. Silva, and M. Vengalattore, Rev. Mod. Phys. **83**, 863 (2011).

[59] M. A. Cazalilla, Phys. Rev. Lett. **97**, 156403 (2006).

[60] A. Iucci and M. A. Cazalilla, Phys. Rev. A **80**, 063619 (2009).

[61] P. Calabrese and J. Cardy, Journal of Statistical Mechanics: Theory and Experiment **2007**, P06008 (2007).

[62] M. Eckstein and M. Kollar, Phys. Rev. Lett. **100**, 120404 (2008).

[63] M. Kollar and M. Eckstein, Phys. Rev. A **78**, 013626 (2008).

[64] L. F. Santos and M. Rigol, Phys. Rev. E **82**, 031130 (2010).

[65] B. Bransden and C. Joachain, *Physics of Atoms and Molecules*, Pearson Education (Prentice Hall, 2003).

[66] I. Bloch, Nature Physics **1**, 23 (2005).

[67] N. Ashcroft and N. Mermin, *Solid state physics* (Saunders College, 1976).

[68] M. Gertsenshtein and V. Vasilev, Theory of Probability & Its Applications **4**, 391 (1959).

[69] N. F. Mott, Philosophical Magazine **13**, 989 (1966).

[70] P. W. Anderson, Proc. Natl. Acad. Sci. USA **69**, 1097 (1972).

[71] E. Abrahams, P. W. Anderson, D. C. Licciardello, and T. V. Ramakrishnan, Phys. Rev. Lett. **42**, 673 (1979).

[72] A. D. Mirlin, Y. V. Fyodorov, F.-M. Dittes, J. Quezada, and T. H. Seligman, Phys. Rev. E **54**, 3221 (1996).

[73] E. Cuevas, M. Ortuño, V. Gasparian, and A. Pérez-Garrido, Phys. Rev. Lett. **88**, 016401 (2001).

[74] I. Varga, Phys. Rev. B **66**, 094201 (2002).

[75] C. Yeung and Y. Oono, EPL (Europhysics Letters) **4**, 1061 (1987).

[76] D. S. Fisher, Phys. Rev. B **51**, 6411 (1995).

[77] E. Lieb, T. Schultz, and D. Mattis, Annals of Physics **16**, 407 (1961).

[78] A. P. Young and H. Rieger, Phys. Rev. B **53**, 8486 (1996).

[79] A. P. Young, Phys. Rev. B **56**, 11691 (1997).

[80] T. Caneva, R. Fazio, and G. E. Santoro, Phys. Rev. B **76**, 144427 (2007).

[81] M. P. V. Albada and A. Lagendijk, Phys. Rev. Lett. **55**, 2692 (1985).

[82] D. S. Wiersma, P. Bartolini, A. Lagendijk, and R. Righini, Nature **390**, 671 (1997).

[83] B. Damski, J. Zakrzewski, L. Santos, P. Zoller, and M. Lewenstein, Physical Review Letters **91**, 080403 (2003).

[84] G. Roati, C. D'Errico, L. Fallani, M. Fattori, C. Fort, M. Zaccanti, G. Modugno, M. Modugno, and M. Inguscio, Nature **453**, 895 (2008).

[85] S. Aubry and G. André, Ann. Israel Phys. Soc. **3**, 133 (1980).

[86] P. Jordan and E. Wigner, Zeitschrift für Physik **47**, 631 (1928).

[87] D. Grempel, S. Fishman, and R. Prange, Physical Review Letters **49**, 833 (1982).

[88] C. Aulbach, A. Wobst, G.-L. Ingold, P. Hänggi, and I. Varga, New Journal of Physics **6**, 70 (2004).

[89] A. L. Fetter and J. D. Walecka, *Quantum Theory of Many-Particle Systems* (McGraw-Hill, New York, 1971).

[90] S. Ziraldo and G. E. Santoro, Phys. Rev. B **87**, 064201 (2013).

[91] E. Barouch, B. M. McCoy, and M. Dresden, Phys. Rev. A **2**, 1075 (1970).

[92] E. Barouch and B. M. McCoy, Phys. Rev. A **3**, 786 (1971).

[93] E. Barouch and B. M. McCoy, Phys. Rev. A **3**, 2137 (1971).

[94] F. Iglói and H. Rieger, Phys. Rev. Lett. **85**, 3233 (2000).

[95] D. Rossini, A. Silva, G. Mussardo, and G. E. Santoro, Phys. Rev. Lett. **102**, 127204 (2009).

[96] D. Rossini, S. Suzuki, G. Mussardo, G. E. Santoro, and A. Silva, Phys. Rev. B **82**, 144302 (2010).

[97] F. Iglói and H. Rieger, Phys. Rev. Lett. **106**, 035701 (2011).

[98] S. Suzuki, D. Rossini, and G. E. Santoro, ArXiv e-prints (2009), arXiv:0910.4055 .

[99] S. Ziraldo, A. Silva, and G. E. Santoro, Phys. Rev. Lett. **109**, 247205 (2012).

[100] K. Binder and A. P. Young, Rev. Mod. Phys. **58**, 801 (1986).

[101] L. C. Venuti and P. Zanardi, Phys. Rev. E **87**, 012106 (2013).

[102] C. Gramsch and M. Rigol, Phys. Rev. A **86**, 053615 (2012).

[103] K. He, L. F. Santos, T. M. Wright, and M. Rigol, Phys. Rev. A **87**, 063637 (2013).

[104] J. Sokoloff, Physics Reports **126**, 189 (1985).

[105] P. Reimann, Phys. Rev. Lett. **101**, 190403 (2008).

[106] P. Reimann, Physica Scripta **86**, 058512 (2012).

[107] R. E. Belardinelli, S. Manzi, and V. D. Pereyra, Phys. Rev. E **78**, 067701 (2008).

[108] P. Ojeda, M. E. Garcia, A. Londoño, and N. Y. Chen, Biophysical Journal **96**, 1076 (2009).

[109] E. B. Kim, R. Faller, Q. Yan, N. L. Abbott, and J. J. de Pablo, The Journal of Chemical Physics **117**, 7781 (2002).

[110] M. Mller and J. de Pablo, in *Computer Simulations in Condensed Matter Systems: From Materials to Chemical Biology Volume 1*, Lecture Notes in Physics, Vol. 703 (Springer Berlin Heidelberg, 2006) pp. 67–126.

[111] B. J. Schulz, K. Binder, M. Müller, and D. P. Landau, Phys. Rev. E **67**, 067102 (2003).

[112] K. Binder, Zeitschrift für Physik B Condensed Matter **43**, 119 (1981).

[113] A. Pal and D. A. Huse, Phys. Rev. B **82**, 174411 (2010).

[114] S. Iyer, V. Oganesyan, G. Refael, and D. A. Huse, Phys. Rev. B **87**, 134202 (2013).

[115] A. D. Luca and A. Scardicchio, EPL (Europhysics Letters) **101**, 37003 (2013).

[116] R. Walter, *Principles of Mathematical Analysis* (McGraw-Hill, 1976).

[117] S. Bochner and K. Chandrasekharan, *Fourier transforms*, Annals of mathematics studies (Kraus Reprint Corp., 1965).

[118] P. Ring and P. Schuck, *The Nuclear Many-Body Problem*, Physics and astronomy online library (Springer, 2004).

[119] C. Bloch and A. Messiah, Nuclear Physics **39**, 95 (1962).

INDEX